SELECTION OF SMALL PRETARGETING PEPTIDES WITH AFFINITY FOR RADIOCHELATES AND SEPARATION AND PURIFICATION OF RADIOLANTHANIDES

A Dissertation

Presented to

The Faculty of the Graduate School

University of Missouri-Columbia

In Partial Fulfillment of

the Requirements for the Degree

Doctor of Philosophy

by

NEBIAT SISAY

Dr. Silvia S. Jurisson, Dissertation Supervisor

Dr. Cathy S. Cutler, Dissertation Supervisor

MAY 2014

The undersigned, appointed by the dean of the Graduate School, have examined the dissertation entitled

SELECTION OF SMALL PRETARGETING PEPTIDES WITH AFFINITY FOR RADIOCHELATES AND SEPARATION AND PURIFICATION OF RADIOLANTHANIDES

Presented by Nebiat Sisay,

a candidate for the degree of doctor of philosophy,

and hereby certify that, in their opinion, it is worthy of acceptance.

Professor Silvia S. Jurisson

Professor Cathy S. Cutler

Professor Susan Z. Lever

Professor Paul R. Sharp

This work is dedicated to my late grandfather,
Abraham Asfaw

ACKNOWLEDGMENTS

My gratitude goes to almighty God in giving me the patience and strength to fulfill my dreams. I would like to thank my advisors Dr. Silvia Jurisson and Dr. Cathy Cutler for their unwavering support and guidance in my study as graduate student. They were extremely patient and supportive from the time I was an undergraduate research intern to a graduate student. I also would like to thank my other committee members: Drs. Paul Sharp and Susan Lever for their assistance in developing the project. I would like to thank all the collaborators that I worked with in various projects; specially, Dr. George Smith, for his inspiring motivation. His dedicated support taught me valuable lessons. I was fortunate to work s at the University of Missouri Research Reactor Center (MURR), a great facility that provided the platform to educate students in various research and developments. I would like to mention those whom I have worked closely including Stacy Wilder, Mary Embree, and Leanne Forbis for showing me the way in the lab. Also, I am grateful to Drs. John Lever and Jeff Smith for approving the animal study protocol and Lisa Watkinson and Terry Carmack for conducting the studies and providing the data. My graduate studies will not have been possible without the financial assistance provided by the Chemistry Department, in addition to the research funding from the Department of Energy (DOE -DE-SC0003851), and National Cancer Institute (NCI-R21CA127339) grants.

I would like to thank my undergraduate advisor Dr. Carl Johnson for his encouragement and assistance in my academic life. My special appreciation goes to my parents: Sissay Ashenfi and Birhan Abraham, my siblings and relatives: Michael Ashenafi and his wife Selam Adenew, Mariamawit Sisay, Adonay Sisay, Daniel

Abraham and Emebet Abraham. I am grateful for Rahel Sinu for her continuing support. They all have provided me the support and kind advice when I needed it.

TABLE OF CONTENTS

LIST OF FIGURES

LIST OF TABLES Page

APPENDIX LIST OF FIGURES

LIST OF ABBREVIATIONS

Abbreviation	Definition
A	Alanine
AABD	Acrylamidobenzyl DOTA
ABD (*t*-Bu)$_4$	Amidobenzyl DOTA (acetic acid-*t*-butyl ester)
ACN	Acetonitrile
AmMABD	Amidomaleic aminobenzyl DOTA
BFCA	Bifunctional chelating agent
C	Cysteine
D	Aspartic acid
DCM	Dichloromethane
DIPEA	N-Ethyldiisopropylamine
DMF	Dimethylformamide
DOTA	1, 4, 7, 10-tetraazacyclododecane-N, N', N'', N'''-tetraacetic acid
DTPA	Diethylenetriaminepentaacetic acid
E	Glutamic acid
ECC	Extraction column chromatography
EDC	1-ethyl-3-(3-dimethylaminopropyl)carbodiimide
EDTA	Ethylenediamine tetraacetic acid
EDTMP	Ethylenediamine tetra(methylene phosphonic acid)
ESI-MS	Electrospray ionization mass spectrometry
F	Phenylalanine
FDA	Food and Drug Administration

fmoc	9-Fluorenylmethyloxycarbonyl
G	Glycine
H	Histidine
HA	Hydroxyapatite
HDEHP	(bis(2-ethylhexyl) hydrogen phosphate
HEH(EHP)	(2-ethylhexyl hydrogen (3-ethylheptyl)phosphonate
HPLC	High pressure liquid chromatography
I	Isoleucine
K	Lysine
L	Leucine
LCMS	Liquid chromatography mass spectroscopy
Ln	HDEHP resin
Ln2	HEH(EHP) resin
Ln3+	Lanthanide ion with oxidation number +3
M	Methionine
MABD	2-(4-(cis-3-carboxyacrylamido) benzyl)-DOTA
MURR	University of Missouri Research Reactor Center
N	Aasparagine
nca	No-carrier-added
NHS	N-hydroxysuccinimide
NMP	1-Methyl-2-pyrrolidone
NOTA	1,4,7-triazacyclononane-1,4,7-triacetic acid
P	Proline
PBS	Phosphate buffered saline

PEG	Polyethylene glycol
PET	Positron emission tomography
Q	Glutamine
R	Arginine
RP-HPLC	Reversed-phase high performance liquid chromatography
RPL	Random phage display library
S	Serine
SA	Specific activity
SPECT	Single photon emission computed tomography
SPPS	Solid phase peptide synthesis
T	Threonine
t-Bu	*tert*-butyloxycarbonyl
TFA	Trifluoroacetic acid
THF	Tetrahydrofuran
TIS	Triisopropylsilane
TLC	Thin layer liquid chromatography
TMAS	Tetramethylammonium sulfate
TPB	Tributylphosphate
UV	Ultra-violet
V	Valine
W	Tryptophan
Y	Tyrosine
α HIBA	Alpha-hydroxyisobutyric acid

Abstract

The first objective of this dissertation was to develop metallated chelates with Michael acceptor groups for selecting small peptides from a random phage display library (RPL). The selection is for cysteine bearing peptides, so that the sulfhydryl on cysteine reacts with the reactive electrophilic group conjugated to the 1, 4, 7, 10-tetraazacyclododecane N, $N^{'}$, $N^{''}$, $N^{'''}$, $N^{''''}$–tertraacetic acid (DOTA) chelate. Upon selection of peptides with affinity for the radiochelates, the antibody-conjugated peptides are used in pretargeting tumors. Three radionuclides (^{68}Ga, ^{111}In, and^{177}Lu) were selected for labeling DOTA due to their nuclear properties applicable for radiopharmaceuticals, as well as their ability to form unique coordination geometries with the DOTA chelate. The latter variance is expected to contribute to selecting a peptide that binds specifically to each of the three metallated complexes. The newly synthesized chelate 2,2',2",2"'-(2-(4-(4-amino-4-oxobut-2-enamido)benzyl)-1,4,7,10-tetraazacyclododecane-1,4,7,10-tetrayl)tetraacetic acid (AmMABD) was radiolabeled with ^{68}Ga and^{177}Lu and the complexes were evaluated for their *in vitro* and *in vivo* stabilities and compared to previously reported radiolabeled complexes without electrophilic functional groups. The result from these studies showed the radiolabled (^{68}Ga and ^{177}Lu) AmMABD complexes were *in vitro* and *in vivo* stable. The encouraging biodistribution profile and fast blood clearance of the radioconjugates suggest that they are potential candidates for radiodiagnostic and radiotherapeutic agents.

The second objective of this dissertation focuses on separation and purification of radiolanthanides to achieve high specific activity radioisotopes applicable in nuclear

medicine. The reactor produced radiolanthanides, such as ^{177}Lu, ^{161}Tb and ^{166}Ho, have nuclear properties useful for diagnoses and treatment. The low-energy β^- emitters ^{177}Lu and ^{161}Tb are capable of causing cell damage, which is useful to localize and target metastasized large tumors. These radioisotopes also emit low energy photons useful for gamma camera imaging. In contrast, ^{166}Ho emit high energy β^- particles to deliver higher doses of radiation for effective therapeutic applications. In order to utilize these radionuclides for targeted radiodiagnosis or radiotherapy, the product radioisotopes must be separated from the irradiated target and other impurities encountered in the production process. Of the different chemical separation processes explored, the separation by utilizing chromatographic media enabled the removal of the bulk of the irradiated targets. An alternative separation method that chemically reduces enriched Yb^{3+} targets and exploits the oxidation state differences between the Yb^{2+} and Lu^{3+} was also explored. This multistep separation of Yb^{2+} from $^{177}Lu^{3+}$ is advantageous over chromatographic separation since it minimizes mixed radioactive wastes generated and lowers processing time. A method to reduce Yb^{3+} to Yb^{2+} was developed, however due to the high potential of the Yb^{3+}/Yb^{2+} redox couple (-1.05 V measured against Ag/AgCl reference electrode), reoxidation of the Yb^{2+} back to 3+ remains to be overcome.

Chapter 1

1.1 Introduction to Development of Radiopharmaceuticals

The development of radiopharmaceuticals involves preparation of molecules that contain radioactive atoms for potential applications in nuclear medicine. These radioisotopes with suitable nuclear properties can be used for diagnoses and/or therapy. Nuclear medicine takes advantage of radioisotopes that undergo radioactive decay to attain stability by releasing particles or electromagnetic radiations. The nuclear properties of a spontaneously decaying isotope, including its decay modes, the energies emitted, and the half-life, are fundamental in selecting radioisotopes for medicinal applications. Although these properties are discussed upfront, equally important are the production and availability of radioisotopes, the chemistry of the radioisotopes, and the molecules in which the radioisotope is incorporated.

In 1898 Henry Becquerel was the first to report the biological effects of radioactivity after experiencing skin burn from exposure to radiation.[1] This precedent led to an investigation of biological effects from radiation exposure and the application of radioisotopes in medicine. In the early 1930s the construction of cyclotron accelerators by Earnest Lawrence revolutionized the technology of producing radioisotopes for pharmaceutical purposes. This investigation led to the development of radioisotope production for medicinal applications.[2]

1.2 Diagnostics and Imaging

The radioisotopes utilized for diagnostics and imaging decay by emitting gamma or annihilation photons. The gamma photons are emitted if the nucleus is in an excited energy state above the ground state. The term isomeric transition indicates the decay pathway of gamma photon emission from an excited to a lower exited state to attain stability. Similarly, radioisotopes with their nucleus in an excited state can transfer energy to an electron from an inner orbital. This decay mode is termed internal conversion. The primary detection method utilized to register the incident photons emitted from a radiation source administered to patients is known as single photon emission computed tomography (SPECT). SPECT is used for radioisotopes that emit gamma photons with optimal energies in the range of 100-200 keV. However, radioisotopes with emitted energies lower or higher than the optimal range are currently being used for SPECT (e.g., ^{131}I and ^{201}Tl have γ photons of 382 and 71 keV, respectively).[3-4] The difficulties experienced in SPECT are related to quantitative measurements of the regional radioactivity *in vivo* using external detectors. Only a fraction of the photons emitted from the radioactive source reach the external detector. Other photons undergo interactions within the tissue that result in loss of energy. Some are absorbed by the tissue, while others undergo a change in direction. These multiple problems of absorption and scattering make it very difficult to perform accurate quantitative measurement of regional radioactivity with conventional external detector systems in clinical nuclear medicine.

The imaging modality that utilizes positron emission tomography (PET) from annihilation photons can minimize the aforementioned problems in using SPECT. The

detection of radioactivity in PET takes advantage of the physical properties of the radioisotopes that emit a positively charged electron (also known as a positron, β^+). A nuclide with a high ratio of protons to neutrons (Z/N) than the stable nuclide decays by β^+ emission or electron capture. At the end of the path of the β^+, they will combine with electrons in the surrounding matter and undergo annihilation, with each event giving rise to two photons of 511 keV that are emitted in 180° apart from each other. Because of the nature of the physics involved in the coincidence detection of photons in PET, the scattering or absorptions of photons caused by surrounding tissues is easily avoided by applying attenuation corrections.

1.3 Radiotherapy

Radioisotopes that decay by emitting particles are used for therapy. The commonly utilized decay modes for therapy are α, β^-, and Auger electrons. The radioactive atoms that undergo decay by releasing alpha particles ($^4_2He^{2+}$) are usually produced by heavy element radioisotopes (usually $Z \geq 83$).[5] Beta decay (β^-) is a type of radioactive decay mode that allows the conversion of a neutron to a proton within the nucleus and releases negatively charged electrons. The other ionizing radiation source is the Auger electrons, which are generated by filling the vacancy of the inner electron orbitals following electron capture or internal conversion decay modes. The choice of radioisotopes for radiotherapy considers the characteristics of the decay modes. Alpha particles deliver a high radiation dose over a short range (few cell diameters, 2-3) when compared with β^- particles (tens of cell diameters depending on their energies). Since these radioisotopes are damaging to cells *in vivo*, the diseased cells are targeted by

biological molecules labeled with radioisotopes to deliver radiation doses to the intended targets. Beta particles are less densely ionizing and are more penetrating than alpha particles. Long-range ionzing radiation from β^- decay delivers the desired radiation dose to cancer cells further removed from the delivery site. Conversely, cancer cells that are localized in small regions of the body can be treated with Auger electrons, which are low in energy. For this type of decay mode to be utilized in radiotherapy, the radiolabeled compound must be delivered to the nucleus to receive the dose required for cell damage.

Another important factor in considering radioisotopes for nuclear medicine is the half-life**.** The rate of decay of a radioisotope follows first order kinetics and is characterized by its half-life. That is the time necessary for one half of the radioactive atoms of a sample to decay. The relationship between half-life ($T_{1/2}$) and the decay constant (λ) is illustrated in **Equation1-1**.

Equation 1-1. $$T_{1/2} = \frac{\ln(2)}{\lambda}$$

The physical half-life of the radioisotope should exceed the biological molecule's *in vivo* half-life for targeted diagnosis or therapy. These requirements are critical if the biological molecule is an antibody or large molecule that has a long circulation and clearance time.

1.4 Production of radioisotopes

The majority of radioisotopes for medical applications are artificially produced by irradiating highly enriched targets. The production of radioisotopes in general can be classified as accelerator-produced or reactor-produced. Cyclotron produced radioisotopes

are bombarded with accelerated charged particles such as protons, deuterons, or α particles. Radioisotopes produced by this reaction are generally no-carrier-added because the radioisotope can be separated from the target since they are different elements. Reactor-produced radioisotopes are generated by neutron capture by a stable isotope**.** In this case target nuclei are bombarded with neutrons in a nuclear reactor to produce a radioisotope, which will generally decay by β^- emission. The factors that affect routine production of radioisotopes are associated with the nuclear properties of the target and the desired radioisotope, the facilities needed to irradiate the targets, and the cost of routine production and shipment of radioisotopes. Higher standards are set for purity levels in radiopharmaceuticals.

1.5 Radiodiagnostic and therapy development and approaches

Different approaches are utilized to deliver a formulation of radiolabeled compounds in the biological system. The differences mainly lie in the methodology utilized to deliver the dose to the desired destination with a minimum loss to other regions of the body. The three general approaches that are used to deliver radiation doses to intended targets are an integrated approach, the bifunctional chelate approach, and the pretargeting approach. Radiometals are frequently applied in diagnosis and therapy because of the established chelating ligands that can accommodate a host of metal ions. Since this study focuses on using radiometals, the examples used for the different approaches listed above are associated with radiometals. The integrated approach (**Figure 1-1 A.**) involves a radiolabeled chelate where the metal is an integral (required) component, as is the chelate, for the drug to reach its destined target.[6] The following commercialized radiopharmaceuticals can be used as example for the integrated approach for delivering

radiolabeled compounds to patients: ^{99m}Tc-sestamibi (myocardial perfusion agent) and ^{153}Sm-EDTMP (palliative treatment of bone pain).[7] **Figure 1-2** shows the chemical structures of ^{99m}Tc-sestamibi (a) and ^{153}Sm-EDTMP (b).

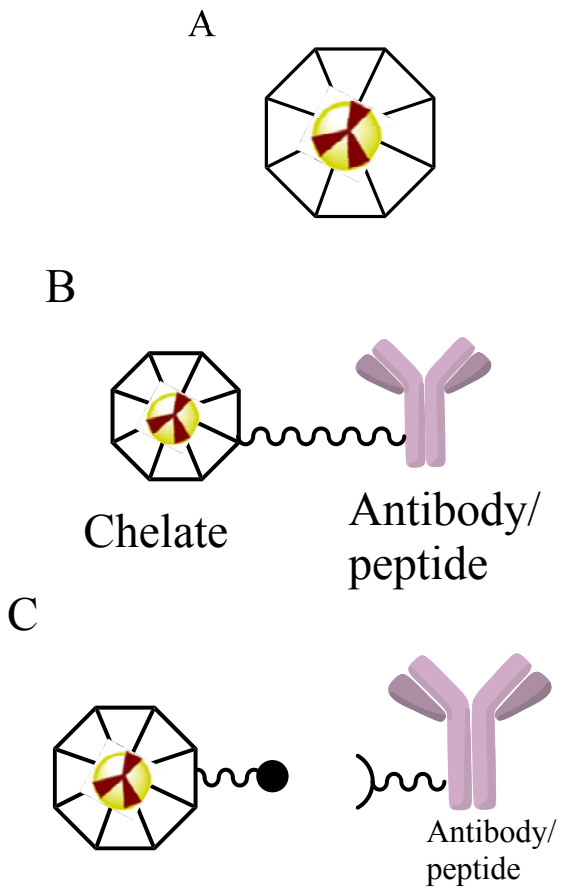

Figure 1-1. Schematic diagram of (A) the integrated approach, (B) the bifunctional chelate approach, and (C) the pretargeting approach

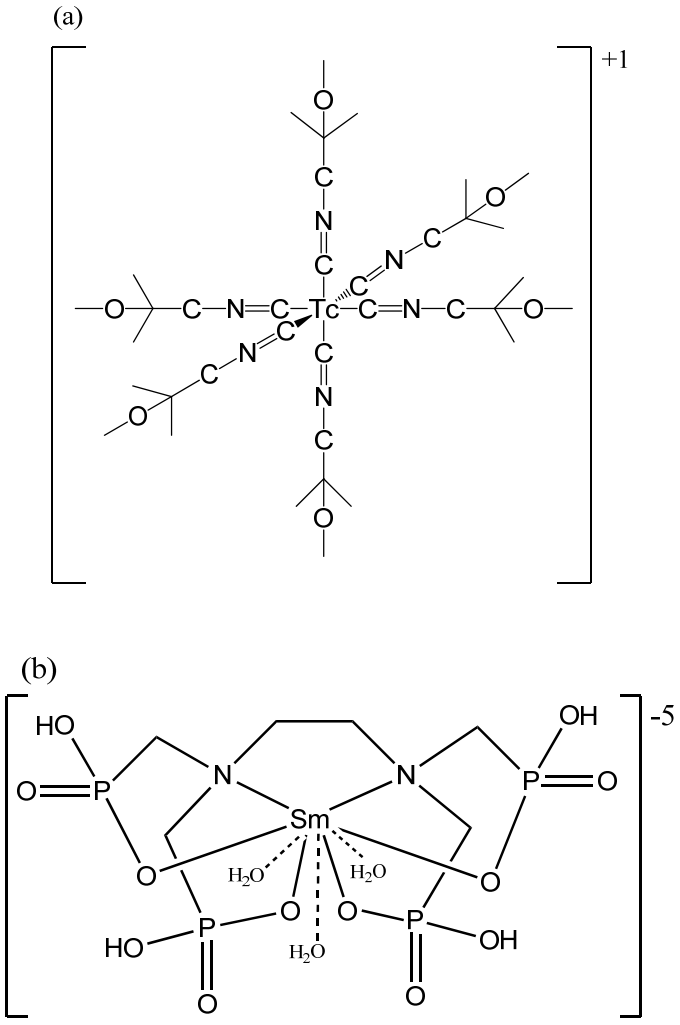

Figure 1-2. Chemical structures of ^{99m}Tc-sestamibi (a) and ^{153}Sm-EDTMP (b)

1.6 The bifunctional chelate approach (BFCA)

Target specific radiotherapy contains a receptor specific targeting moiety such as antibodies, an antibody fragment, or peptide and a chelating moiety **(Figure 1-1 B)**. The chelating molecules have a dual function, one capable of linking to biomolecules and the other to coordinate radiometals. These two functional parts of the molecule are joined covalently by linking groups. The linker additionally can be used to modify the pharmacokinetic properties of the radiopharmaceutical. The ideal BCA would contain a

targeting moiety that probes for cells of interest and a chelating moiety that coordinates a radiometal with nuclear properties suitable for imaging or treatment. The coordination chemistry of the radiometal will determine the geometry and chemical stability of the metal chelate. The chemical stability of a radiolabeled compound from the thermodynamic point view, as indicated in the following **Equation 1-2**, is obtained when the coordinating donor atoms match the hard/soft metal ligand interactions. Accordingly, hard metals form more stable complexes with hard ligands that have donor atoms such as oxygen and nitrogen and the soft metals form more stable complexes with soft ligands that have donor atoms such as sulfur and phosphorous.[8]

$$K_{eq} = \frac{k_{asscciation}}{k_{dissociation}}$$

Equation 1-2 Rate equation for a general forward and reverse reaction

For radioisotopes with short half-lives, the K_{eq} has to be high enough for a complete association to obtain higher yields. However, more attention is given to the kinetic inertness that is determined by the rate of dissociation (k_d). The kinetic inertness is important since the radiolabeled compound is administered to the body in nanomolar to picomolar concentrations where endogenous competing proteins acting as ligands are available at much higher concentrations and could cause the dissociation of the bound metal ion and potentially complex the radiometal. **Figure 1-3** shows the chemical structure of some commonly used chelates that are used to radiolabel +3 and +2 radiometals such as Ga^{3+}, Cu^{2+}, or Lu^{3+}. While acyclic chelates (EDTA and DTPA) provide a faster complexation time, which is helpful for short-lived radioisotopes, the

macrocylic ligands (DOTA and NOTA) provide greater stability for the coordinated metal center and are the preferred complexing agents.[9]

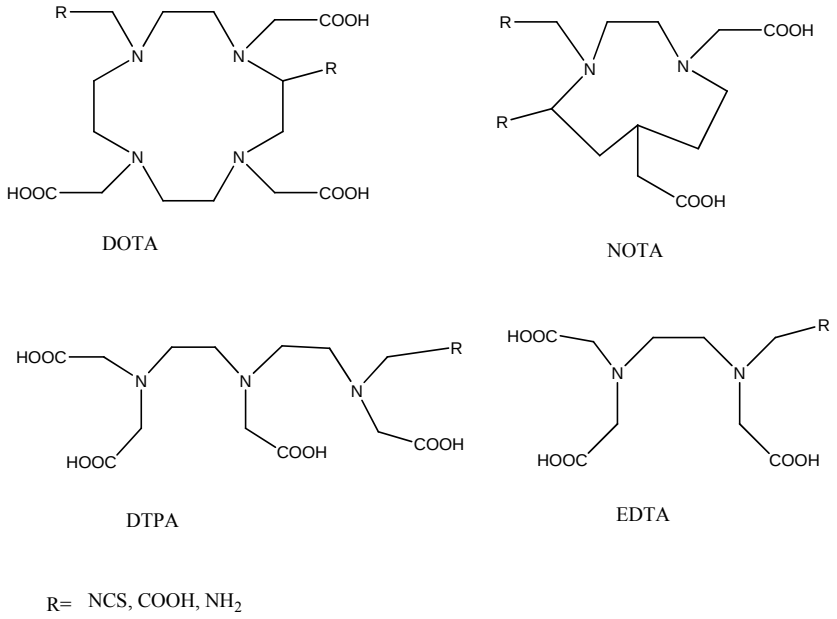

Figure 1-3. The chemical structures of DOTA, NOTA, DTPA, and EDTA chelators that coordinate +2 and +3 metal ions are illustrated with functional groups (R-) available for synthesis to link with targeting biological molecules.

1.7 Pretargeting approach

The frequently experienced difficulty in BCA targeted radiation therapy derives from the poor pharmacokinetics of large biological targeting molecules such as antibodies. If the radiolabled biological targeting molecule takes longer periods of time to find its target, this will result in radiation exposure to vital organs. The pretargeting approach separates the radioconjugate from the targeting vector, mainly antibodies, to minimize the injected radiation dose to normal tissues. The first step in pretargeting is the delivery of an antibody or a peptide that upon injection circulates *in vivo*, and is given time to reach its maximum accumulation at the target site, with the rest clearing the body. The

subsequently injected radioconjugate is then captured by the pretargeting module, while the unbound radioconjugate clears rapidly from the body. **Figure 1-1 C** illustrates the two separately administered components of pretargeting approach.

Pretargeting is advantageous as it (1) spares radiolabeling of antibodies from harsh reaction conditions, (2) significantly reduces the radiation burden to the antibody therefore no time restrictions on the biodistribution of the Ab, (3) minimizes the time invested to radiolabel and purify compounds, and (4) allows the use of short-lived radioisotopes for hospitals that have limited access to isotope production.

This dissertation describes two projects related to radiopharmaceutical chemistry:

1) An investigation of a new pretargeting approach that links radiolabeled conjugates to small peptides, which have high affinity for radioconjugates is described, including the *in vitro* and *in vivo* stability of the newly prepared radioconjugate that are useful in pretargeting.

2) The evaluation of the separation methods of ^{177}Lu, ^{161}Tb, and ^{166}Ho from enriched targets using chromatographic, chemical and electrochemical methods is described in Chapters 3 & 4.

1.8 References

1. Weslch, M. J.; Redvanely, C. S., *Handbook of Radiopharmaceuticals*. John Wiley & Sons Ltd.: Wiltshire, UK, 2003.
2. Choppin, G.; Liljenzin, J.-O.; Rydberg, J., Radiochemistry and nuclear chemistry. Butterworth-Heinemann: Woburn, 2002; pp ix-x.
3. Reichert, D. E.; Lewis, J. S.; Anderson, C. J., Metal complexes as diagnostic tools. *Coordination Chemistry Reviews* **1999,** *184* (1), 3-66.
4. Rahmim, A., PET vs. SPECT: in the Context of Ongoing Developments. *Iran J Nucl Med* **2006,** *26* (14), 1-20.
5. Loveland, W. D. M., David J.; Seaborg, Glenn T., *Modern Nuclear Chemistry*. John Wiley & Sons: 2005.
6. Jurisson, S. S.; Lydon, J. D., Potential Technetium Small Molecule Radiopharmaceuticals. *Chemical Reviews* **1999,** *99* (9), 2205-2218.
7. Cutler, C. S.; Smith, C. J.; Ehrhardt, G. J.; Tyler, T. T.; Jurisson, S. S.; Deutsch, E., Current and potential therapeutic uses of lanthanide radioisotopes. *Cancer Biother Radiopharm* **2000,** *15* (6), 531-45.
8. Gerloch, M.; Constable, E. C., *Transition Metal Chemistry:The Valence Shell in d-Block Chemistry*. Wiley-VCH Verlag GmbH & Co. KGaA: 1994; p 223.
9. Bartholomä, M. D., Recent Developments in the Design of Bifunctional Chelators for Metal-Based Radiopharmaceuticals used in Positron Emission Tomography. *Inorganica Chimica Acta* **2012,** *389* (1), 36-51.

Chapter 2

Selection of peptides from random phage display peptide library with affinity for metallated chelates

Introduction

Pretargeting is an extensively investigated approach for delivering radionuclides to target cells of interest. The difficulty in designing a biological molecule that has the ability to capture the radiolabeled chelate *in vivo* has been discussed by Orcutt and co-workers.[1] The biotin–streptavidin system that has been the most studied in pretargeting ($K = 10^{15}$) [2-6] links the preadministered antibody to the radioconjugates has been reported to have limitations. Primarily, the presence of endogenous biotin that competes for the preadministered streptavidin-antibody can result in occupying the available binding sites at nanomolar concentrations, blocking subsequently administered biotinylated radioconjugates. An additional unfavorable feature in using the biotin-streptavidin system for pretargeting is that the immunogenicity of streptavidin (SA) limits the preadministered SA-ab to a single use, which is often less than optimal.

An alternative to the streptavidin-biotin system is to chemically engineer antibodies that assume dual responsibilities, i.e., target cells of interest and capture the second injected radioconjugate. A study reported by Meares et al. describes the use of an antibody engineered to trap specifically and permanently its cognate binder, the radioconjugate, which has a functionalized redox-reactive group.[7-12] The development scheme relies on a Michael addition reaction that occurs between a cysteine of a bi-specific monoclonal antibody 2D12.5 and an acryl-based functional group derivatized on

a 1, 4, 7, 10-tetraazacyclododecane-N, N', N'', N'''-tetraacetic acid (DOTA) chelator (**Figure 2-1**).[9] Two different types of interaction were observed for the antibody metal chelator binding. The antibody CHA255 were selective in binding benzyl-EDTA chelates with different coordinating metals ($In^{3+} > Fe^{3+} > Cd^{2+} > Sc^{2+} > Ga^{3+}$) .[11] However, for the 2D12.5 antibody, which binds DOTA complexed to various lanthanides, no selective metal binding was observed between the antibody and the metal centers and thus no difference in binding was noted between the different metals including copper, which is known to exhibit a much different coordination to DOTA than the lanthanides. The drawback of using an antibody and a radioconjugate as the coupling agents is that the binding interaction between antibodies and radioconjugates is monovalent and gains no avidity advantage for the radioconjugate to form a strong binding. A monovalent engineered antibody against a small molecule will remain bound to its ligand for an average period of a few minutes to a few hours[13], whereas a biotin molecule will remain bound to streptavidin with a half-life of about 35 h.[14]

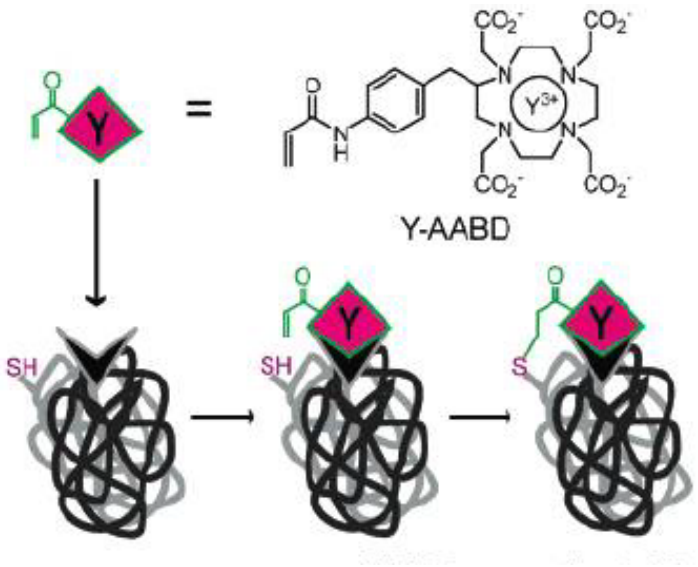

Figure 2-1. A schematic diagram showing the reaction between [Y^{3+}] AABD (acrylamido benzyl DOTA) metallated with an antibody that contains cysteine positioned close to the encapsulated chelate to form a covalent bond.

Building on the work described by Meares, this study proposed an alternative linking mechanism between pretargeting antibodies and the radioconjugates that could enhances the avidity interaction between the capturing moiety and the radioconjugate. Instead of using engineered antibodies for capturing the radioconjugates, this proposal embarks on using small short cysteine-bearing peptides. This new approach of using peptides as the radioconjugate capturing moiety is expected to occur at a faster rate since the reactive thiol of the antibody is not in an optimal position for the required nucleophilic attack. Due to difficulties in determining "the perfect" amino acid sequence that weakly interacts with the derivatized radioconjugates and will bind covalently at the Michael acceptor site, a combinatorial searching method was employed. **Figure 2-2** shows the chemical structure of the DOTA type chelator that has a functionalized Michael acceptor group.

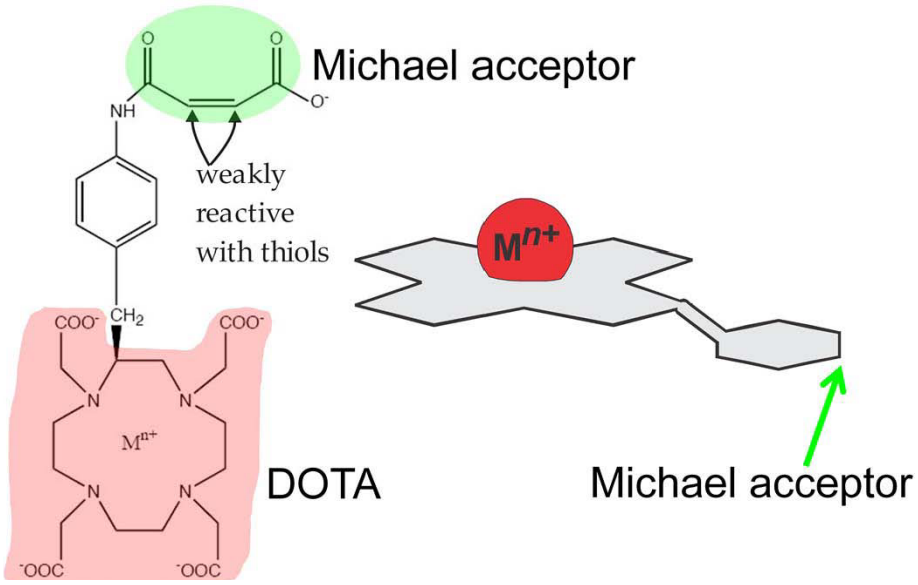

Figure 2-2. A DOTA type chelator that contains two functional moieties: the chelator DOTA (pink shading), which can be metallated with various radionuclides useful for *in vivo* imaging or therapy; and the Michael acceptor (green shading), which serves as a chemical "fastener." The Michael acceptor couples covalently to the thiol group of the amino acid cysteine.

The selection of small peptides using phage display techniques is a powerful tool to identify peptide sequences that successfully bind the selector (metallated ligand).[15-16] The advantage of choosing small peptides over streptavidin for binding the second injected radioconjugate would have important advantages: (1) they are easy to couple chemically to most targeting modules; (2) they can be synthesized chemically making fully synthetic pretargeting probes possible, which would be resistant to proteolytic degradation; (3) they will not be immunogenic, and therefore can be used more than once in the same subject; and (4) a single 'generic' peptide could be used with numerous stable, non-radioactive antibodies.

As was indicated from the Meares publications, the engineered antibodies (Ab) with cysteine are potential candidates for pretargeting. The affinity binding can be enhanced if the Ab has a cysteine at an optimal position to obtain fast binding of the radioconjugate. The task to find an amino acid sequence with an optimal conformation for binding the radioconjugate is tedious. This study, therefore, utilized an established technique to rapidly screen effective magic peptides from a huge library of random peptides displayed on phage particles that have affinity for the metallated selectors. **Figure 2-3** illustrates a phage particle that displays a random amino acid sequences designated as 'X' and fixed amino acids are coded in single letters.

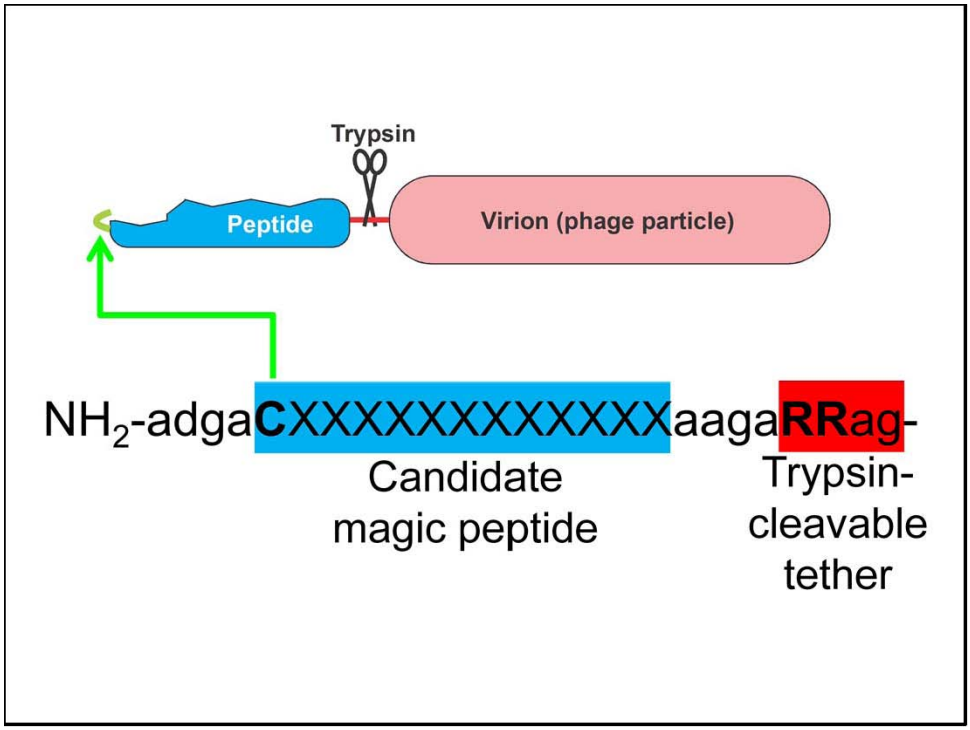

Figure 2-3. A random phage display library containing 12 random amino acids. Each displayed peptide would have a sequence of the form CXXXXXXXXXXXX and is susceptible to cleavage by enzyme trypsin.

Modification of Chelates selected for radiolabeling. From the list of chelates functionalized with electrophilic groups that were evaluated by Meares, we have chosen

one with a weak electrophilic group, (*S*)-2-(4-(*cis*-3-carboxyacrylamido) benzyl)-DOTA [MABD][9]. The factors that contributed to select the weak Michael acceptor instead of the strong one are two-fold. A peptide selected against weak Michael acceptor chelates is anticipated to have the conformations necessary to bind the selector molecule. A peptide that only binds strong Michael acceptor chelates (if the selection was performed using strong Michael acceptor chelates) could face stiff competition from endogenous proteins with strong nucleophiles by binding all the Michael acceptor radioconjugates that are only administered in small concentrations. Second, the selection of peptides from the random phage display library requires the selector metallated chelates to be tethered on a solid support. The MABD has a functional group that lends a free carboxylic acid for attaching a moiety such as biotin to immobilize the entire selector molecule on a plastic material coated with streptavidin (**Figure 2-2).** Another diagram (**Figure 2-4**) is shown to represent a selector molecule with three important components: the metal ion, the coordinating chelator with a Michael acceptor group, and a biotin tag.

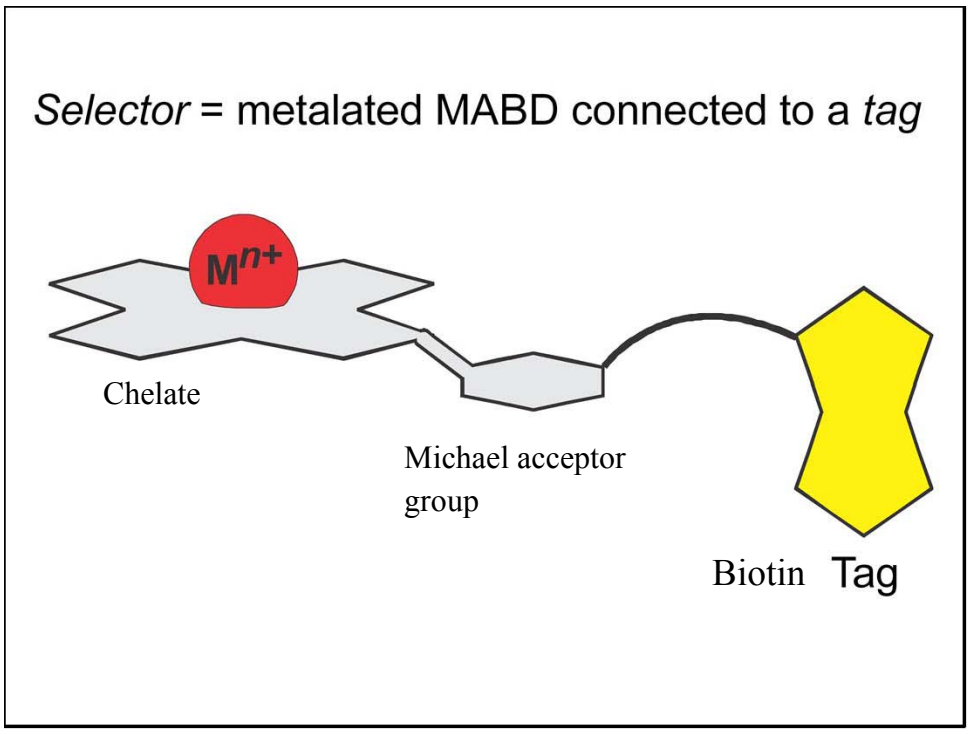

Figure 2-4. A structure that represents the selector molecule. A functinalized DOTA chelate metallated with either Ga^{3+}, In^{3+}, or Lu^{3+} ion. This molecule is also tagged with biotin for imoblizing the selector to a plastic plate coated with streptavidin to conduct the selection.

The functional groups that have to be linked to the DOTA chelate, in addition to the Michael acceptor molecule, are compounds that have a high binding affinity to the immobilizing plastic support. A common practice in phage display selection is to synthesize biotinylated biological molecules to take advantage of the high binding affinity between biotin and the streptavidin coated plastic material. In this study biotin was attached to the DOTA type chelate in a position that does not affect the binding between the metal and the chelate. Also, since the reaction media for the selection was aqueous, PEGylated biotin was chosen for the biotinylation of the selector molecule. **Figure 2-5** shows the structure of the entire selector molecule with the tagged biotin for capturing the selector onto streptavidin coated plates.

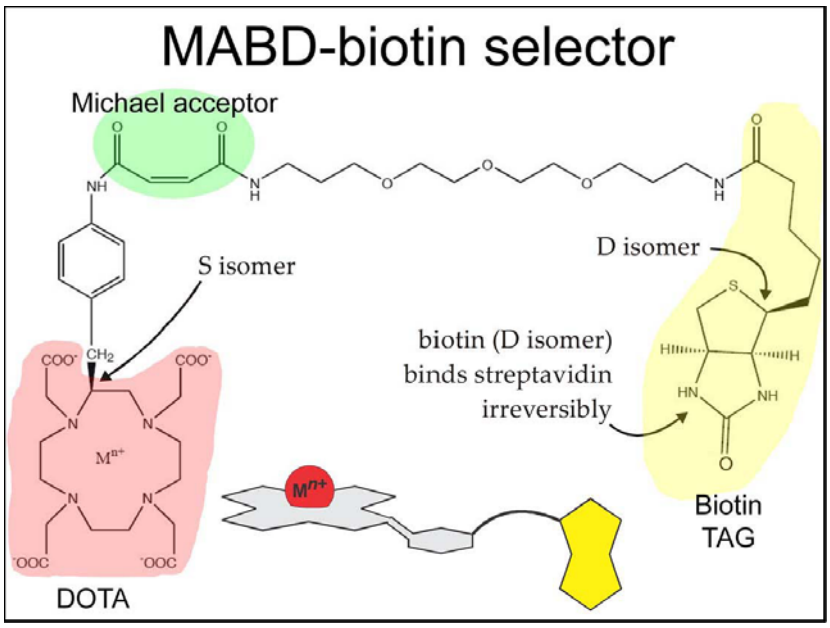

Figure 2-5. The metallated (Ga^{3+}, In^{3+}, and Lu^{3+}) MABD-PEG-Biotin complex are the selector compounds. The yellow colored cartoon is biotin for capturing the selector compound on a plastic plate coated with streptavidin.

This modification of the metallated selector molecule (MABD-PEG-Biotin), however, does affect the structure of the MABD at the carboxylic acid terminus, where the biotinylated MABD-PEG-Biotin has an amide between the PEG and the Michael acceptor. It is important to note here that once the selection process is completed the selector molecule [M] MABD-PEG-biotin is no longer required for the pretargeting studies. Instead, the MABD with a carboxylic acid terminus will be the one used in the radioconjugate molecule. The structural differences between MABD and the selector molecule [M] MABD-PEG-biotin may become problematic for the performance of the selected peptides in the pretargeting applications. So, a similar DOTA type chelate with an amide terminus was prepared to evaluate its *in vivo* and *in vitro* stabilities. Accordingly, the carboxylic acid terminus of MABD was converted to an amide terminus to form maleamic amino benzyl DOTA (AmMABD) that more closely resembles that of

the corresponding selector in terminating with an uncharged amide rather than a charged carboxylic acid.

Geometric conformation of metal complex promotes selection of peptides. This study uses three selector and one counter selector compounds that are prepared by metal ion (Ga^{3+}, In^{3+}, and Lu^{3+}) complexation with DOTA type ligands with distinct different coordination geometries for each metal. The Ga^{3+} and In^{3+} DOTA complexes have a coordination number of 6 and 7, respectively,[17-18] whereas Lu^{3+} has a coordination number of 9 when complexing DOTA chelates with four nitrogen and four oxygen from the DOTA chelate and one water molecule.[18] **Figure 2-6** shows the complexation of the three metal ions (Ga^{3+}, In^{3+}, and Lu^{3+}) to MABD. Such different three dimensional configurations could prompt selection of unique amino acid sequences from a random phage display library for each of the metal complexes.

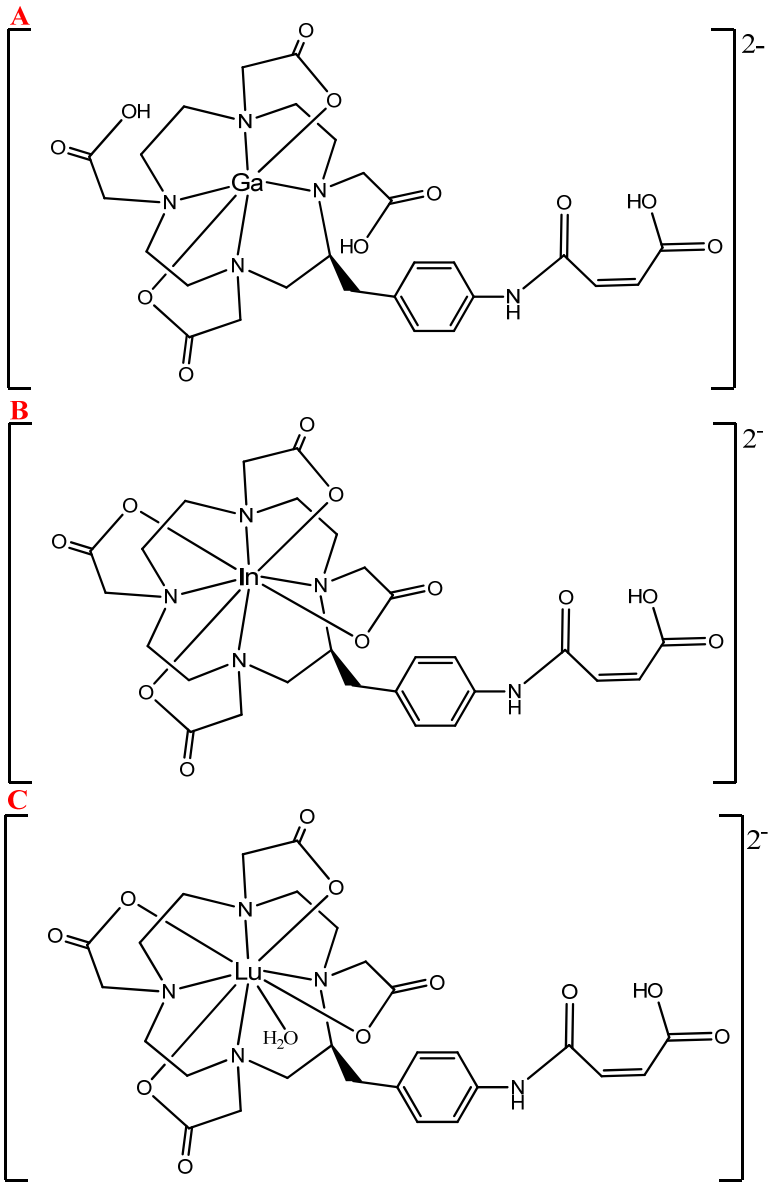

Figure 2-6. Chemical structures of Ga^{3+}, In^{3+}, and Lu^{3+} MABD compounds in A, B, and C, respectively.

The nuclear properties of the radioactive analogues of these metals are equally important considerations for imaging and therapy. The generator produced ^{68}Ga ($t_{½}$ = 68 m; β^+ max 1900 keV) radionuclide decays by emitting a positron that upon annihilation with an electron forms two 511 keV photons, which can be used for imaging by positron emission tomography (PET).[19] The accelerator produced ^{111}In ($t_{½}$ 2.8 d, γ 170, 250

keV) is used as the SPECT imaging surrogate of ^{90}Y (t ½ 2.7 d, β^- max 2.28 MeV); a therapeutic radioisotope that only emits β^- and not a traceable photons. The reactor produced ^{177}Lu ($t_{½}$ = 6.7 d; γ 208 keV; β^- max 0.5 MeV) decays to its ground state ^{177}Hf, and emits both gamma rays and beta particles desirable for imaging and therapy.[20]

Counter-selection of phage clones from the RPL

Before selecting phage-borne peptides that couple to the Ga^{3+}, In^{3+} and Lu^{3+}MABD-biotin selectors, the goal was to deplete the phage peptide library of those peptides that couple to the Ca^{2+} MABD-PEG-Biotin counter-selector. The reason for counter-selection is to simplify preparation of radioactive MABD for administration to a subject. When chelators are labeled with radioactive metals, the metal is in a vast molar deficit compared to the chelator. When MABD is reacted with radioactive Ga^{3+}, for instance, only a tiny fraction of the MABD is metallated. The goal is to avoid having to separate that tiny fraction from unmetallated MABD. The strategy is to metallate all non-radio-metallated MABD with a vast excess of non-radioactive Ca^{2+}, an ion that is abundant in blood and natural body fluids. In order to implement this strategy, we must ensure that the peptides that couple themselves effectively to Ga^{3+}, In^{3+} or Lu^{3+}MABD do not couple to Ca^{2+}MABD, even when the latter is in vast molar excess. In view of the substantial differences in three-dimensional structures between Ca-MABD and the other chelates, it is not unreasonable to imagine a magic peptide that could discriminate between them. That is the reason for counter-selection with Ca^{2+}-MABD-biotin, and **Figure 2-7** depicts the advantage of the counter-selection by giving an example where unmetallated DOTA type chelates could easily form complexes with endogenous Ca^{2+} ions that are present at higher concentrations compared to the administered chelates. The

presence of the unmetallated chelate does not interfere with the biodistribution, since the preadministered peptide is selective for the Ga^{3+}, In^{3+} or Lu^{3+}MABD complexes.

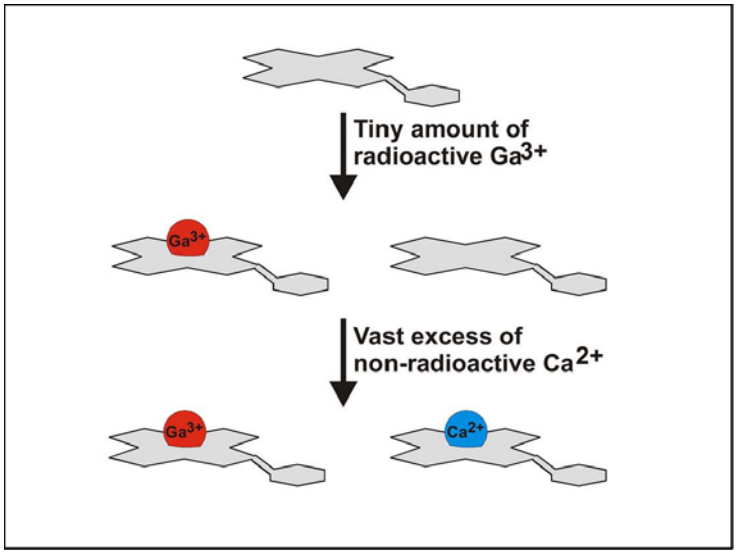

Figure 2-7. This figure illustrates the advantage of using peptides that preferentially binds the Ga^{3+}, In^{3+} or Lu^{3+}MABD complexes and not the unmetallated MABD. The counter-selection process would enable depletion of the library that binds Ca^{2+}MABD-PEG-Biotin

Positive Selection of phages from the RPL. Three separate positive selection series were carried out in parallel, one series with each of the three positive selectors: Ga^{3+}, In^{3+} or Lu^{3+}MABD-PEG-Biotin. The input to the first round of all three series was the counter-selected library described above; the input to each subsequent round of a series was the output of the previous round in that series.

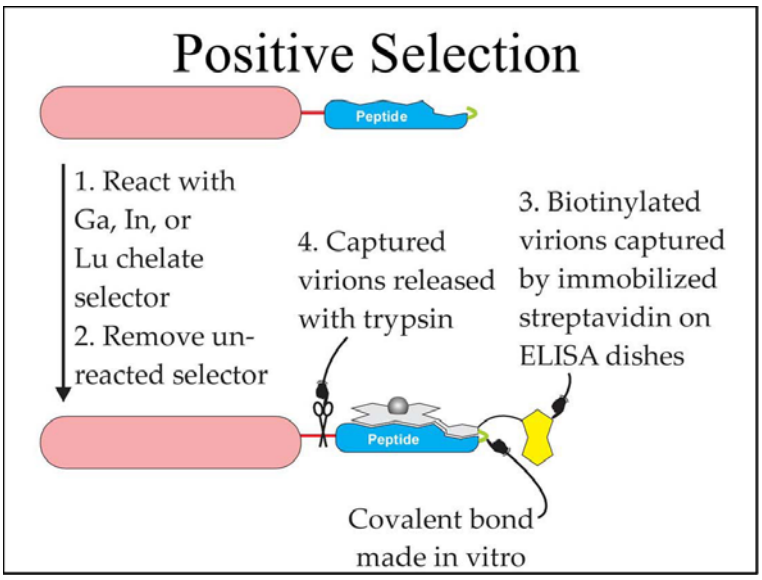

Figure 2-8. An illustration of selection process: steps 1 and 2 involves the input virions reaction with the appropriate selector Ga^{3+}, In^{3+} or Lu^{3+}MABD-PEG-Biotin; in step 3 the reacted phage would then be captured by the streptavidin via the biotin tag; and in step 4 the captured phage is released by reaction with the trypsin enzyme to amplify the phages using *E. coli* cells.

Project Objectives

The project is classified into two parts. The first project is to synthesize chelates that have the Michael acceptor functional groups, coordinate them with radiometals, evaluate their *in vitro* and *in vivo* stability. The second part is to find peptides that have high affinity for the metallated conjugates from a random phage display library.

Two ligands were prepared that have a Michael acceptor group, one terminating with a carboxylic acid (MABD) and the other with an amide (AmMABD). The position of the carbon-carbon double bond on the amidobenzyl-DOTA chelator affects the rate in which the thiolate (a strong nucleophile) forms a stable covalent bond with the carbon of the double bond (a very weak electrophile). The incorporation of such a functionality enables pretargeting peptides to capture the metallated complex. The radioconjugate with weak electrophilic functional groups may encounter strong nucleclophiles in the blood,

creating unwanted competition with the preadministered peptides. Such undesirable interactions between potent nucleophiles in the blood or tissues and the radioconjugate could nullify the use of these radioconjugates in pretargeting. Therefore, *in vitro* and *in vivo* stability studies on the ^{68}Ga and ^{177}Lu AmMABD radioconjugates were performed and are reported herein. Additionally, a comparison of the biodistribution results in normal mice with published biodistribution profiles of similar radiolabeled hapten molecules to determine the viability of the radioconjugates in pretargeting is described.

2.1 Experimental

2.2.1 Chemicals and Reagents. The starting material (S)-2-(4-aminobenzyl)-DOTA tetra-*tert*-butyl ester (ABD-(*t*-Bu_4)) was purchased from Macrocyclics (Dallas, TX). Maleic anhydride and other reagents, if not specified, were purchased from Fisher Scientific (St. Louis, MO). Maleamic acid was purchased from Sigma Aldrich (St Louis, MO). A $^{68}GaCl_3$ generator was purchased from Eckert & Ziegler Isotope Products, Inc. (Berlin, Germany) and ^{68}Ga was eluted with 0.1 N high purity HCl. Lutetium-177 chloride ($^{177}LuCl_3$) was obtained from the University of Missouri Research Reactor (MURR) in 0.05 M HCl. Hydroxyapatite (microcrystalline hydroxyapatite 40% by weight in cross linked 4% beaded agarose) was purchased from Sigma Aldrich (St. Louis, MO). $^{57}CoCl_2$ (specific activity 8.433 Ci/mg, $t_{½}$ 271 d; γ 122 KeV) was purchased from PerkinElmer (Boston, MA) in 0.1 M HCl with specific activity of 8.433 Ci/mg. HPLC grade reagents were obtained from Fisher Scientific, (St. Louis, MO). All chemicals were used as received unless otherwise stated. Mouse serum was purchased from Innovative Research (Novi, MI). Aqueous solutions were prepared with an in-house Milli-Q water system (Millipore Corp., Bilerica, MA).

HPLC methods. HPLC analysis was performed on either a Beckman Coulter System Gold chromatograph equipped with a 168 diode array detector (Beckman Coulter, Fullerton, CA) or a Varian Prostar HPLC system. A reversed phase C-18 Vydac (4.6 × 150 mm, 5 μm, 100 Å) column was used for analytical HPLC analysis. A reversed-phase C-18 Jupiter column (10 x 250 mm, 5 μm, 300Å) purchased from Phenomenex (Torrance, CA) was used for semi-preparative work. The flow rates for analytical and semi-preparative experiments were 1 mL/min and 4 mL/min, respectively, while the

wavelengths were set at 214 nm and 280 nm for both. HPLC methods for (1) semi-preparative purification and (2) analytical evaluations were as follows: (1) (A) 0.1% trifluoroacetic acid in water and (B) 0.1% TFA in acetonitrile with a gradient of 40-70 % of B over 45 min. (2) (A) 0.1% TFA in water and (B) 0.1% TFA in acetonitrile with a gradient going from 3-60% of B over 45 min.

2.2.2 Synthesis of (s)-2-(4-(cis-carboxylamido)benzyl)-1,4,7,10-tet-razacyclododecane-N,N',N'',N'''-tetraacetic Acid (MABD). The synthesis method of the MABD compound was analogous to what was reported previously.[9] Briefly, ABD (*t*-Bu)$_4$ (100 mg, 0.14 mmole) was added to 2 mL of dimethylformamide (DMF) solvent in a 10 mL conical vial. N, N-diisopropylethylamine (DIPEA) (22 µL, 0.1 mmole) was then added and the reaction mixture was stirred for 30 min. To the ABD (*t*-Bu)$_4$ solution a 1.6 molar excess of maleic anhydride (12 mg, 0.1 mmole) was added dropwise and the reaction mixture was then stirred under argon for 24 h. The solvent was removed under reduced pressure. The dried product was dissolved in 10 mL of dichloromethane, and 5 mL of 0.1 M sodium bicarbonate solution was added to hydrolyze the unreacted maleic anhydride. While the target molecule remained in the organic phase, the hydrolyzed maleic acid was extracted into the aqueous phase. The extracted MABD (*t*-Bu)$_4$ was dried over anhydrous Na_2SO_4, and the solvent removed by vacuum to yield the crude product. A fraction of the crude product was removed for analysis using LC/ESI-MS and ^{1}H NMR (**Figure A 2-2 and A 2-3)**. ESI/MS $C_{43}H_{69}N_5O_{11}$: m/z calculated $(MH)^+$ 831.5 g/mole, found 832.3 g/mole;^{1}H NMR (500 MHz, $CDCl_3$, δ ppm): 1.4-1.7 (s = 36 H), 1.80-3.6 (m= 25 H), 5.85 (d, J = 13 Hz, 1H), 6.35 (d, J = 13.5 Hz, 1H), 6.36 (d, J = 8 Hz, 1H), 6.86 (d, J = 8.5 Hz, 1H), 7.65 (d, J = 7 Hz, 2H), 14.76 (d, J= 28.5 Hz, 1H). In order to deprotect the

tertiary ester groups from the DOTA chelates to obtain four carboxylic acid groups, the solid product was dissolved in 800 μL of a cocktail mixture of trifluoroacetic acid, triethylsilane, and water with a ratio of 90/5/5 (TFA/TIS/H_2O), respectively. After the deprotection, the solvent volume was reduced under a stream of N_2 gas. To the resulting solid product 2 mL of a mixture of H_2O/ACN (50/50) was added; the product was then precipitated with 500 μL of cold diethyl ether, and re-dissolved in a H_2O/ACN (50:50) mixture for reversed-phase HPLC analysis. The crude mixture was purified by HPLC using a semi-preparative reversed phase C-18 column, and the fractions of the target molecule were collected and lyophilized. (ESI-MS $C_{27}H_{37}N_5O_{11}$ (Figure A 2-4): *m*/*z* calculated (MH^+): 608.26. Found: 608.2 g/mole **(Figure A 2-3)**.

2.2.3 Synthesis of (s)-2-(2-(4-(4-amino-4-oxobut-2-enamido)benzyl)-1,4,7,10-tetrazacyclododecane-N, N', N'',N'''-tetraacetic Acid (AmMABD). To the ABD (*t*-Bu)$_4$ (28 mg, 0.34 mmole) mixture in basic solution (preparation described above), previously prepared 1-ethyl-3-(3-dimethylaminopropyl)carbodiimide (EDC), *N*-hydroxysuccinimide (NHS; 0.34 mmole, 56 mg), and maleamic acid (40 mg, 0.34 mmole) were added in 1 mL of DMF . The reaction mixture was stirred overnight under argon. The solvent was removed under reduced pressure and the product was dissolved in dichloromethane and dried over anhydrous Na_2SO_4. The crude product (28 mg of AmMABD) was dissolved in water and the tertiary protecting groups of the carboxylic arms were removed by following the same procedure as described above.[14] The crude mixture was purified by HPLC using a semi-preparative reversed phase C-18 column, and the fractions of the target molecule were collected and lyophilized. (ESI-MS $C_{27}H_{38}N_6O_{10}$ *m*/*z* calculated (MH^+): 608.28 g/mole; found: 608.35 g/mole) **(Figure A 2-**

-4). ^{1}HNMR (500 MHz, D_2O) δ: 4.2-2.9 (m = 25 H), 7.05 (d, J = 13.8 Hz, 1H), 6.29 (d, J= 13.8 Hz, 1H), 7.49 (d, J = 7 Hz, 2H), 7.27 (d, J = 8 Hz, 2H) **(Figure A 2-5 and A 2-6)**.

2.2.4 Radiolabeling. The solid MABD and AmMABD ligands were dissolved in 0.1 M NH_4OAc at pH 5 to final concentrations of 2.8 μg/μL and 3.6 μg/μL, respectively. Radiolabeling with the generator-eluted $^{68}GaCl_3$ in 0.1 N HCl was conducted by mixing 500 μL of the ^{68}Ga solution into a vial containing 800 μL of 0.4 M NH_4OAc pH 5 buffer and 20 μL of the ligand with subsequent microwave heating of the reaction mixture for 1 min at a power setting of 100 watts. For the ^{177}Lu labeling, the solutions containing 20 μL of the ligand and 150 μL of 0.1 M NH_4OAc buffer were mixed with 20 μL of $^{177}LuCl_3$ in 0.05 N HCl and heated for 1 h at 100° C. The radiolabeling yield was evaluated by radio-TLC using C-18 reversed-phase plates analyzed using an AR-2000 Bioscan. The developing solution was 0.1 M NH_4OAc: MeOH (50:50). The radiolabeled chelates travel toward the solvent front (R_f = 0.7), whereas the free radioisotope remains at the origin (R_f = 0).

2.2.5 Serum stability studies. The stability of the ^{68}Ga and ^{177}Lu labeled MABD and AmMABD chelates in rat serum was determined following a referenced report that measured the extent of the transchelation of the radiometals from the chelates to the serum proteins.[21] The radiolabeled complexes (50 μL) were incubated in serum (450 μL) at 37 °C for up to 4 h for the ^{68}Ga complexes and out to 6 days for the ^{177}Lu complexes. The evaluation of intact complex was performed by spotting 1.5 μL aliquots for each time point on silica-gel fluorescent active TLC plates and developing with the mobile phase stated above. Under these conditions the radiolabeled complex moved with the solvent

front (R_f = 0.7 while free and serum protein bound ^{68}Ga or ^{177}Lu complexes remained at the origin (R_f = 0).

2.2.6 Hydroxyapatite challenge study. Hydroxyapatite (HA) challenge was performed by mixing HA (0.5 g) with 2 mL of 50 mM Tris buffer solution (pH 7.8) and incubating in a water bath maintained at 37° C.[22] In two separate vessels that contained the HA solutions, 50 μL of the ^{177}Lu MABD or ^{177}Lu AmMABD were added and incubated for a time period extended out to 6 days. The samples were passed through 0.2 μm filters and were washed three times with milli Q water. The stability of the radiolabeled compound in HA challenge is expressed in percent by taking the ratio between the counts from the eluted solution and the HA bound radioisotope.

2.2.7 Biodistribution. Biodistributions of the radiolabeled ^{68}Ga AmMABD and ^{177}Lu AmMABD conjugates were determined after intravenous administration in normal mouse models employed for drug discovery (n=3). All animal studies were performed under protocols approved by the University of Missouri Animal Care and Use Committee. Twelve normal adult CF-1 mice were injected with ^{68}Ga AmMABD (42 μCi/100 μL) radioconjugate. A group of three mice were sacrificed by cervical dislocation at the specified time points (15 m, 30 m, 2 h, and 4 h) and organs of interest were harvested to measure radioactivity of the samples in a γ-counter together with a series of dilutions of the injected material to determine the percent injected dose per gram. Similarly, another fifteen adult CF-1 mice were injected with 22 μCi/100 μL of ^{177}Lu-AmMABD conjugate and groups of three mice were sacrificed as described above at the specified time points, and organs of interest were measured for activity in a γ-counter.

2.2.8 Synthesis of MABD-PEG-Biotin. The diagram for the synthesis of MABD-PEG-Biotin by utilizing solid phase peptide synthesis is shown in **Figure 2-9**. The MABD (*t*-Bu)$_4$ was prepared using the procedure listed under section 2.2.2. Briefly, ABD (*t*-Bu)$_4$ (100 mg, 0.14 mmole) was dissolved in 2 mL of dimethylformamide and to this mixture DIPEA (N,N-diisopropylethylamine) (22 µL, 0.1mmol) was added and stirred under argon. After 30 min of stirring, 1.6 equivalent of maleic anhydride (21.8 mg, 0.2 mmol) was added to reaction drop wise and continued to stir for 24 h. The solvent was removed under reduced pressure and the resulting crude product was dissolved in dichloromethane, mixed with $NaHCO_3$, and vortex agitated to extract the unreacted maleic acid from the reaction mixture into the aqueous phase. This extraction was performed using a separatory funnel to isolate the product in the organic phase from the aqueous layer. The solvent of the organic layer was removed under reduced pressure and the resulting product was analyzed by LC/MS to determine the target molecule. A reversed phase C-18 column was utilized to evaluate the compound synthesis of MABD(*t*-Bu)$_4$ using the following mobile phases with gradient flow at 1 mL/min. [(A) 0.1% TFA in water and (B) 0.1% TFA in ACN with a gradient 3-60% for 45 min of B in A]. The MABD(*t*-Bu)$_4$ crude product (80 mg, 0.096 mmole) was dissolved in 2 mL of N-Methyl-Pyrrolidone (NMP) and 1.5 equivalents of benzotriazol-1-yl-oxytripyrrolidinophosphonium hexafluorophosphate (PyBOP) (150 mg, 150 µmol) was added and vortexed for 20 min to allow the formation of active ester at the carboxylic acid terminus. To this reaction mixture PEG-biotin resin was added (preparation of PEG-biotin is described below) and vortexed for a further 26 h. The crude sample was filtered to remove uncoupled MABD (*t*-Bu)$_4$ residues as well as activating reagents. Treatment of

the MABD (t-Bu)$_4$-PEG-Biotin resin with trifluoroacetic acid removed the protecting t-butyl esters from MABD(t-Bu)$_4$-PEG-biotin and cleaved the MABD-PEG-biotin from the resin. An aliquot of the crude MABD-PEG-biotin compound was analyzed by LC/MS and the solvent of the reaction mixture was removed by evaporation under reduced pressure. The product was confirmed by ESI/MS. (expected mass M= 1035.49 g/mole: found M^+ = 1036.5 g/mole) **(Figure A 2-7)**.

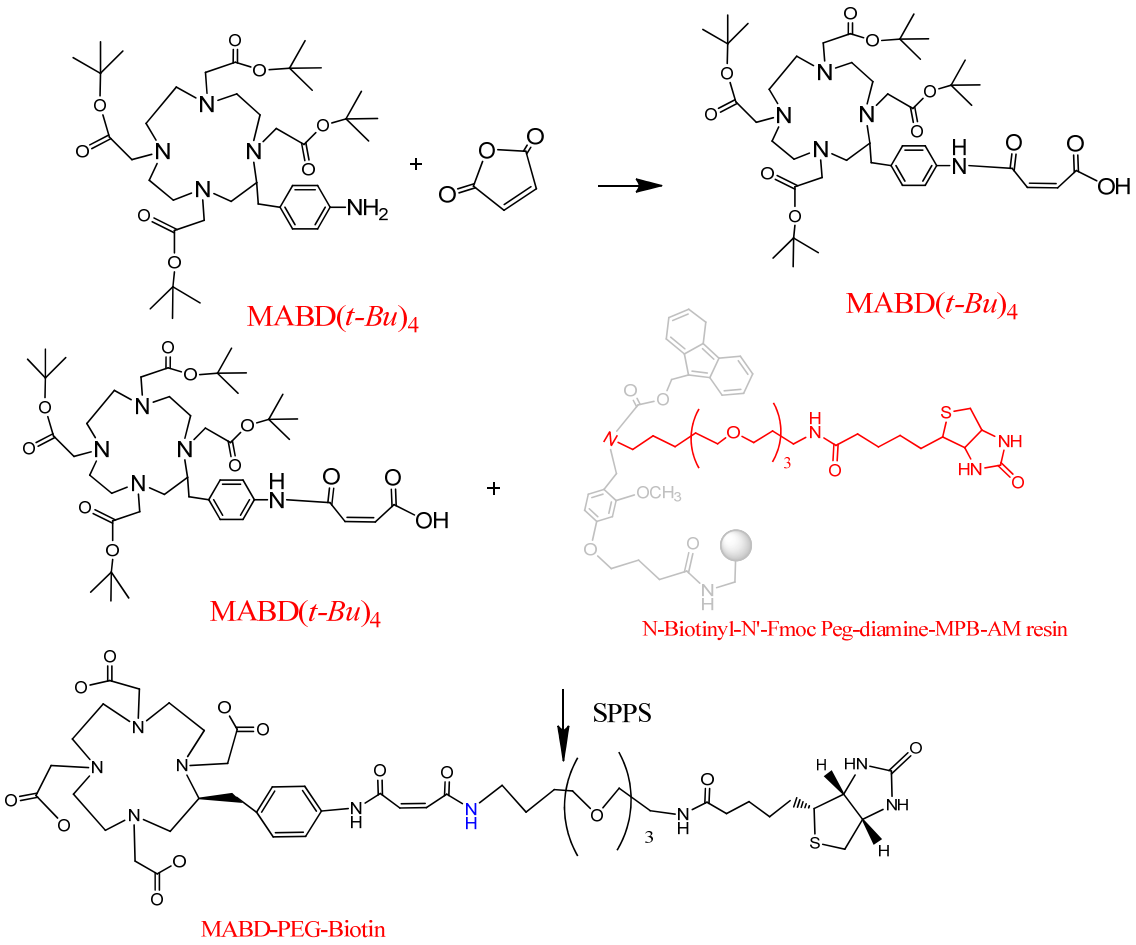

Figure 2-9. Diagram of the reaction scheme for the formation of MABD-PEG-Biotin

2.2.9 Determination of level of substitution of PEG-Biotin resin. Manufacturers' declared substitution level of the biotin-PEG Nova tag resin™ (0.20 - 0.50 mmole/g resin)

was determined from the amount of Fmoc-chromophore liberated upon treatment of the resin with piperdine/ dimethylformamide.[23] Briefly, Biotin-PEG-resin (100 mg) was treated with 1 mL of 25% piperidine in dimethylformamide for 1 h to cleave the Fmoc-chromophore. The filtered Fmoc-chromophore solution was diluted 1 to 10 in N-methylpyrolidone (NMP) and 20 μL aliquots were injected on a C-18 reversed-phase column. Fmoc-Gly/Sieber amide resin standards of known amounts were used as standards to determine the amount of Fmoc-chromophore that was released from the biotin-PEG resin by comparison of the chromatography peak area of Fmoc-chromophore with the standard. The experimentally determined value of biotin-PEG Nova tag resin™ (0.45 mmole/g of resin) was in accordance with the manufacturers' claim.[23]

2.2.10 Quantification of MABD-PEG-Biotin using isotope dilution analysis. A freshly prepared solution of 0.4 mM $CoCl_2$ (23.6 μL, 22.4 mmol) using a cobalt reference standard solution was spiked with 5 μL of the ^{57}Co activity (0.1 M HCl, 54.21 mCi/mL). This solution was added to reaction vessels that contained known amounts of MABD-PEG-biotin in 0.1 M NH_4OAc pH 5 buffer. The reaction mixture was vortexed for 5 min, an aliquot from each solution was taken out to spot silica-gel TLC plates, and the plates were developed with a 0.1 M NH_4OAc pH 5 buffer. The [^{57}Co] Co-MABD-PEG-biotin complex migrated to the solvent front on the TLC plate, whereas the unreacted/free [^{57}Co]$CoCl_2$ remained at the origin. The plates were cut in two pieces, 2 cm from the spot and each piece was counted for activity on a NaI (Tl) detector. The counts from the samples for various concentrations of Co^{2+}MABD-PEG-biotin were plotted as labeled MABD-PEG-biotin vs concentration of the radiolabeled compound **(Table 2-1)**.

	0.1 M NH_4OAc	MABD-Biotin	0.4 mM ^{57}Co			MABD-Biotin mM	weight of MABD-B in 3.5 ml (mg)
	vol µL	vol (µL)	vol (µl)	µmol	final µM		
1	10	5	5	0.002	100	0.40	1.45
2	10	3	5	0.002	111	0.67	2.42
3	10	3	8	0.0032	152	1.07	3.87
4	10	3	10	0.004	174	1.33	4.83
5	**10**	**3**	**11**	**0.0044**	**183**	**1.47**	**5.32**
6	10	3	12	0.0048	192	1.60	5.80
7	10	3	13	0.0052	200	1.73	6.29
8	10	3	14	0.0056	207	1.87	6.77
9	10	3	15	0.006	214	2.00	7.25
10	10	0	5	0.002	100	-	-
11	10	0	15	0.006	214	-	-

Table 2-1. The volume and concentration of the [^{57}Co]$CoCl_2$ metal ion and the MABD-PEG-biotin ligand used to determine the concentration of the ligand by isotope dilution analysis methodology. The highlighted row indicates the amount of $CoCl_2$ needed to metallate all of the available DOTA chelator, which determined the concentration of the chelator.

2.2.11 Metallation of the MABD-PEG-biotin. Four metal ions (Ca^{2+}, Ga^{3+}, In^{3+}, and Lu^{3+}) were used to metallate the MABD-PEG-bitoin ligand. An excess of $CaCl_2.6H_2O$ (1.5 eq, 1.67 µmoles) was added to a reaction vessel that contained 1.13 µmoles of the ligand. A similar reaction protocol was used for $Ga(NO_3)_3.6H_2O$. The calculated concentration for Ca^{2+} and Ga^{3+} metallated complexes were 1.68 and 3.93 mM, respectively. For Lu_2O_3 (67.8 mg, 170 µmoles) and In_2O_3 (4.8 mg, 17.3 µmoles), solid powders were added to the reaction vessels that contained 1.13 µmoles of the ligand and the reaction mixtures were stirred at 80°C for 24 h. The unreacted metal powders were removed from the reaction mixture by filtration. The concentration for the In^{3+} and Lu^{3+} complexes were 1.69 and 1.96 mM, respectively. The metal ligand complexations were evaluated by ESI MS and are tabulated below (**Table 2-2**).

Metallated chelates	Calculated molecular weight (g/mole)	Observed molecular weight $[M+H]^+$ (g/mole)
Ca^{2+}MABD-PEG-Biotin	1173.44	1175.01
Ga^{3+}MABD-PEG-Biotin	1102.4	1102.73
Lu^{3+}MABD-PEG-Biotin	1206.4	1208.5
In^{3+}MABD-PEG-Biotin	1146.37	1146.8

Table 2-2. A list of the calculated and measured molecular weights using ESI/MS **(Figure A 2-8 to A-2-11)** of the metallated [Ca^{2+}, Ga^{3+}, In^{3+}, and Lu^{3+}] MABD-PEG-Biotin complexes.

2.2.12 Selection of peptides from RPL. A cysteine tagged random peptide library was constructed as described in the literature.[24] The random phage display peptide library was constructed in Dr. George Smith's lab using the random coding inserts indicated in the accompanying **Figure 2-10.** The phage preparation protocol to make a RPL with 1.3 x10^9 primary clones can be accessed from the University of Missouri Biological Sciences Department website.[25] Each phage from this library displays a randomized amino acid sequence represented by X_{12} (X_{12} stands for one of the possible 12-mer peptides shown in the dark background in **Figure 2-10**) with flanking fixed amino acids. The arginine, on one side of the amino acid sequence that is in close proximity to the phage, is sensitive to trypsin. The cysteine fixed next to the randomized amino acids bears the peptide's reactive thiol.

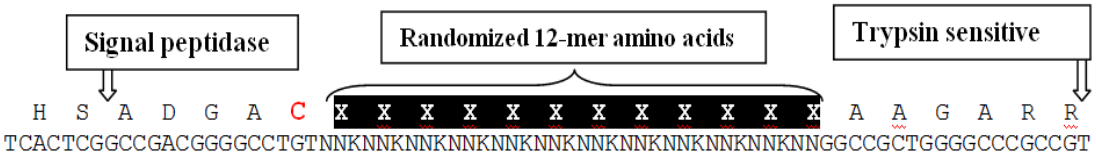

Figure 2-10. Randomized 12 amino acid sequences in the displayed peptides with signal peptidase and trypsin sensitive alanine and arginine in each side of flanks.

The experiments conducted are classified into two parts: counter selection and positive selection of peptides from the RPL. First, to obtain a phage population that is free of

peptides that have affinity for Ca^{2+} chelates, the RPL with 1.3 x10^9 primary clones were reacted with the [Ca^{2+}] MABD-PEG-Biotin. Second, the peptides of the RPL underwent counter selection to deplete the library of peptides that have affinity for streptavidin. The remaining library was used for positive selection using the Ga^{3+}, In^{3+}, or Lu^{3+} MABD-PEG-Biotin selector molecules. The procedure is described below.

(1) Into a 4-mL vial 2 mL of 3.94 x 10^{14} virions , 1.3 mL of 10 mM tris(carboxyethyl) phosphine (TCEP) and 250 μL (1.47 μmol) of Ca-MABD-biotin were added. The reaction was vortexed and allowed to react for 2 h at room temperature. (2) The reaction mixture was added to a larger vessel (50 mL) that contained 20 mL of Ca^{2+}/Mg^{2+} free Dulbecco's buffer. The insoluble salts precipitated and formed a pellet upon centrifugation. The supernatant was added to 3 mL of PEG/NaCl to isolate the phage in solid form by centrifugation. This step was repeated three times more by dissolving the pellet using the buffer solution. (3) The reaction mixture was then added to magnetized beads coated with streptavidin. These beads were magnetized to capture the phage that reacted with the Ca^{2+}-MABD-PEG-biotin via the streptavidin biotin reaction. (4) The phages that did not get captured by the streptavidin beads were removed from the reaction mixture by centrifugation. (5) Evaluation of residual biotinylated virions were performed by comparing the RPL that did not react with the counter selecting Ca^{2+}MABD-PEG-biotin using enzyme-linked immunosorbent assay (ELISA).

ELISA analysis. Phage detection and quantification are accomplished by ELISA following standard protocols with a primary polyclonal antiphage antibody[26]. The general scheme of phage captured on a streptavidin coated plate is shown in **Figure 2-11**. A stepwise addition of anti-phage antibody (extracted from mouse serum) and anti-mouse

antibody to the captured phage (by virtue of the biotinylated selector molecules) results in a signal that is detected at 425 nm using a spectrophotometer. From the selection of peptides from the RPL, if specific binding is observed, the positively tested clones are sequenced.

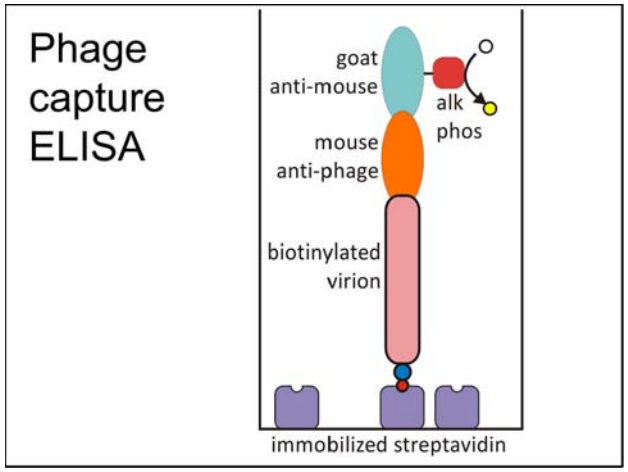

Figure 2-11. A schematic diagram showing the evaluation of the capurted phage using ELISA to detect the signal from the alkaline phosphatase upon reaction with antiphage antibody. The resulting signal is then used to deternine the quantity of phages that was captured on the tethering material.

The phage library that was counter selected with [Ca^{2+}]MABD-PEG-biotin was used for the positive selection using the three selector molecules [Ga^{3+}, In^{3+}, or Lu^{3+}] - MABD-PEG-Biotin in 3.9, 1.6 and 1.9 mM concentrations, respectively. The selection of peptides from the RPL was conducted using four different concentrations of the selector molecules (0.1, 1, 10, and 100 μM). As the selector concentration decreased a total of 12 samples of phages were amplified and the total number virions listed in **Table 2-3** represents the selector concentration reacted and the total virions obtained after the selection and amplification.

[Ga^{3+}]MABD-PEG-Biotin				
Selector conc.	100 μM	10 μM	1 μM	0.1 μM
Total virions	3.99E+14	4.01E+14	3.93E+14	3.58E+14
[In^{3+}]MABD-PEG-Biotin				
Selector conc.	100 μM	10 μM	1 μM	0.1 μM
Total virions	4.07E+14	4.00E+14	4.30E+14	4.01E+14
[Lu^{3+}]MABD-PEG-Biotin				
Selector conc.	100 μM	10 μM	1 μM	0.1 μM
Total virions	3.99E+14	3.89E+14	3.74E+14	3.69E+14

Table 2-3. The Ga^{3+}, In^{3+}, and Lu^{3+} MABD-PEG selector concentrations and the number of virions obtained after selection and amplification

To evaluate the selection of peptides from the RPL, the phages that had undergone selection were reacted with the selector molecules once again in the presence of a strong Michael acceptor molecule, N-ethylmaleimide (NEM). The NEM was added to the samples to compete against the selectors with a weak Michael acceptor group for cysteine bearing peptides in the RPL. Accordingly, a graded concentration of NEM (0, 0.006, 0.032, 0.16, 0.8, 4, 20, and 100 mM) was mixed with 30 nM of the selector (Ga^{3+}, In^{3+}, and Lu^{3+} MABD-PEG-Biotin) and the counter selector (Ca^{2+}-MABD-PEG-Biotin) molecules to which the RPL solution was added to make a total of 32 samples. Each of these samples was evaluated using the ELISA method. In order to evaluate the amino acid sequenced phage binding ability to the selector metallated chelates, timed reactions were performed between individual phage (with known amino acid sequences) and the metallated selectors. Two types of plates that were coated with either streptavidin or neutravidin were utilized to capture biotinylated phage. The output from the third round

of selection, which was sequenced and amplified (12 peptides), was reacted with metallated chelates and poured into wells coated with streptavidin and neutravidin. The wells were washed vigorously as in the final round of selection, including a 1-hour biotin block and stripped with the strongly denaturing stripping buffer (6 M urea buffered at pH 2.2). Wells were developed as usual for phage capture ELISA, as described earlier. In this manner, the percent of input virions that remained captured after washing could be quantified.

2.3 Results and Discussion

The objective of this project was to utilize the binding affinity between an antibody linked peptide and a metallated chelate in pretargeting. Two derivatized DOTA ligands were synthesized and radiolabeled with ^{68}Ga and ^{177}Lu. The MABD compound, previously reported by Meares[9], is different from the AmMABD in that the AmMABD has an amide terminus whereas the MABD has a carboxylic acid terminus. The synthesis of MABD and AmMABD, the *in vitro* and *in vivo* stability of ^{68}Ga and ^{177}Lu radiolabeled conjugates, and the biological characteristics of the small radioconjugates in comparison with similar hapten molecules are discussed. Also, the results from the selection of the peptides from RPL with affinity for the metallated chelates are described.

2.3.1 Synthesis of MABD and AmMABD. The starting material, ABD-(*t*-Bu$_4$), was used to synthesize the carboxylic acid and amide terminal chelators (MABD and AmMABD) according to modifications adopted to convert the carboxylic acid terminus to an amide.[9] The *t*-butyl protected DOTA allowed for easy manipulation and purification of the derivatives. A similar preparation protocol for the synthesis of MABD using unprotected

ABD·4HCl as the starting material was reported by Meares et al.[9] The result in the referenced study matches what is reported here, namely the ^{1}H NMR of the protected MABD (*t*-Bu)$_4$ and the LC/MS for the MABD. Also, the synthesis of AmMABD, which has not been reported before, was analyzed by LC/MS and ^{1}H NMR. The semi-preparative reversed-phase HPLC/MS purification of each of the deprotected chelates afforded pure complexes.

2.3.2 Radiolabeling with MABD and AmMABD with ^{68}Ga and ^{177}Lu. The radiolabeling of AmMABD and MABD chelates with ^{68}Ga and ^{177}Lu was evaluated by TLC. Accordingly, the ^{68}Ga radiolabeled MABD/AmMABD conjugate yields were 89 % and 91%, respectively, whereas the ^{177}Lu radiolabeled MABD/AmMABD conjugate yields were approximately 98% for both complexes.

2.3.3 Stability studies of ^{68}Ga and ^{177}Lu MABD and AmMABD Complexes in mouse serum. A radiolabeled compound is challenged *in vivo* by transchelating proteins; the thermodynamics favors the transchelation because of the overwhelming concentration difference between the serum proteins might and the radiolabeled chelates. Moreover, the fact that the chelate contains a Michael acceptor group, there is a possibility that nucleophilic reactive thiols on proteins compete with the selected peptides that are preadministered for the electrophilic carbons (weak Michael acceptor). Translating this outcome *in vivo* could mean a prolonged blood residence time for the radioconjugates, which would result in an obscured image and potential radiotoxicity to the blood cells. In the presence of 1 mM thiols in the form of mouse serum albumin, the electrophilic MABD and AmMABD chelates displayed no binding. This is significant since all four radioconjugates exhibited no binding in blood to the albumin, which contains high levels

of thiolates (strong nucleophiles) and suggests that these chelates should also be unreactive in the blood for the length of time needed for pretargeting. The results from serum stability studies are comparable to similar studies performed on stronger electrophilic radioconjugates reported by Meares.[27]

The radiolabeled ^{68}Ga MABD and ^{68}Ga AmMABD were incubated in mouse serum. After 98 min of incubation, TLC analysis showed the ^{68}Ga MABD and ^{68}GaAmMABD complexes maintained stability with only a low level of transchelation, with 94 % remaining bound (**Figure 2-12**). Similarly, 92 % of the ^{177}Lu MABD and 96 % of the ^{177}Lu AmMABD conjugates incubated in mouse serum remained stable.

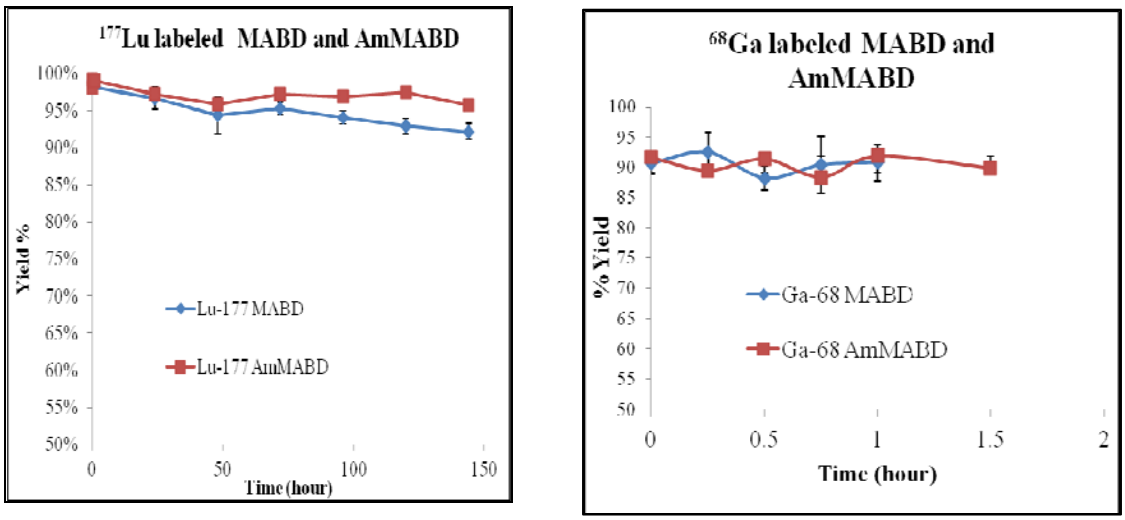

Figure 2-12. Serum stability study of the ^{68}Ga and ^{177}Lu AmMABD/MABD conjugates incubated in mice serum at 37 ˚C. The percentage of the ^{68}Ga /^{177}Lu associated with the chelates was analyzed by TLC.

2.3.4 Hydroxyapatite (HA) challenge study. A customary way of determining the transchelation level of a calcium mimic radiometal that is bound to a complex is to incubate the radiocomplex in HA media.[28-29] Adsorption of the ^{68}Ga and ^{177}Lu complexes onto HA was evaluated by incubation with HA. The yield from the

incubation of ^{68}Ga MABD and AmMABD conjugates in HA over 2 h showed 90% and 95% remained intact, respectively. The percent intact complex from the HA challenge study of ^{177}Lu conjugates showed a slightly reduced rate from 98% to 84% for ^{177}Lu MABD and from 98% to 94% for ^{177}Lu AmMABD for the time incubated (0, ¼, ½, 1, 24, 48, 72, 96, 120, and144 h). The nominal fraction of ^{177}Lu adsorbed onto the HA could be due to slow transchelation of Lu (calcium ion mimic) by HA over the incubation period extended for one half-life of the isotope, ~ 6 d.

2.3.5 Biodistribution in Normal Mouse. A biodistribution study was done in normal CF-1 mice to evaluate the small radioconjugates that exhibited high stability to serum challenge studies and HA with the intended use for pretargeting applications. A radiolabeled ligand functionalized with a weak electrophilic groups such as the MABD or AmMABD that remained stable in mouse serum (1 mM concentration of cysteine) is expected to overcome the interference from high sulfhydryl containing proteins *in vivo*.[30]

A favorable outcome from the biodistribution profile would be that these radioconjugates with weak electrophilic groups do not react with random endogenous nucleophiles and exhibit fast blood clearance and high renal clearance without significant retention in any specific organs. Therefore, ^{68}Ga and ^{177}Lu labeled AmMABD were administered to normal mice. These mice were sacrificed at various time points and radioactivity from extracted organs were counted and evaluated to determine whole body retention and clearance. The biodistribution of all of the radioconjugates exhibited low whole-body retention. The biodistribution of these radioconjugates are presented in **Tables 2-4 and 2-5** for ^{68}Ga and ^{177}Lu-AmMABD, respectively. The results are expressed as injected dose per gram for the organs of interest. For both ^{68}Ga and ^{177}Lu-

AmMABD, a significantly fast blood clearance was exhibited (at 15 min) and the majority of the activity was found in the kidneys and urine (^{68}Ga AmMABD, 94 % and ^{177}Lu AmMABD 95 %) with minimal retention, which is indicative of renal clearance. In addition, very little accumulation of activity was observed in the major organs (% ID of ^{68}Ga and ^{177}Lu conjugates; heart 0, brain 0, spleen 0, and liver 1.1 ± 0.28, 0.2 ± 0.01) for either radioconjugate over 4 h and 24 h for ^{68}Ga and ^{177}Lu conjugates, respectively; this is additional evidence indicating minimal non-specific binding.

Organs	15 m		30 m		2 h		4 h	
	% ID/g	stdev	% ID/g	stdev	% ID/g	stdev	% ID/g	stdev
Blood	**4.65**	**0.85**	**1.35**	**0.47**	**0.00**	**0.04**	**0.00**	**0.08**
Heart	0.11	0.09	0.0	0.09	0.00	0.54	0.00	0.44
Lung	1.98	0.46	0.09	0.13	0.00	0.30	0.00	0.28
Liver	**2.95**	**0.31**	**1.78**	**0.42**	**1.19**	**0.28**	**0.97**	**0.37**
Spleen	0.0	0.51	0.0	0.18	0.00	0.59	0.00	0.47
Stomach	0.51	0.31	0.0	0.10	0.00	0.04	0.00	0.17
L Int	0.51	0.15	0.09	0.06	0.59	0.64	3.78	1.12
Sm Int	0.90	0.13	0.68	0.06	1.65	0.65	0.63	0.15
Kidney	**10.28**	**1.84**	**4.21**	**1.80**	**2.12**	**0.45**	**2.11**	**0.58**
Feces	0.0	0.26	0.0	75.81	0.00	1.14	0.00	2.63
Muscle	0.0	0.03	0.0	0.09	0.00	0.33	0.00	0.09
Bone	0.0	0.93	0.0	1.33	0.00	2.70	0.00	2.74
Bladder	**10.86**	**11.28**	**0.0**	**1.34**	**0.00**	**4.44**	**0.00**	**2.85**
Brain	0.0	0.11	0.0	0.05	0.00	0.14	0.00	0.12
Pancreas	0.0	1.08	0.0	1.34	0.00	2.44	0.00	1.30
Carcass	1.29	0.18	0.50	0.21	0.13	0.03	0.15	0.03

Table 2-4. Biodistribution of the percent injected dose/gram of the ^{68}GaAmMABD after iv injection of mice at four different time points (n=3)

Organ	15 m		30 m		2 h		4 h		24 h	
	%ID/g	STDEV	%ID/g	STDEV	%ID/g	STDEV	%ID/g	STDEV	%ID/g	STDEV
Blood	**2.58**	**0.21**	**0.69**	**0.05**	**0.03**	**0.03**	**0.11**	**0.17**	**0.00**	**0.00**
Heart	0.97	0.16	0.23	0.03	0.02	0.00	0.01	0.00	0.01	0.00
Lung	1.53	0.26	0.52	0.02	0.05	0.01	0.03	0.00	0.02	0.01
Liver	**2.39**	**0.23**	**1.66**	**0.21**	**0.69**	**0.06**	**0.40**	**0.12**	**0.08**	**0.01**
Spleen	0.61	0.06	0.21	0.02	0.04	0.01	0.04	0.00	0.03	0.01
Stomach	0.40	0.10	0.65	0.87	0.09	0.08	0.08	0.04	0.08	0.02
L Int	0.45	0.09	0.12	0.01	1.15	0.20	2.31	0.63	0.19	0.11
Sm Int	0.72	0.07	0.72	0.11	1.23	0.35	0.88	0.25	0.06	0.02
Kidney	**6.44**	**0.65**	**2.28**	**0.28**	**1.25**	**0.29**	**1.06**	**0.06**	**0.62**	**0.23**
Muscle	0.57	0.12	0.15	0.01	0.01	0.00	0.01	0.00	0.01	0.01
Bone	**0.51**	**0.06**	**0.21**	**0.06**	**0.07**	**0.03**	**0.06**	**0.02**	**0.10**	**0.02**
Bladder	12.33	6.90	2.11	1.16	0.19	0.25	0.10	0.03	0.01	0.01
Brain	0.12	0.01	0.04	0.01	0.01	0.00	0.01	0.00	0.00	0.00
Pancreas	0.80	0.13	0.27	0.04	0.08	0.08	0.01	0.02	-0.01	0.02
Carcass	1.16	0.17	0.33	0.02	0.04	0.01	0.04	0.00	0.02	0.00

Table 2-5. Biodistribution of the percent injected dose/gram of the ^{177}LuAmMABD after iv injection of mice at five different time points (n=3)

The counts from the blood fractions taken from the mice sacrificed at various time points were plotted versus time (**Figure 2-13 (a)** ^{68}GaAmMABD and **(b)** ^{177}LuAmMABD compounds).The blood clearance shown in the graphs for both ^{68}Ga AmMABD and ^{177}Lu-AmMABD radioconjugates was fast, comparable to similar weak electrophilic functionalized ^{111}In conjugates reported by Meares.[27] This report also noted that, of the evaluated derivatized electrophilic radioconjugates, the stronger electrophilic radioconjugates reacted with endogenous nucleophilic molecules *in vivo*. The weak electrophilic radioconjugates, however, exhibited no significant interactions, which is in agreement with what was observed from the biodistribution of the ^{68}Ga and ^{177}Lu labeled AmMABD.

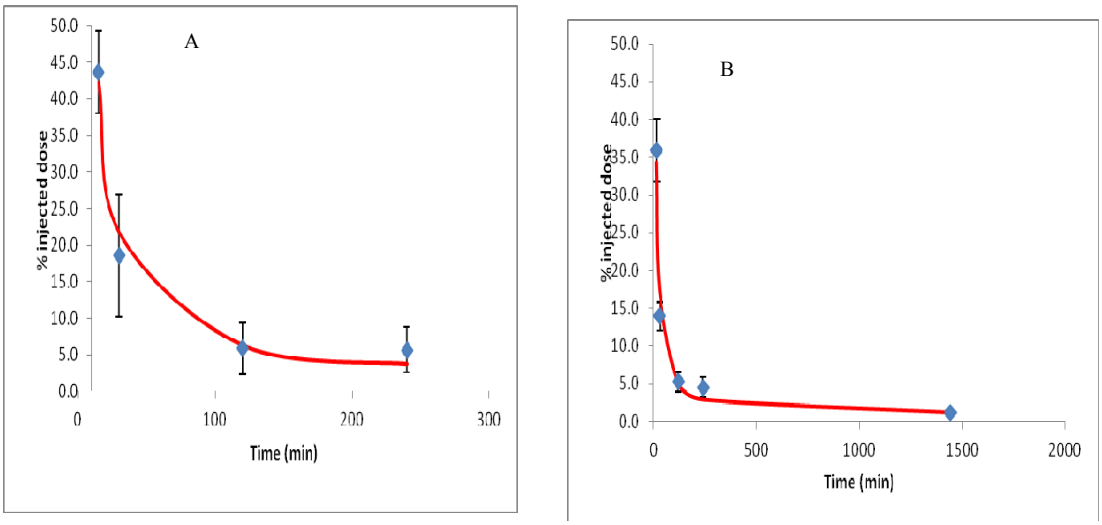

Figure 2-13. Blood clearance of (A) ^{68}Ga AmMABD and (B) ^{177}Lu AmMABD over 4h and 24 h duration, respectively.

The stability and biodistribution of selected ^{68}Ga radioconjugates were reported by Ferreira et al.[31] For comparison, **Table 2-6** lists selected data reported by Ferreira for the whole body retention and blood clearance profile of the functionalized p-Bn-NOTA radioconjugates along with biodistribution from ^{68}Ga AmMABD. For ^{68}Ga AmMABD the random dose retention in the various organs is slightly less than that of the radioconjugates with no functionalized electrophilic groups attached.

Organ	Ga-AmMABD		Ga-p-NO2-Bn-PCTA*	Ga-p-NO2-Bn-Oxo*	Ga-p-NO2-Bn-DOTA*	Ga-p-NO2-Bn-NOTA*
Blood	0.00	±0.04	11.51	2.58	4.57	0.35
Heart	0.00	±0.54	5.14	1.14	1.77	0.23
Liver	1.19	±0.30	4.52	0.96	2.86	0.63
Spleen	0.00	±0.59	4.11	0.90	1.20	0.00
Kidney	2.12	±0.45	8.49	2.52	8.06	38.10
Muscle	0.00	±0.33	4.38	0.60	1.14	-
Brain	0.00	±0.14	0.34	-	0.17	-

Table 2-6. Biodistribution of ^{68}Ga labeled radioconjugates after 2 h of post injection in normal mice (% ID/g, n =3). The ^{68}Ga AmMABD complex is compared with other small hapten molecules labeled with ^{68}Ga.

* Ferreira, C. L.; Lamsa, E.; Woods, M.; Duan, Y.; Fernando, P.; Bensimon, C.; Kordos, M.; Guenther, K.; Jurek, P.; Kiefer, G. E., Evaluation of Bifunctional Chelates for the Development of Gallium-Based Radiopharmaceuticals. *Bioconjugate Chemistry* **2010,** *21* (3), 531-536.

A similar comparison can be made to the biodistribution analysis of the ^{177}Lu AmMABD conjugate and ^{177}Lu labeled DOTA type complexes reported by Orcutt et al.[1] The ^{177}Lu AmMABD has a Michael acceptor group, which is more likely to react with endogenous nucleophiles than the hapten molecules reported by Orcutt. The biodistribution data of ^{177}Lu labeled AmMABD **(Table 2-5)**, however, is similar to what was reported by Orcutt for ^{177}Lu labeled DOTA, DOTA-benzene, and DOTA-biotin complexes with fast blood clearance and low non-specific tissue binding. The whole body retention of ^{177}Lu AmMABD is minimal (% ID remaining in the whole body was less than 4.5% at 4 h and 1.3 at 24 h), which suggests a high signal-to-background ratio for pretargeting, an important parameter in therapy of cancer that affords minimal exposure to normal tissues and organs.

2.3.6 Selection of peptides from RPL. Phage constructs with a 12 mer peptide phage library were utilized to select metallated chelates (Ga^{3+}, In^{3+}, and Lu^{3+}) MABD-PEG-Biotin. The phage displayed peptide library was comprised of 1.3 $x10^{9}$ individual clones, with 3.06 % infective units. The two important characteristics of the random phage display library, other than the random amino acid sequence, are all displayed peptides contain cysteine and have tryspsin sensitive arginine/alanine amino acid sequences as illustrated in **Figure 2-3**.

The trypsin sensitive amino acid sequences enabled the extraction of phages that presumably formed strong covalent bonds with the selectors and were captured on the immobilizing plastic plate. For the selection process to deliver those peptides with affinity for the selectors, three primary components of the selector molecule needed to be in place. These are the metallated DOTA type chelate, the Michael acceptor functionality, and the biotin linkage. A molecule that lacked one of these components could interfere with the selection.

2.3.7 Counter selection of peptides. This preliminary screening experiment was conducted to deplete the library of peptides that either directly bind streptavidin or have an affinity for [Ca^{2+}]MABD-PEG-Biotin. As a result of the counter selection process, 1:1000 of the phage library were found to either directly react with the streptavidin or the Ca^{2+}MABD-PEG-Biotin (biotinylated peptides in such reaction would then be captured by streptavidin) and removed. A follow up analysis of the counter selected phage peptides resulted in 67 % or 6.49 x 10^{13} virions/mL recovered from the RPL. These recovered phage virions were used for the positive selection of peptides using the three metallated selectors.

2.3.8 Selection of peptides with the metallated selectors (Ga^{3+},In^{3}, and Lu^{3+} MABD-PEG-Biotin). The preliminary selection experiments showed varying levels of response to the selector molecules during the evaluation. The phage selected for affinity against Ga^{3+} chelates with a concentration of 10 μM and 1 μM exhibited high absorption signal with no response to the competing NEM compound at all concentrations of NEM. The phage selected at lower concentrations of Ga chelates (100 nM and 1 nM) however, showed a decreasing signal with increasing concentration of the NEM. Phages selected for Ga^{3+}, In^{3+} or Lu^{3+} chelates were also reacted with Ca^{2+} chelates. In some instances the results showed phage tested in the presence of Ca^{2+} chelates were similar to the metallated chelates (Ga^{3+}, In^{3+}, or Lu^{3+} MABD-PEG-Biotin) they were selected against. This led to an investigation of the amino acid sequence of the peptides displayed on the phage that gave signals at higher concentrations of NEM. The phage that were harvested were considered strong binders to the metallated chelates since they stood up to the competition of the high concentrations of NEM and they responded to the trypsin cleavage, indicative of phage capture via the P3 displayed peptides from the selection, and not a random binding by virtue of the outer protein coat.

The amplification of phage was narrowed down to phages selected against low concentrations of selector chelates (10 nM Ga^{3+} and Lu^{3+}-MABD-PEG-Biotin and 100 nM of In^{3+}-MABD-PEG-Biotin) and reacted in the presence of high concentrations of NEM up to 66.7 mM). The captured phage were released by adding the enzyme trypsin to the plastic wells. The released phage comprised the output of selection. Those output virions were used to infect fresh *E. coli* host cells, which were cultured overnight in growth medium. The output phages thus increased in numbers by a factor of a million or

more. The DNA nucleotide bases of the amplified clones were sequenced and the amino acid sequences were identified **(Table 2-7).**

Name of clone	Displayed peptide sequence	Ga	In	Lu
DOTA01	adgacTFQRGTHPQFETaagarr	6		54
DOTA02	adgacSFVCWSGHPQNSaagarr	22	17	21
DOTA03	adgacMRCMAWGGYHPQaagarr	8	7	13
DOTA04	adgacFSHYSWGGDHPMaagarr	18		
DOTA05	adgacHFSQPHPQFEQPaagarr			18
DOTA06	adgacFYPVSDRHPQAGaagarr	5		5
DOTA07	adgacPWAFSHPQFETEaagarr	8		
DOTA08	adgacGAGIGNYYNLGLaagarr			8
DOTA09	adgacFWSFDPDFVKMTaagarr	2	4	
DOTA10	adgacAWTGWHPQGDLPaagarr	6		
DOTA11	adgacFLCVSRPDEFSSaagarr		4	
DOTA12	adgacGRAWHPQFGPPLaagarr	1		3
DOTA13	adgacSWGKTWGGRHPMaagarr	2		
DOTA14	adgacIWRWRLEPYDLRaagarr	1		
DOTA15	adgacLWEGFPWGGYCKaagarr	1		
DOTA16	adgacAWGSLDRYSWQWaagarr	1		
DOTA17	adgacWQFRYYQIGSYKaagarr	1		
DOTA18	adgacPWTLWTFIEGVSaagarr			1
DOTA19	adgacSHLDDSQLTPETaagarr		1	
DOTA20	adgacCAWGGFHPQGPGaagarr	1		
DOTA21	adgacAWGSHRHPMSPLaagarr	1		
DOTA22	adgacCYYVVGHPQGDPaagarr	1		
DOTA23	adgacVFNKTCNHPQFEaagarr	1		
DOTA24	adgacWFCGHPQFQNPPaagarr	1		
DOTA25	adgacSSWCYLIYDHPQaagarr			
DOTA26	adgacVECFFMDHPQNMaagarr			1
DOTA27	adgacFIGHPQFAGYGWaagarr			1
IV1	adgaRGGRCLLCCLCLWWAgaag	36	37	
IV2	adgaAVAGGRSVVDARVARgaag		54	

Table 2-7. The amino acid sequences from the selected phage are listed along with their frequency of appearances. The amino acid sequences in the randomized positions are printed in capital letters; other amino acids are printed in lower-case letters. Cysteine (C) are printed in red letters. A streptavidin-binding motif HPQ or HPM (histidine, proline, and gluthamine or methionine) observed in most of the peptides is printed in blue letters. The 9 peptides that do not have this motif are highlighted in yellow. A distribution of sequenced phages among three selector chelates is shown.

The presence of HPQ (histidine, proline, and glutamine) or HPM (histidine, proline, and methionine) motifs suggest that most of the peptides were selected by virtue

of their ability to bind directly to the immobilized streptavidin, rather than by virtue of their ability to couple to the selector. It was a surprise that the streptavidin-binding peptides emerged from the selections in spite of the strong measures taken (counter selection to avoid Ca^{2+} chelates or streptavidin binding peptides, phage precipitation to discard random binding of peptides during phage the positive selection, and applied strong wash media multiple times). A few of the selected peptides, highlighted in yellow, do not have the streptavidin-binding motif; they perhaps are the best prospects for being the desired peptides.

The signal from the ELISA reading showed that all the phage on the streptavidin coated plates had varying levels of signal whereas similar reaction mixtures reacted with the NA coated plates presented minimal signal. **Figure 2-14** shows two batches of selector metallated chelates (Ga^{3+}, In^{3+}, and Lu^{3+}) and the counter-selector Ca chelates (biotin is the control) and the selected and sequenced phage.

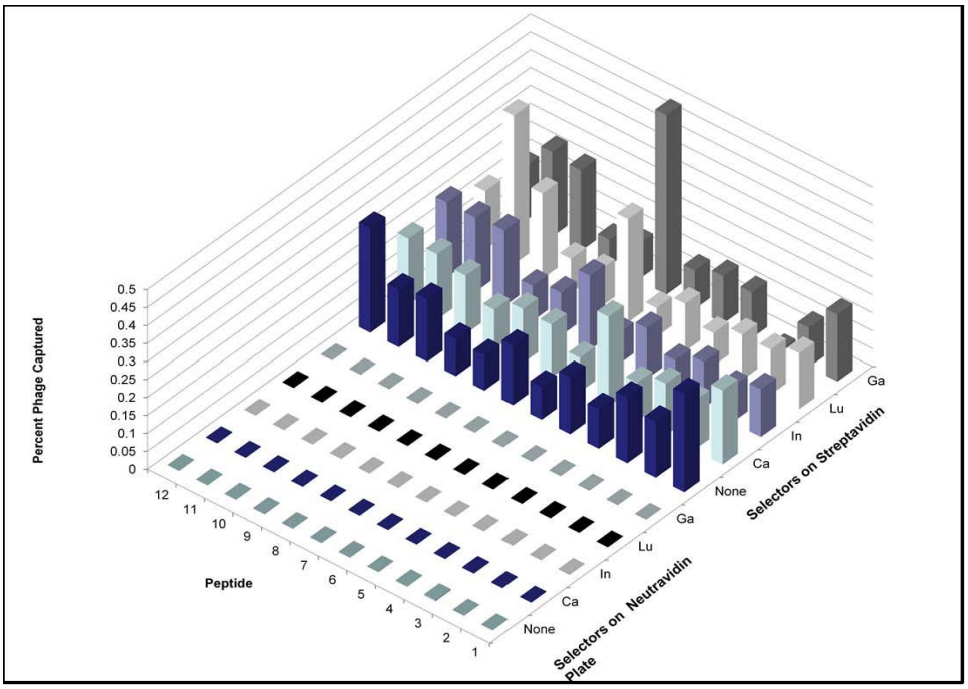

Figure 2-14. Peptides with known amino acid sequences reacted with selector chelates and the control (Ca^{2+} chelates and boitin). A magic peptide that was biotinylated by coupling to the counter-selector or the selector would be captured by both streptavidin and neutravidin. Second, the virions were captured by streptavidin even in the control wells where no selector was present, indicating that they were captured directly rather than because they coupled to the selector.

The alternative to eliminate the possibility of direct interaction between phage and the streptavidin is to use neutravidin, a deglycosylated protein capable of binding biotin with a high association rate $[k_a = 10^{15}]$[32] and minimal nonspecific adsorption. A repeat of the experiment that produced the sequenced peptide in **Table 2-7** was conducted using neutravidin coated plastic plates coated, instead of streptavidin. The final round of selection was repeated using three selector molecules ([Ga^{3+}, In^{3+}, and Lu^{3+}]-MABD-PEG-Biotin) with graded concentrations of the NEM competitor. The selection resulted in 48 amplified outputs, 16 each for the ([Ga^{3+}, In^{3+}, and Lu^{3+}]MABD-PEG-Biotin selectors, (rather than individual phage clones). The evaluation from this experiment showed only one of the output captured significantly above background. The percent of

input virions captured from this output population was quite high (1-4 percent). Evidently, this output population was subsequently shown to be dominated by a single clone displaying the peptide adgacWAWWTYDIKGCMaagarr, which presumably is responsible for the population's neutravidin-binding activity. **Figure 2-15** shows the performance of the virions selected for the metallated chelates and tested against the same chelates plus biotin and Ca^{2+} chelates. This specific clone did not show any response when it was tested against the different metal ion (Ga^{3+}, In^{3+}, or Lu^{3+}) complexes. Although multiple attempts were made to find a peptide that has an excellent conformation, there is no indication that the output population includes virions displaying effective peptides.

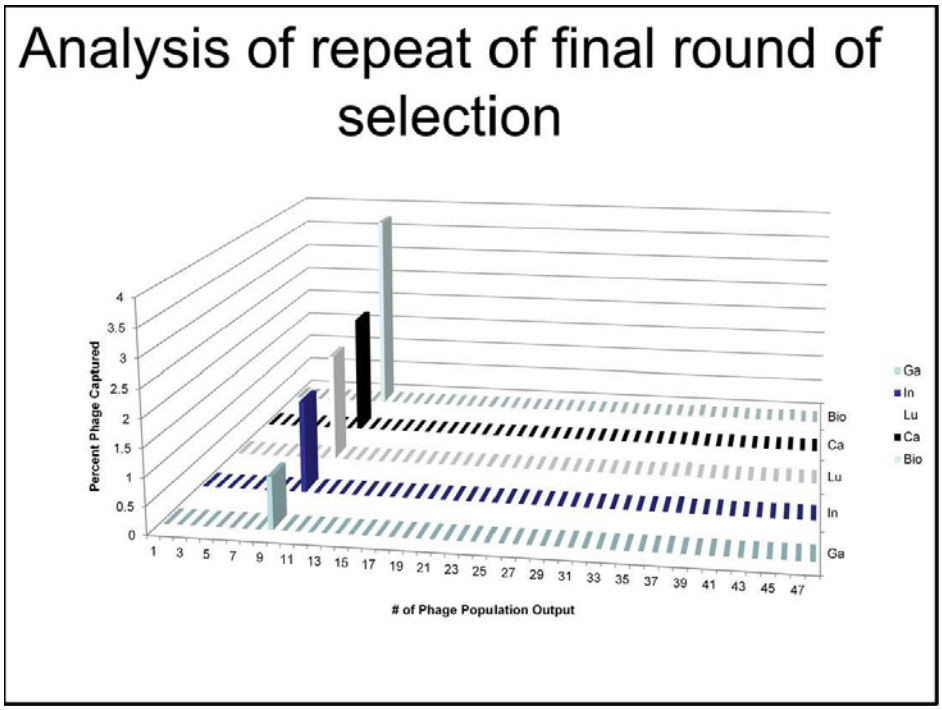

Figure 2-15. The 48 phage clones amplified to react with the three metallated chelates, selectors ([Ga^{3+}, In^{3+}, and Lu^{3+}]MABD-PEG-Biotin) and samples that are considered as blanks such as the Ca^{2+} chelates and a biotin that is not linked to a DOTA chelator. The ELISA analysis of this samples showed one of the 48 phage clones presented a new amino acid sequence that directly interacts with the plastic plate coated with neutravidin.

2.4 Conclusion

For a radioconjugate to be considered in pretargeting, it needs to demonstrate a high affinity for its cognate peptide, a high stability *in vivo*, and a favorable pharmacokinetic profile, all of which ensures fast blood clearance and excretion through the kidneys without any significant retention by any organs. Based on the results obtained in this study, serum stability studies indicate the Michael acceptor groups are not susceptible to nucleophilic attack in the presence of thiols. This could be due to the weak Michael acceptor group that is less likely to react with free sulfhydryl as opposed to the strong Michael acceptor groups, which are more reactive in similar incubation media. Similarly, the biodistribution profiles of $^{68}Ga^{3+}$ and $^{177}Lu^{3+}$ AmMABD indicates minimal non-specific binding and fast blood clearance, which is consistent with the biodistribution profiles of $^{111}In^{3+}$ labeled EDTA ligands functionalized with a Michael acceptor group.[27] The selection of peptides with affinity for the metallated chelates did not yield the amino acid sequences that we anticipated. The presence of contaminant peptides that overwhelmed the final positively selected library have effectively diminished the chances of finding the desired sequence during the intermediate steps of phage amplifications. Although, the selection process has attempted from the start to eliminate such possibilities by conducting counter selections, the contaminant HPQ motifs were resistant in the unfavorable reaction media for random binding. This study has developed $^{68}Ga^{3+}$ and $^{177}Lu^{3+}$ AmMABD radioconjugates with favorable characteristics with both *in vivo* and *in vitro* stabilities for potential pretargeting applications.

2.5 Future Studies

The selection strategy developed in this project could serve to select strong radioconjugate binding peptides, with the appropriate changes in the design of the library and the structure of the selectors. In particular, the trypsin-release vector developed in this project is highly applicable to any selection for irreversible covalent coupling rather than reversible non-covalent binding. The obvious modification that would be made for further selection of peptides from the RPL would be to use neutravidin coated capturing plates instead of streptavidin. Although, the study showed there could be some amino acid sequences that directly bind the capturing plate, those virions clones can easily be eliminated during counter selection. There is a high possibility for the counter selection to eliminate these unwanted clones because the neutravidin is a deglycosylated compound and discourages random binding of peptides, such as one displayed on phage.

Other changes that could enhance the affinity selection are increasing the concentrations of the selector molecules. This study used 100 nM selector concentrations and the future study should consider 50-100 μM concentrations of the metallated chelate to encourage the reactivity between the peptide and the selector chelates. Although, the selection stringency could suffer from the increase in the concentration of the selector molecule, it could still benefit from the fact that the selector has a weak reactive group, which requires an excellent conformation of the peptide to form covalent binding. In addition, the stipulated concentration of the selector chelates can still be accommodated by the binding sites of the capturing neutravidin coated plates.

2.5 Appendix

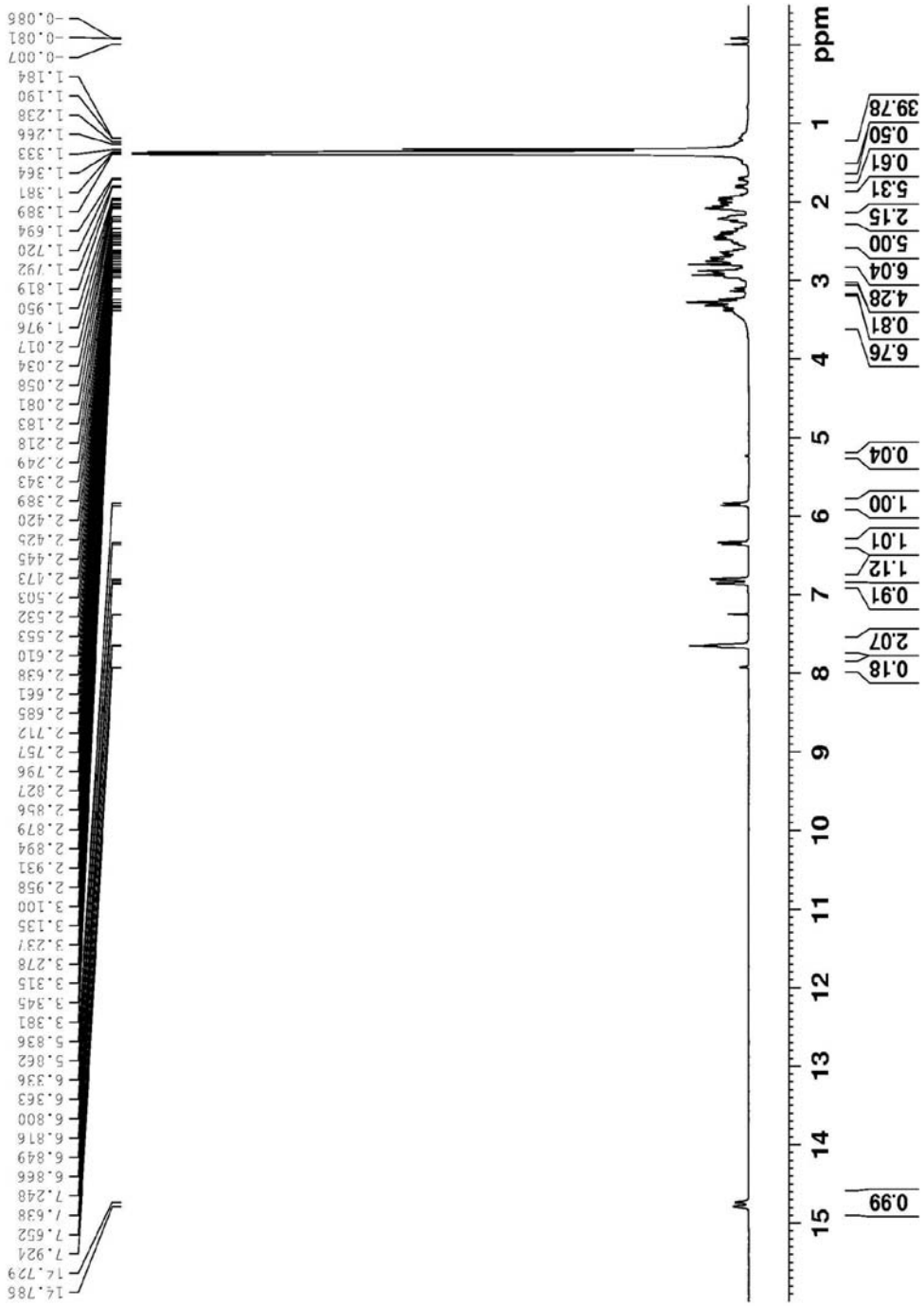

Figure A 2-1. ^{1}H NMR experiment of MABD(t-Bu)$_4$ in $CDCl_3$ solvent on 500 MHz

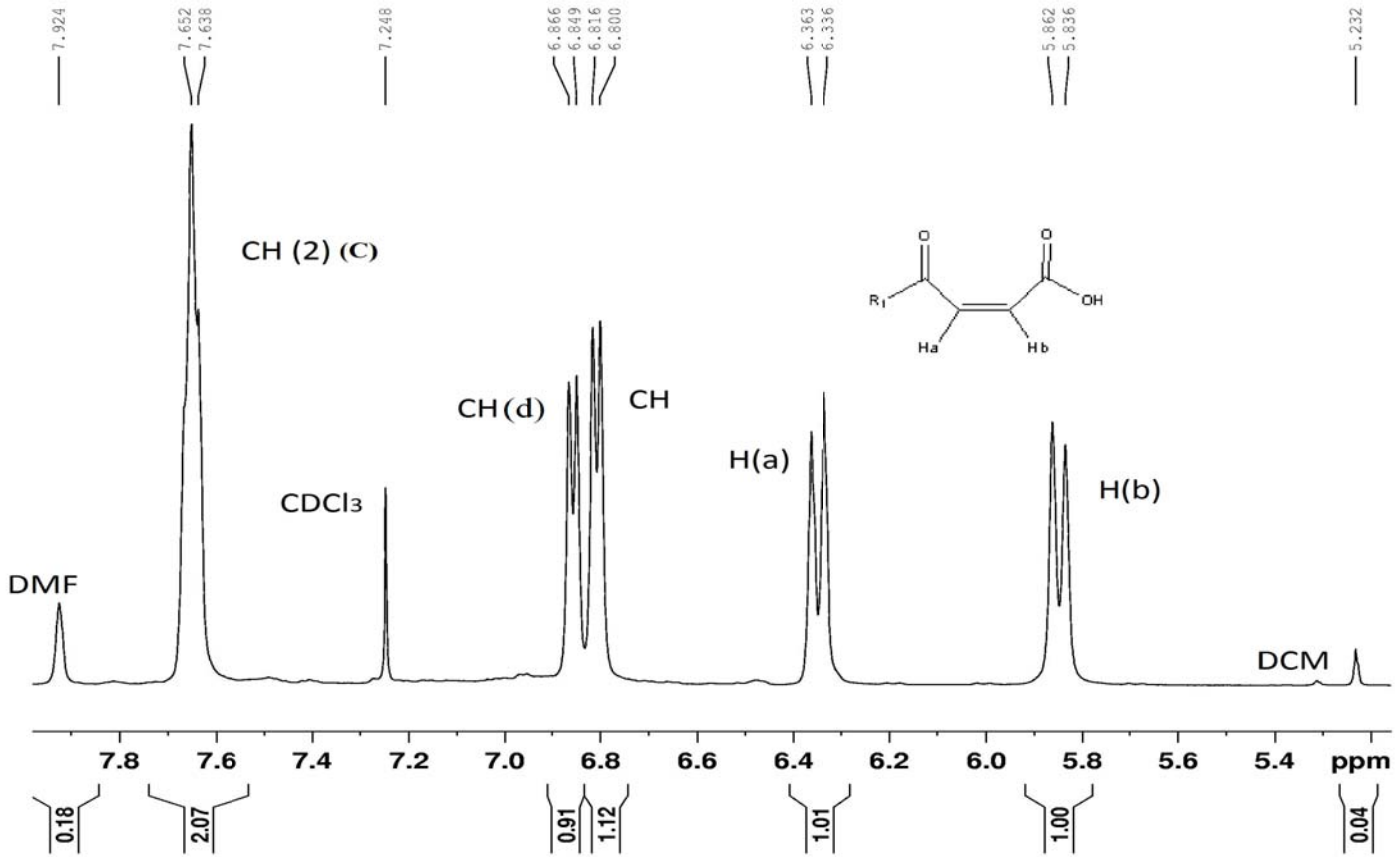

Figure A 2-2. ^{1}H NMR experiment of MABD(t-Bu)$_4$ in $CDCl_3$ solvent on 500 MHz

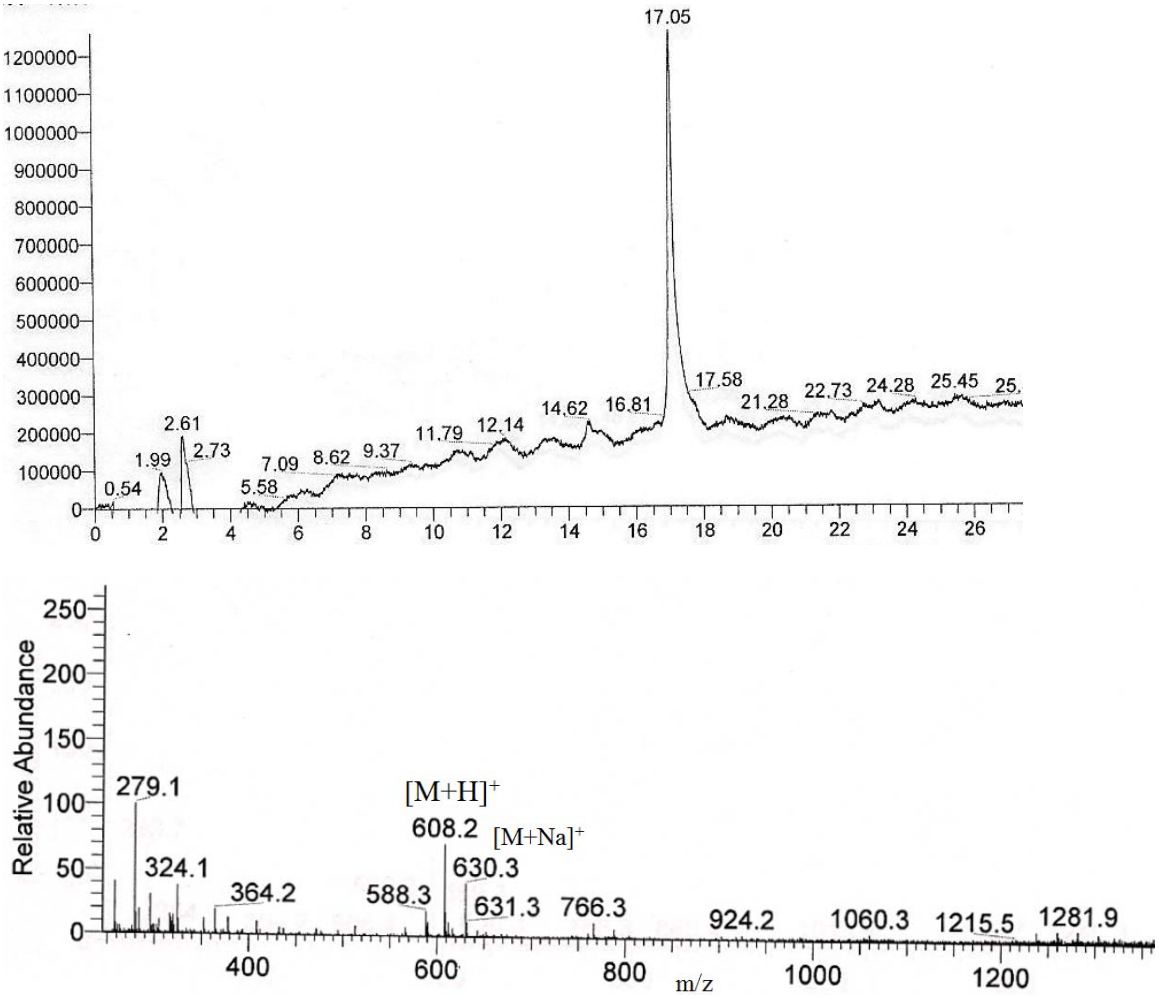

Figure A 2-3. The LC/MS on C-18 reversed phase column analysis of the MABD

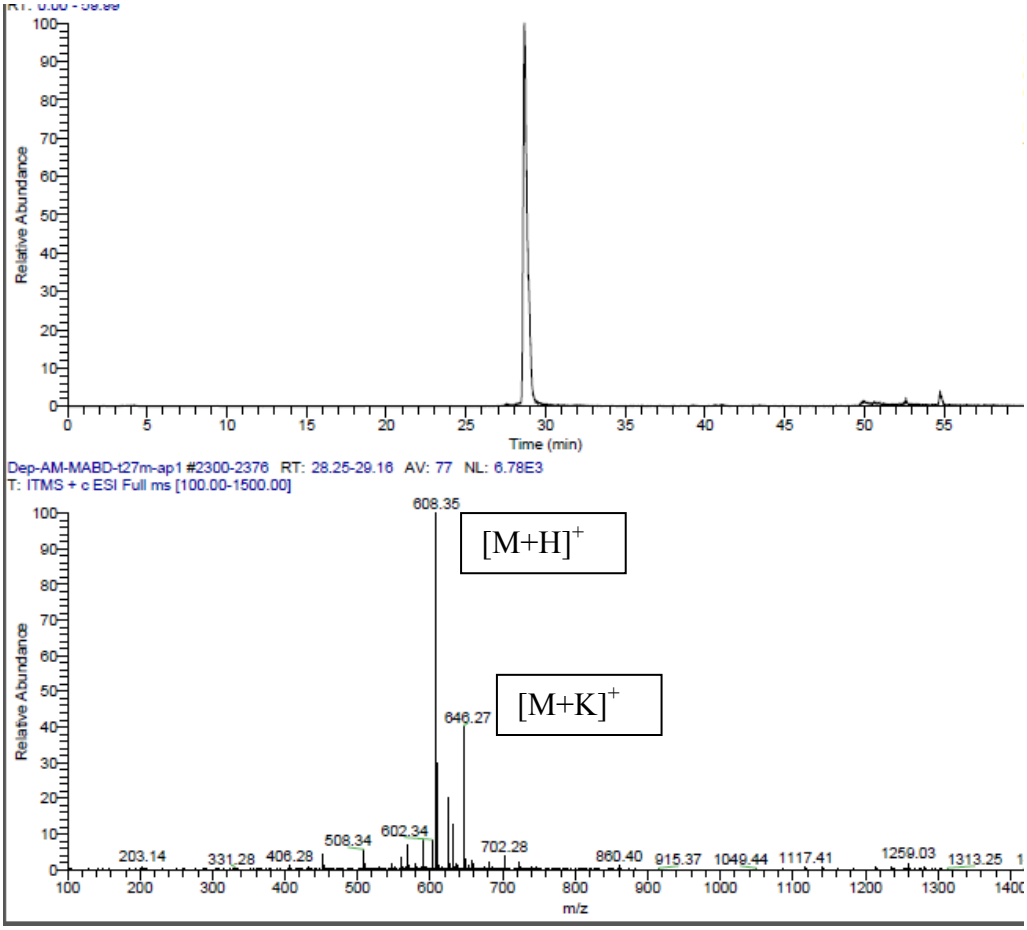

Figure A 2-4. The LC/MS on C-18 reversed phase column analysis of the AmMABD

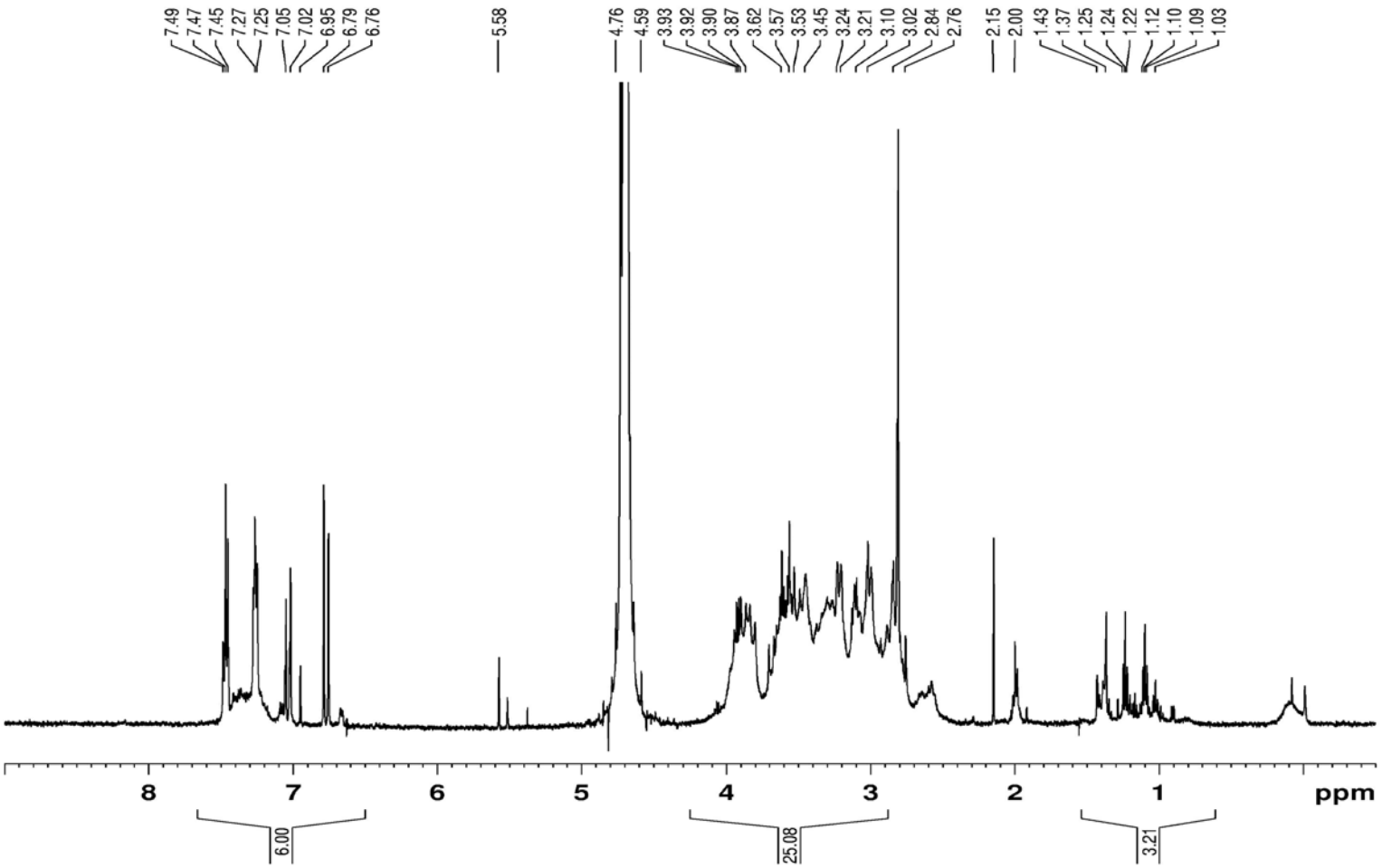

Figure A 2-5. ^{1}H NMR experiment of AmMABD(t-Bu)$_4$ in D_2O solvent on 500 MHz

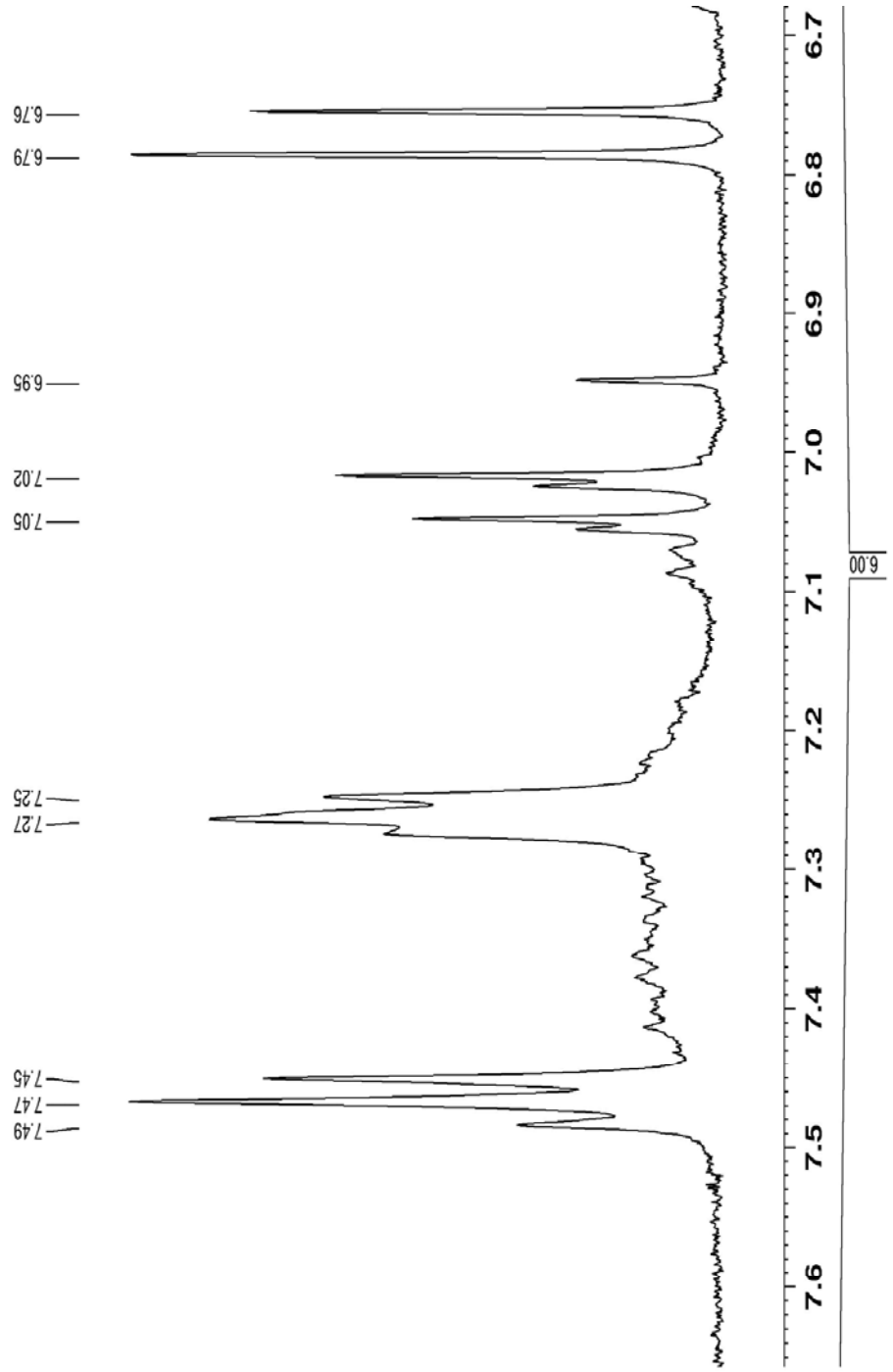

Figure A 2-6. ^{1}H NMR experiment of AmMABD in D_2O solvent on 500 MHz

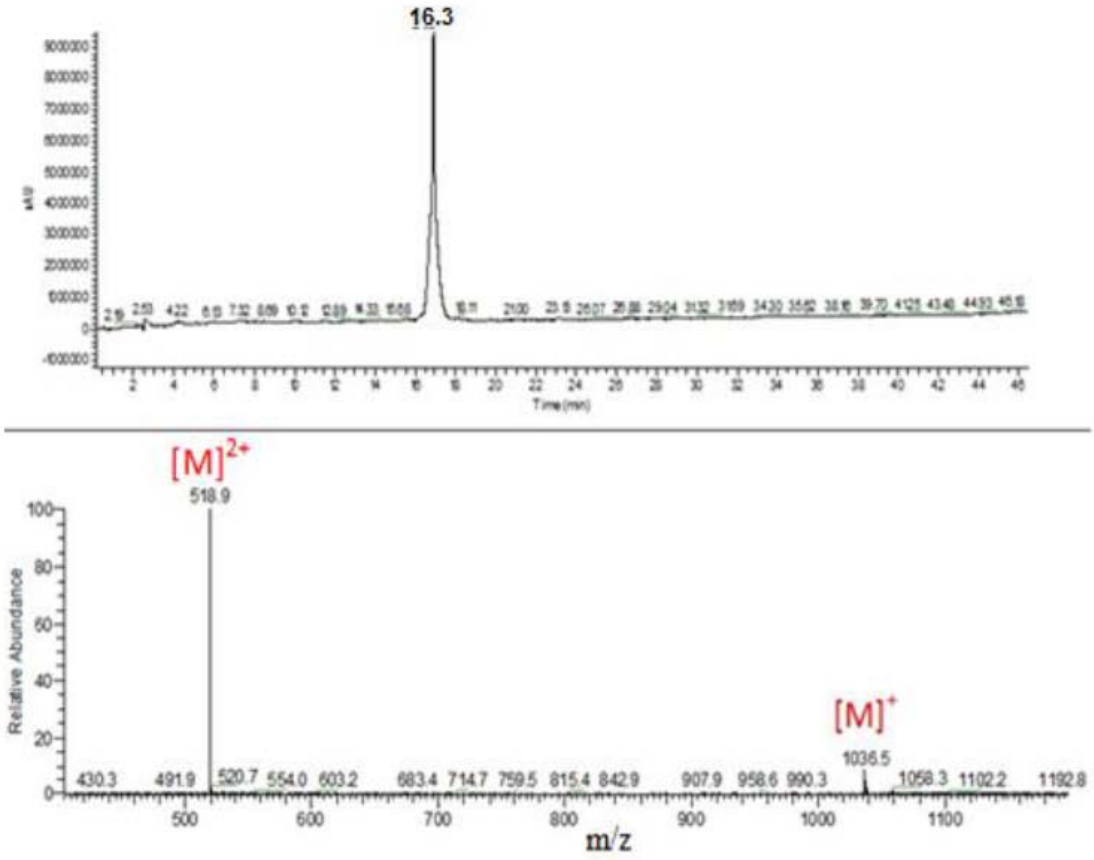

Figure A 2-7. C-18 reversed phase HPLC- ESI-MS analysis of the purified MABD-PEG-Biotin

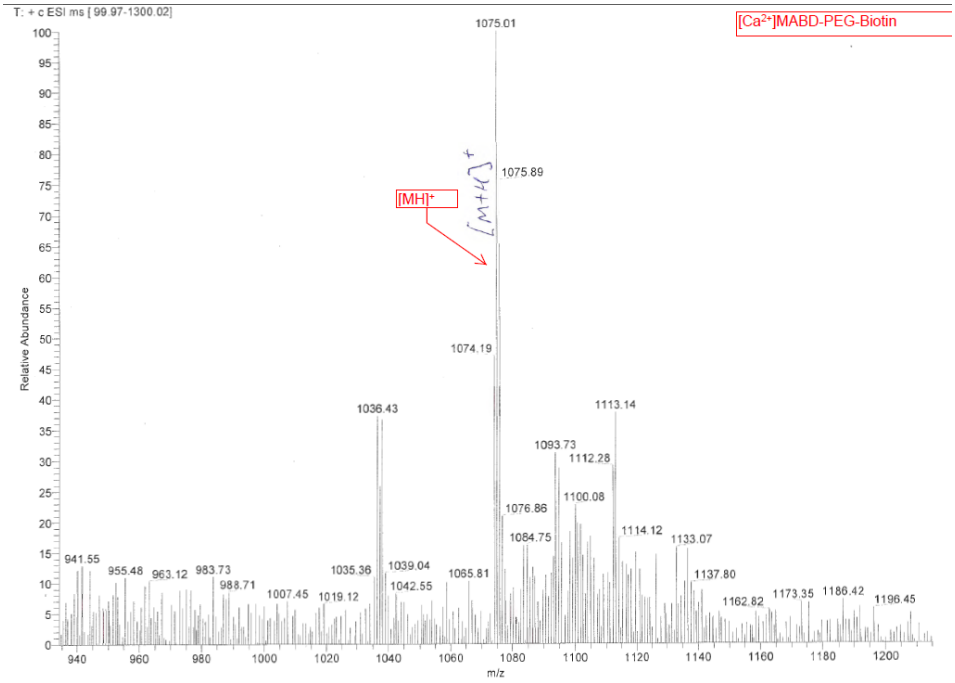

Figure A 2-8. ESI/MS Ca^{2+}MABD-PEG-Biotin

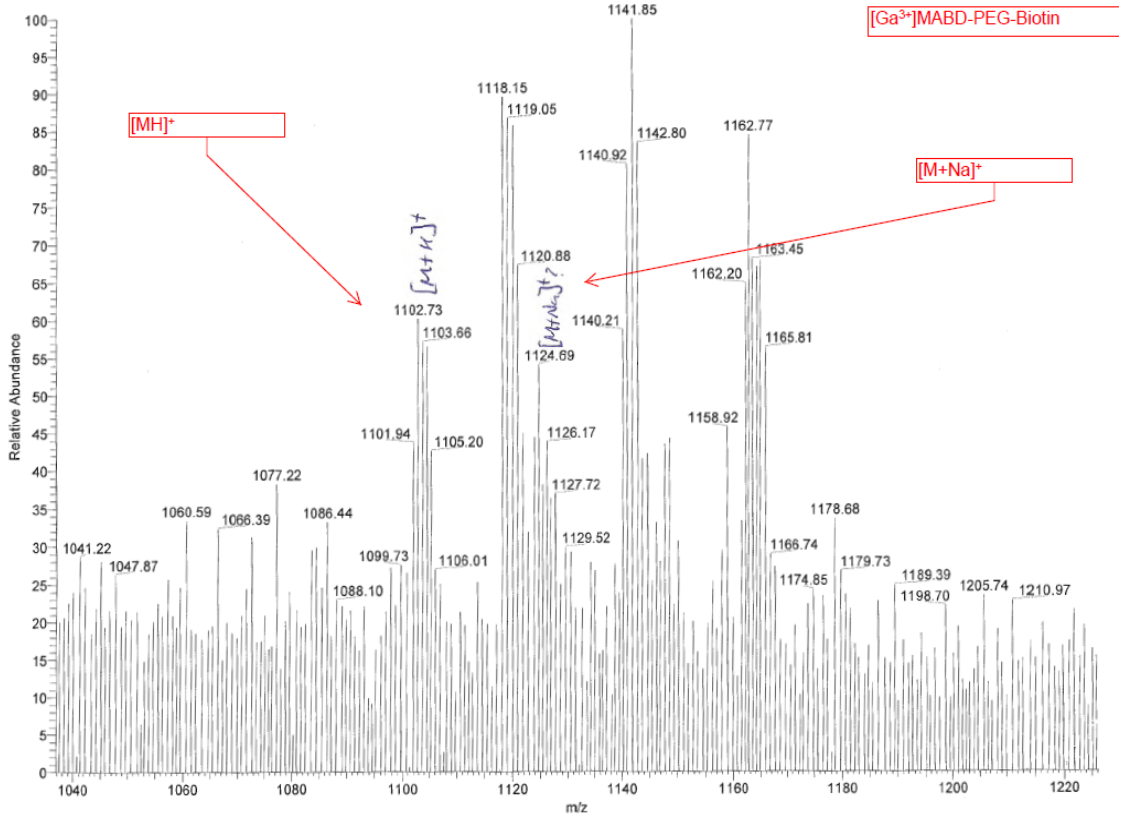

Figure A 2-9. ESI/MS Ga^{3+}MABD-PEG-Biotin

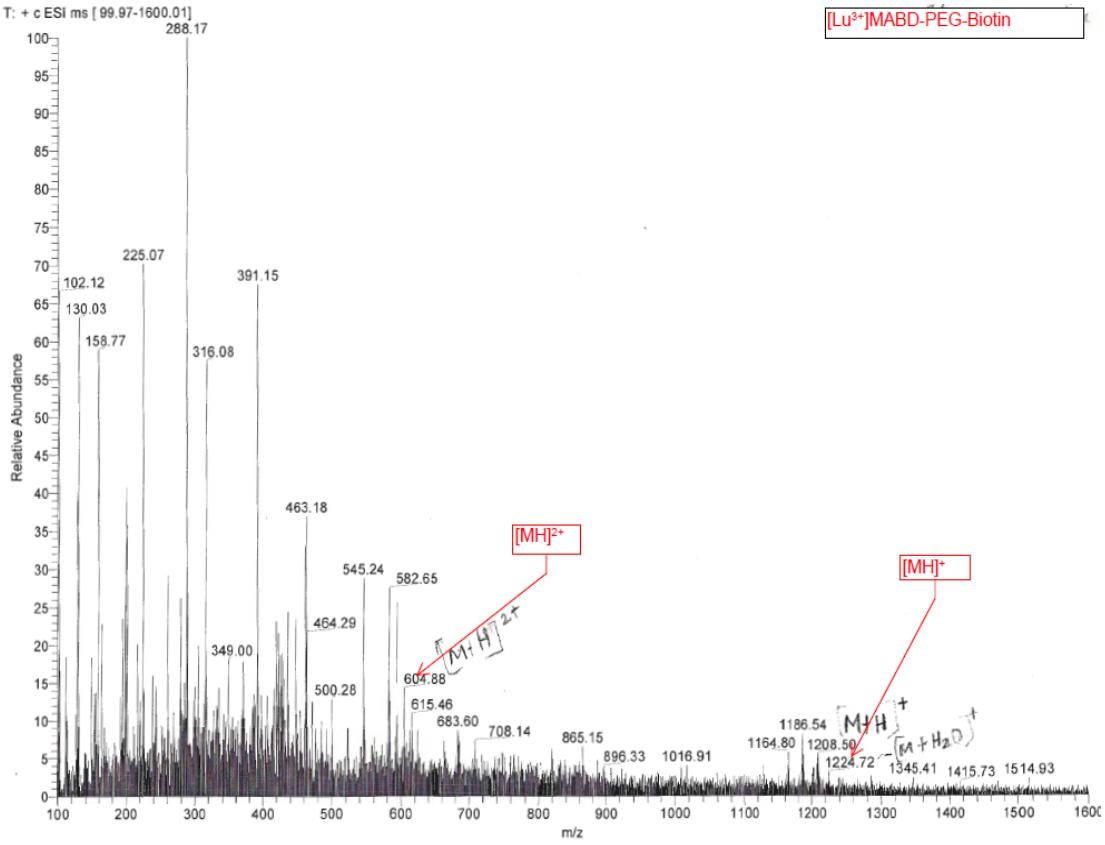

Figure A 2-10. ESI/MS Lu^{3+}MABD-PEG-Biotin

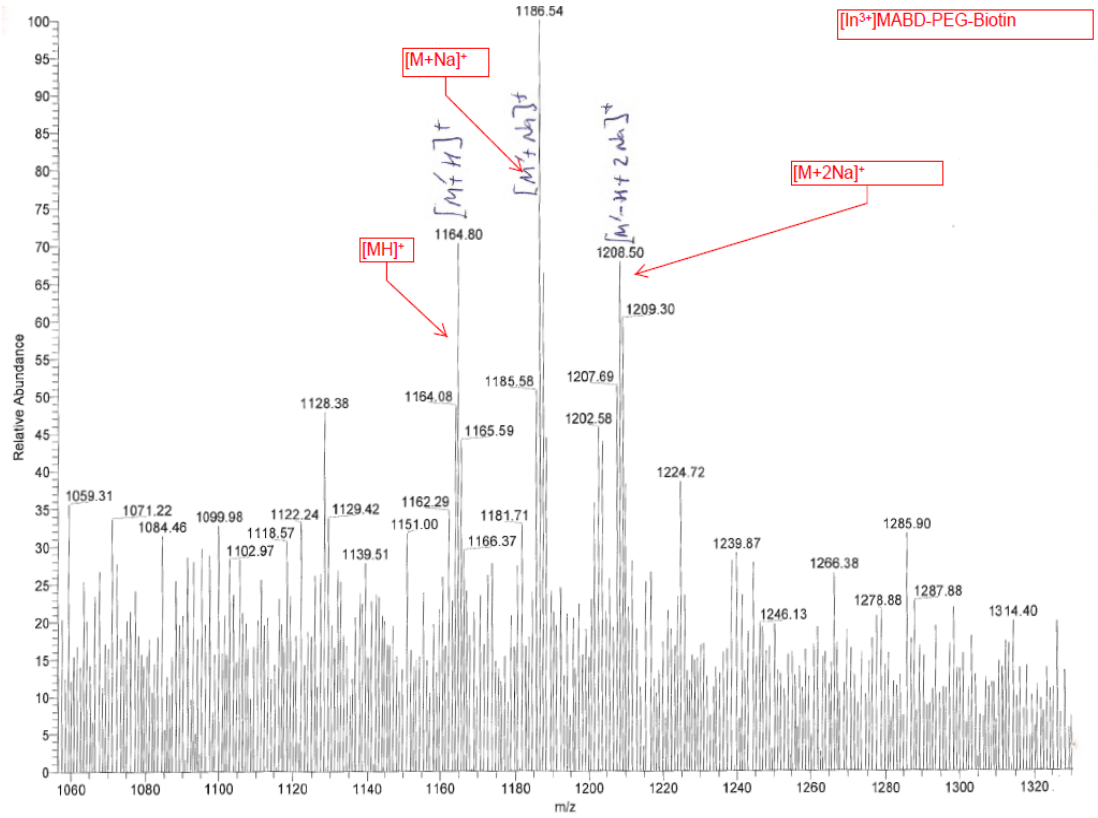

Figure A 2-11. ESI/MS In^{3+}MABD-PEG-Biotin

2.6 References

1. Orcutt, K.; Nasr, K.; Whitehead, D.; Frangioni, J.; Wittrup, K., Biodistribution and Clearance of Small Molecule Hapten Chelates for Pretargeted Radioimmunotherapy. *Molecular Imaging and Biology* 2011, *13* (2), 215-221.
2. DJ, H.; F, V.; M, R., Investigations of avidin and biotin for imaging applications. *J Nucl Med* 1987, *28* (8), 1294-302.
3. Goldenberg, D. M.; Sharkey, R. M.; Paganelli, G.; Barbet, J.; Chatal, J.-F., Antibody Pretargeting Advances Cancer Radioimmunodetection and Radioimmunotherapy. *J Clin Oncol* 2006, *24* (5), 823-834.
4. Lewis, M. R.; Wang, M.; Axworthy, D. B.; Theodore, L. J.; Mallet, R. W.; Fritzberg, A. R.; Welch, M. J.; Anderson, C. J., In Vivo Evaluation of Pretargeted 64Cu for Tumor Imaging and Therapy. *Journal of Nuclear Medicine* 2003, *44* (8), 1284-1292.
5. Wilbur, D. S.; Chyan, M.-K.; Pathare, P. M.; Hamlin, D. K.; Frownfelter, M. B.; Kegley, B. B., Biotin Reagents for Antibody Pretargeting. 4. Selection of Biotin Conjugates for in Vivo Application Based on Their Dissociation Rate from Avidin and Streptavidin. *Bioconjugate Chemistry* 2000, *11* (4), 569-583.
6. James, H.; Harrison, P.; Mather, S. J., Preparation and characterization of a DOTA-Lysine-biotin conjugate as an effector molecule for pretargeted radionuclide therapy. *Bioconjugate Chem.* 2005, *16*, 1468-1474.
7. Goodwin, D. A.; Meares, C. F.; McTigue, M.; Chaovapong, W.; Diamanti, C. I.; Ransone, C. H.; McCall, M. J., Pretargeted immunoscintigraphy: effect of hapten valency on murine tumor uptake. *J Nucl Med* 1992, *33* (11), 2006-13.
8. Reardan, D. T.; Meares, C. F.; Goodwin, D. A.; McTigue, M.; David, G. S.; Stone, M. R.; Leung, J. P.; Bartholomew, R. M.; Frincke, J. M., Antibodies against metal chelates. *Nature* 1985, *316* (6025), 265-268.
9. Corneillie, T. M.; Lee, K. C.; Whetstone, P. A.; Wong, J. P.; Meares, C. F., Irreversible Engineering of the Multielement-Binding Antibody 2D12.5 and Its Complementary Ligands. *Bioconjugate Chemistry* 2004, *15* (6), 1392-1402.
10. Corneillie, T. M.; Whetstone, P. A.; Lee, K. C.; Wong, J. P.; Meares, C. F., Converting Weak Binders into Infinite Binders. *Bioconjugate Chemistry* 2004, *15* (6), 1389-1391.
11. Chmura, A. J.; Orton, M. S.; Meares, C. F., Antibodies with infinite affinity. *Proceedings of the National Academy of Sciences of the United States of America* 2001, *98* (15), 8480-8484.
12. Butlin, N. G.; Meares, C. F., Antibodies with infinite affinity: origins and applications. *Acc Chem Res* 2006, *39* (10), 780-7.
13. Meyer, D. L.; Fineman, M.; Unger, B. W.; Frincke, J. M., Kinetics of the dissociation of indium-(para-substituted-benzyl)ethylenediaminetetraacetic acid hapten analogs from the monoclonal anti-hapten antibody CHA255. *Bioconjugate Chemistry* 1990, *1* (4), 278-284.
14. Chilkoti, A.; Stayton, P. S., Molecular Origins of the Slow Streptavidin-Biotin Dissociation Kinetics. *Journal of the American Chemical Society* 1995, *117* (43), 10622-10628.
15. Smith, G. P.; Petrenko, V. A., Phage Display. *Chem Rev* 1997, *97* (2), 391-410.

16. Smith, G. P.; Petrenko, V. A.; Matthews, L. J., Cross-linked filamentous phage as an affinity matrix. *Journal of Immunological Methods* 1998, *215* (1-2), 151-161.
17. Liu, S.; He, Z.; Hsieh, W.-Y.; Fanwick, P. E., Synthesis, Characterization, and X-ray Crystal Structure of In(DOTA-AA) (AA = p-Aminoanilide): A Model for ^{111}In-Labeled DOTA-Biomolecule Conjugates. *Inorganic Chemistry* 2003, *42* (26), 8831-8837.
18. Wadas, T. J.; Wong, E. H.; Weisman, G. R.; Anderson, C. J., Coordinating Radiometals of Copper, Gallium, Indium, Yttrium, and Zirconium for PET and SPECT Imaging of Disease. *Chemical Reviews* 2010, *110* (5), 2858-2902.
19. Reichert, D. E.; Lewis, J. S.; Anderson, C. J., Metal complexes as diagnostic tools. *Coordination Chemistry Reviews* 1999, *184* (1), 3-66.
20. Cutler, C. S.; Smith, C. J.; Ehrhardt, G. J.; Tyler, T. T.; Jurisson, S. S.; Deutsch, E., Current and potential therapeutic uses of lanthanide radioisotopes. *Cancer Biother Radiopharm* 2000, *15* (6), 531-45.
21. Moi, M. K.; DeNardo, S. J.; Meares, C. F., Stable Bifunctional Chelates of Metals Used in Radiotherapy. *Cancer Research* 1990, *50* (3 Supplement), 789s-793s.
22. Suzuki, K.; Satake, M.; Suwada, J.; Oshikiri, S.; Ashino, H.; Dozono, H.; Hino, A.; Kasahara, H.; Minamizawa, T., Synthesis and evaluation of a novel 68Ga-chelate-conjugated bisphosphonate as a bone-seeking agent for PET imaging. *Nuclear Medicine and Biology* 2011, *38* (7), 1011-1018.
23. Reagents for labeling and ligation. In *Peptide Synthesis* [Online] Novabiochem: EMD Millipore, 2012; p. 43. (accessed 12/12/2013).
24. Thomas, W. D.; Smith, G. P., The case for trypsin release of affinity-selected phages. *BioTechniques* 2010, *48* (3), 651-654.
25. Smith, G. P. http://www.biosci.missouri.edu/smithgp/PhageDisplayWebsite/PhageDisplayWebsiteIndex.html (accessed 06/01/2010).
26. Petrenko, V. A.; Smith, G. P.; Gong, X.; Quinn, T., A library of organic landscapes on filamentous phage. *Protein Engineering* 1996, *9* (9), 797-801.
27. Chmura, A. J.; Schmidt, B. D.; Corson, D. T.; Traviglia, S. L.; Meares, C. F., Electrophilic chelating agents for irreversible binding of metal chelates to engineered antibodies. *Journal of Controlled Release* 2002, *78* (1–3), 249-258.
28. Li, W. P.; Ma, D. S.; Higginbotham, C.; Hoffman, T.; Ketring, A. R.; Cutler, C. S.; Jurisson, S. S., Development of an in vitro model for assessing the in vivo stability of lanthanide chelates. *Nuclear Medicine and Biology* 2001, *28* (2), 145-154.
29. Couto, R. M.; De Barboza, M. F.; De Souza, A. A.; Muramoto, E.; Mengatti, J.; De Araujo, E. B., In vivo comparative study of hydroxyapatite labeled with different radioisotopes: evaluation of the scintigraphic images. *Cellular and molecular biology* 2010, *56* (2), 6-11.
30. Schwöbel, J. A. H.; Wondrousch, D.; Koleva, Y. K.; Madden, J. C.; Cronin, M. T. D.; Schüürmann, G., Prediction of Michael-Type Acceptor Reactivity toward Glutathione. *Chemical Research in Toxicology* 2010, *23* (10), 1576-1585.
31. Ferreira, C. L.; Lamsa, E.; Woods, M.; Duan, Y.; Fernando, P.; Bensimon, C.; Kordos, M.; Guenther, K.; Jurek, P.; Kiefer, G. E., Evaluation of Bifunctional

Chelates for the Development of Gallium-Based Radiopharmaceuticals. *Bioconjugate Chemistry* 2010, *21* (3), 531-536.
32. Hiller, Y.; Gershoni, J. M.; Bayer, E. A.; Wilchek, M., Biotin binding to avidin. Oligosaccharide side chain not required for ligand association. *Biochemical Journal* 1987, *248* (1), 167-171.

Chapter 3

Separation and purification of no carrier added ^{161}Tb, ^{166}Ho, and ^{177}Lu by column chromatography

Introduction

The radiolanthanides have extensively been evaluated in nuclear medicine for potential targeted radiotherapy. The radiolanthanides are useful in treating rheumatoid arthritis, which is mainly localized in the synovium.[1] The aim of radiation synovectomy is to reduce pain, improve mobility, and preserve joint function.[1] Hydroxyapatite (HA) $[Ca_{10}(PO_4)_6(OH)_2]$ is a major chemical constituent of skeletal bone matrix. The similar chemical properties between the lanthanides and Ca^{2+} ions prompted the development of radiopharmaceuticals that use radiolabeled HA as a vector to deliver the radiation dose to the target. Radiolanthanides (^{177}Lu and ^{153}Sm) are frequently used to label HA particulates for synovectomy radiation. The radioisotopes that are utilized for therapy are also incorporated in bifunctional chelating systems to target biological receptor sites. Radiolanthanides are frequently used in receptor-based radiopharmaceuticals that require high specific activity or no-carrier added (nca) radiolanthanides. Specific activity (SA) is calculated as the activity of the radioisotope per given mass (Ci/mg). To maximize the specific activity, the amount of the non-radioactive mass has to be reduced or eliminated to obtain a no-carrier-added radioisotope. Most of the reactor produced radiolanthanides have low specific activity since the irradiated targets are of the same element as the produced radionuclide. **Table 3-1** illustrates the nuclear properties of ^{161}Tb, ^{166}Ho, and

^{177}Lu and the specific activities, both theoretical and currently achievable. An example for calculating the theoretical specific activity of ^{177}Lu is indicated in **Equation 3-1.**

Radio-nuclide	Target Radio-nuclide	Decay mode	$T_{1/2}$ (h)	Emax β-, MeV	γ energy, keV (% abundance)	Theoretical Specific Activity (Ci/mg)	Achievable Specific Activity (Ci/mg)	Mean* tissue range (cm)
^{177}Lu	^{176}Yb	β^-, γ	161	0.5	208 (11)	110	25‡	0.24
^{166}Ho	^{164}Dy	β^-, γ	26.8	1.86	80.6 (6.2)	704	2.2‡	1.39
^{161}Tb	^{160}Gd	β^-, γ	165.8	0.59	48.9 (17) 74.6 (10)	117	105†	0.2

Table 3-1. The nuclear properties and decay characteristics of the radiolanthanides. The achievable specific activities for ^{177}Lu and ^{166}Ho are obtained after the direct production of each of the radionuclides, while the ^{161}Tb SA is achieved using the indirect nuclear reaction. The symbols *, ‡ and † denote referenced values[2-4].

$$\begin{aligned}
Specific\ \text{activity}_{^{177}Lu} &= \frac{\text{disintigrations (s)}^{-1}}{\text{unit mass}} \\
&= \frac{\text{A (Ci)}}{\textit{unit mass}\ \text{(mg)}} \qquad \text{A} = \text{N(number of atoms)} * \lambda((\ln(2)/\text{half - life}) \\
&= \frac{\ln(2) * 6.022 \times 10^{23}\ \text{atoms/mole}}{((\text{atomic mass (g/mole)}) * (\text{half - life (sec)} * (3.7 \times 10^{10}(\text{atoms disint.(s)}^{-1} / Ci)) * (1g / 1000mg / 1\,g)} \\
&= \frac{ln(2) * 6.022 \times 10^{23}}{((176.94\,g/mole) * (159.36\ h)(3600\,sec/h) * (3.7 \times 10^{10}\text{dps/Ci}) * (1000\,\text{mg}/1\ \text{g})} \\
&= 111\ \text{Ci/mg}
\end{aligned}$$

Equation 3-1. Calculation of the theoretical specific activity

Production of ^{177}Lu. Lutetium-177 is the most widely investigated radiolanthanide for potential radiotherapy applications, especially in receptor mediated peptides such as octreotate (analogue of somatostatin (SSTR(2)). In addition, a radioconjuate linked to Bombesin, a GRP (gastrin releasing peptides)receptor targeting peptide, is used for treatment of a variety of human cancer cell lines including prostate.[5-6] Although, there are numerous publications that indicate the superiority of ^{177}Lu labeled over ^{90}Y

bioconjugates (^{90}Y is a radioisotope approved by the Food and Drugs Administration (FDA))[7] due to its favorable nuclear properties for therapeutic treatment (lower mean energy of the β^- particles and therefore shorter range, which is preferred for therapy of small tumors). However, ^{177}Lu has not been approved for radiopharmaceutical applications in the US, although ^{177}Lu-DOTA-TATE has been approved in some parts of the world (Warsaw, Poland)[8] for radiotherapeutic treatment of patients with disseminated neuroendocrine tumors.

The nuclear reaction that has been frequently used to obtain ^{177}Lu is the direct irradiation of an enriched ^{176}Lu target. Because of the rather large cross section of ^{176}Lu (σ = 2,300 barns), ^{177}Lu can be produced directly with relatively high specific activity at nuclear reactors via the (n,γ) production route. However, during irradiation of the ^{176}Lu target, the long-lived isomer ^{177m}Lu ($T_{1/2}$ = 160.1 d) is also produced

$$^{176}\text{Lu}\ (n,\gamma)^{177}\text{Lu}$$

$$^{176}\text{Lu}\ (n,\gamma)^{177m}\text{Lu}$$

An alternative production route that involves neutron irradiation of an enriched ^{176}Yb target results in an indirect production of no-carrier ^{177}Lu (**Table A 3-1**). This approach, however, requires chemical separation of the^{177}Lu from the Yb target (**Figure 3-1**).

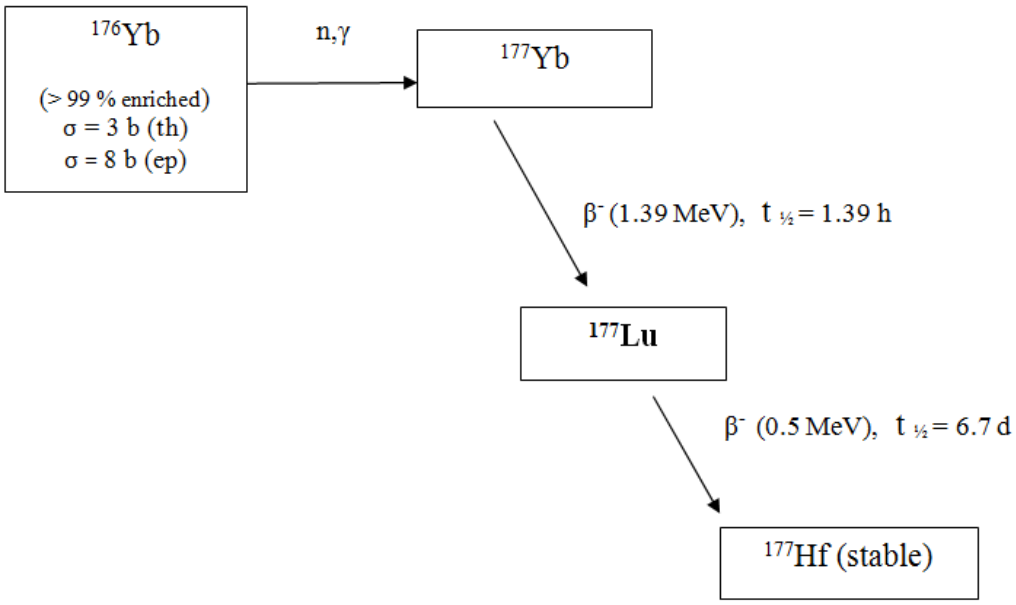

Figure 3-1. Indirect production ^{177}Lu from neutron capture of enriched ^{176}Yb.

Production of ^{166}Ho from an enriched Dy target. ^{166}Ho-DTPA has been proposed as a potential liquid source for filling balloons for endovascular brachytherapy by Hong et al.[9] This report indicated ethylenedicysteine compounds were filled with ^{166}Ho-DTPA solutions and used as an alternative therapeutic agent to that of ^{188}Re labeled therapeutic agents for artherosclerotic coronary artery.

The no-carried-added ^{166}Ho production route involves a double netron capture on an enriched^{164}Dy target to produce the intermediate ^{166}Dy, which then β^- decays to ^{166}Ho. The isolation of ^{166}Ho, as shown in **Figure 3-2**, requires multistep separation to avoid accumulation of ^{165}Ho (stable) from the decay of ^{165}Dy. The enriched ^{164}Dy has a high cross section that proceeds through a single neutron capture to produce ^{165}Dy.[10] The objective of the first separation is to isolate the Dy fraction from the Ho. This is because the accumulation of the ^{165}Ho from the β^- decay of ^{165}Dy results in a neutron capture on

^{165}Ho to produce the long-lived ^{166m}Ho impurity ($t_{1/2}$ = 1,200 y). The calculated decay time to allow the growth of ^{166}Dy is 48 h before performing the separation of ^{166}Dy from ^{166}Ho.

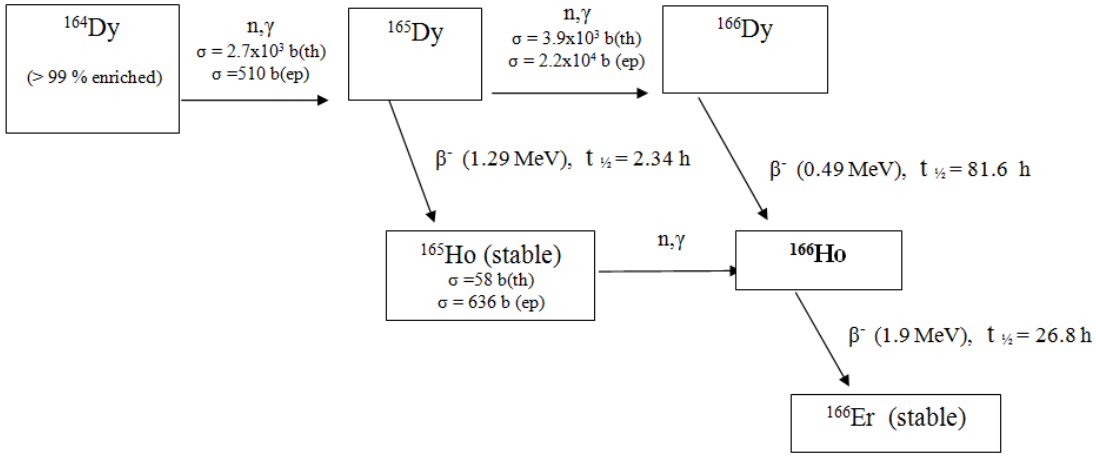

Figure 3-2. ^{166}Ho production scheme

Production of ^{161}Tb. The nuclear properties of ^{161}Tb are similar to those of ^{177}Lu, especially its half-life (6.90 d) and relatively low mean β^- energy. The production of ^{161}Tb involves neutron irradiation of an enriched ^{160}Gd target as shown in **Figure 3-3**. This nuclear reaction yields the ^{161}Gd intermediate, which β^- decays to ^{161}Tb. Because of the low cross section (1.5 b) of the target ^{160}Gd, it requires high quantities of enriched ^{161}Gd target to obtain sufficiently high activity of ^{161}Tb.[4]

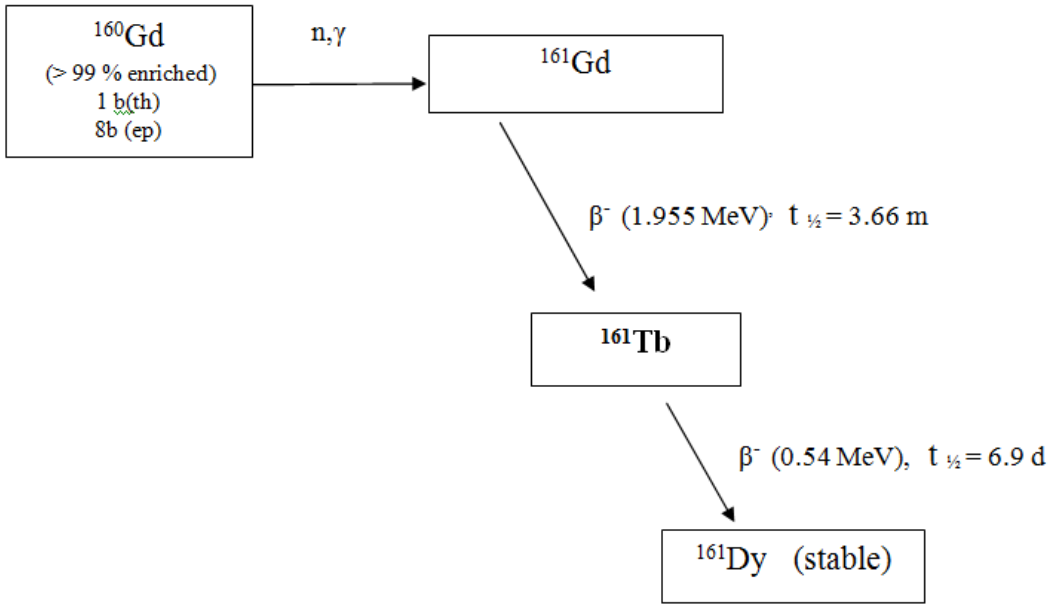

Figure 3-3. ^{161}Tb production scheme

Chemistry of the Lanthanides: The common features in the lanthanide series include (1) Ln ions are stable in their +3 oxidation state (especially, in aqueous media), (2) they form labile ionic complexes, (3) insoluble hydroxides precipitate at neutral pH unless complexing agents are present, and (4) a decrease in radii of the lanthanide ions across the series from La to Lu. The last characteristic is the result of the slight spatial extension of the 4f valence orbitals by the addition of valence electrons that cannot effectively shield the increasing nuclear charge as the atomic number increases across the series. This phenomenon causes shrinkage in the atomic and ionic radius, which is commonly referred as the lanthanide contraction.[11] The Ln^{3+} metal ligand coordination depends on the electronegativity of the coordinating atom with the order of affinity for the Ln^{3+} ions O>N>S. Lanthanide ions have large ionic radii, and are typically hard Lewis acids. Because of ligand bonding with the lanthanide metal ions is electrostatic in nature, the

coordination geometries of lanthanide ions are governed by the steric requirements for the ligand, minimizing ligand-ligand and metal ligand repulsions.[11-12]

Separation of Lanthanides. The general separation scheme to produce high specific activity lanthanides is divided into three types: 1) chemical separations, 2) ion-exchange methods, and 3) extraction column chromatography.1) Chemical separations rely on using the difference in oxidation states between the separating lanthanides ions. For instance, Sm^{2+}, Eu^{2+}, or Yb^{2+} ions are obtained by reducing the +3 oxidation state of the metal ions and can subsequently be isolated from the reaction mixture in the solid state by adding precipitating agents. This multistep separation process is further elaborated in the next chapter. (2) Due to the similarities of the the ionic radii of the individual Ln^{3+} ions, there are not significant differences in their affinities for polystyrene-based cation exchangers. Researchers, therefore, have linked the unsuccessful ion exchange separation process of lanthanide elements using mineral acids (HCl, HBr, HNO_3 and H_2SO_4) to the close chemical properties that exist in the lanthanide series[13-14]. However, Ln^{3+} complexing agents, which are used as eluents, complex quickly with the rare earth elements with different stability constants for the various lanthanide ions.[15] The complexing agents respond to the acidity and ionic strength of the solution and to the presence of metal ions. The strong binding complexing agents such as EDTA and DTPA are effective in chelating lanthanide ions. EDTA is readily available, inexpensive, and easy to regenerate. However, due to EDTA's low solubility, elutions cannot be conducted in acidic environments (**pH <3**).[16]

Various complexing agents and ion exchange chromatography media have been evaluated to separate the lanthanides.[17] Chopin et al investigated the separation factors of

the radiolanthanides using ion exchange chromatography and complexing agents such as glycolic acid, lactic acid, and alpha-hydroxyisobutyric acid (α HIBA). These complexing agents have high affinities for the Ln^{3+} ions (loaded on a cation exchange column), and an increase in the formation constant from left to right across the lanthanide series (complexes most strongly with the smallest Lu^{3+}) provides a convenient method for the chromatographic separation of these ions. Based on these reports, the Ln^{3+} ions were effectively separated with the highest separation factor using α-HIBA. (3) Another separation method takes advantage of the affinity of the Ln^{3+} for phosphonate groups, namely extraction column chromatography (ECC) with organophosphonic acid groups adsorbed onto acrylic ester resins, which are commercially produced and sold by Eichrom LLC as Ln resins. The work reported by Horwitz et al. discussed the separation of $^{177}Lu^{3+}$ from Yb^{3+} using Ln resin.[18-19] Currently, there are a series of Ln resins commercially available with differences in their chemical structures **(Figure 3-4).** A report by Mirzadeh et al. showed the separation of ^{177}Lu from the Yb target using the Ln resin. The separation conditions involved high concentrations of the hydrochloride acid to separately elute the two elements. Since the HDEHP, compared to the HEHEHP (Ln2) is quiet a strong acid that it needed large amount of the eluting solvent to protonate the phosphonate active groups on the resin. The elution profile from the Yb/Lu separation using the Ln resin is referenced in **Figure A 3-8**.[20]In this study the Ln2 resin was prefered to the Ln resin because of its weaker acid that requires less concentrated acidic eluents to push the retained the analytes of the column. Accordingly, the separation of the radiolanthides, $^{177}Lu^{3+}$, $^{166}Ho^{3+}$, and $^{161}Tb^{3+}$ is called the Ln2 resin.

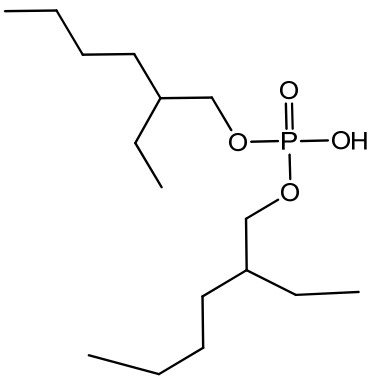

HDEHP

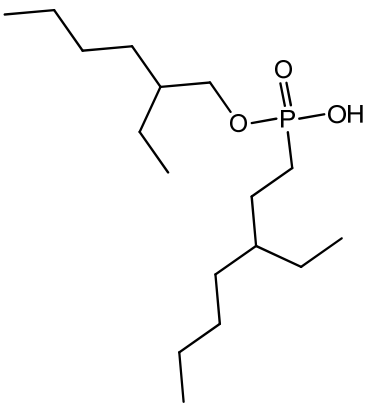

HEH EHP

Figure 3-4. The organophosphorous groups adsorbed on the resin Ln (bis(2-ethylhexyl) hydrogen phosphate (HDEHP)) and Ln2 (2-ethylhexyl hydrogen (3-ethylheptyl)phosphonate (HEH (EHP)) resins.

Various reports have utilized one of the separation methods (ion exchange chromatography or extraction chromatography media) to achieve high SA radiolanthanides (^{177}Lu, ^{166}Ho, and ^{161}Tb). Knapp et al. investigated two types of chromatography media in an attempt to separate ^{166}Ho from Dy targets.[21] The first method was separation by paper electrophoresis using α-HIBA as the complexing agent and a cation exchange resin as the stationary phase. The second separation method evaluated was extraction chromatography, using glass powders that were pre-impregnated with di-(2-ethylhexyl) phosphoric acid (HDEHP). This separation, also referred as partition chromatography, and which is similar to extraction column chromatography, took advantage of the different formation constants of the Ln^{3+} and the ligands (phosphonates) to elute Dy^{3+} first and Ho^{3+} second. The loaded sample (^{166}Dy/^{166}Ho) was eluted using HNO_3 solution. Unlike the cation exchange resins, the stationary phases are usually custom prepared using glass powders or silica impregnated with HDEHP or

tributylphosphate (TPB). In their report a better elution profile with slight shoulder broadening was attained with TPB as the stationary phase and elution with a high concentration of HNO_3 (13 M). The second best elution profile was obtained using HDEHP as the stationary phase and eluting with 1.6 M HNO_3. The authors acknowledged the disadvantage of using high acid concentrations and recommended HPLC assisted column chromatography.

Ramaswami et al. alludes to the process of separation of radioactive $^{157/158}Ho/^{157}Dy$ products obtained by irradiating enriched Eu isotopes.[22] This report established that complexation between HDEHP and the Ln^{3+} increases with decreasing ionic radii of Ln^{3+}.

The objective of the current study was to evaluate the performance of extraction column chromatography media that uses the organophosphoric acid active groups adsorbed on a resin in separating ^{177}Lu, ^{166}Ho, and ^{161}Tb from their corresponding enriched targets. A comparison between previously reported separation techniques and the current study is made to determine the efficiency and reproducibility of extraction column chromatography.

3.2 Experimental

3.2.1 Chemical and reagents. Ytterbium oxide (99.998 % purity), gadolinium oxide (99.99%), and holmium oxide (99.99%) were purchased from Alpha Aesar (Ward Hill, MA). Optima grade quality hydrochloric and nitric acid were purchased from Fisher Scientific (Fairton, New Jersey). Deionized water using a Milli-Q system was18 Ω cm^{-1}.

Radiochemical preparations. A high purity germanium (HPGe) semi-conductor γ-detector was utilized for counting the radioactive samples and fractions. The gamma peak with the highest decay abundance was used to follow the separations for each radionucldie. Yb/Lu (γ-energy intensity for ^{177}Lu and ^{175}Yb is 208 keV and 396 keV, respectively); Dy/Ho (γ-energy intensity for ^{166}Dy and ^{166}Ho is 82.4 keV and 80.5 keV); and Gd/Tb (γ-energy intensity for ^{159}Dy and ^{161}Tb is 75 keV and 365 keV). The γ- decay counts were computed and reported as activity (Genie software 2000).

A typical isotopically enriched target (^{160}Gd, ^{164}Dy, and ^{176}Yb) for irradiation contained 1-2 mg of Gd_2O_3, Tb_2O_3, or Yb_2O_3 (**Figure A 3-1**). The targets were initially converted to the $LnNO_3$ form by dissolving Ln_2O_3 in dilute nitric acid (0.3 M), followed by evaporation to dryness in quartz vials. The quartz vials containing the enriched targets [(^{160}Gd, ^{164}Dy, or ^{176}Yb) NO_3] were irradiated at the University of Missouri Research Reactor Center (MURR). In general two target irradiation positions were used (thermal neutron flux trap and reflector). The thermal neutron flux trap was 3 x 10^{14} neutrons /cm^{2}s and the irradiation time for this position is normally 155 h. The flux in the reflector position was in the range of 1 x 10^{13} to 1 x 14 neutrons /cm^2/sec and the irradiation time last only for 3-4 days. Following irradiation, the samples were dissolved in 500 µL of 0.05 M HCl and mixed with 30-50 mg of their corresponding non-radioactive $LnNO_3$ (Ln = Gd^{3+}, Dy^{3+}, or Lu^{3+}).

3.2.2 Preparation of chromatography columns. The extraction column chromatography Ln2 resin with the (2-ethyl-1-hexyl) phosphonic acid mono (2-ethyl-1-hexyl) ester (HEH[EHP]) reactive group adsorbed on an acrylic ester polymer support (45 µm mesh

size) was acquired from Eichrom Technologies LLC (Lisle, IL). The mobile phases were prepared by diluting optima grade nitric acid.

A water jacketed glass column (to maintain temperature) with internal threaded ends for a screw-cap fittings (dimension 11 ID x 300 mm, 29 mL capacity volume) from Sigma-Aldrich (St. Louis, MO; ACE glass manufacturer) was packed with a slurry of Ln2 (0.1 M HNO_3 is used to make the slurry) resin to a bed volume of 20 mL. The slurry of the Ln2 resin was degassed prior to packing the column to remove air bubbles. The resin slurry was gently added to the column to the desired 20 mL bed volume with the top of the resin covered with a polyethylene frit. After allowing the resin to settle by gravity, the top end of the column was capped and external pressure using nitrogen gas was applied to pack the loose particles with 0.05 M HNO_3. The mobile phases were filtered using 0.45 μm Millipore filters and degassed at room temperature. For trials that have the heat exchange column conditioned at 50 °C, however, the mobile phases were degassed at 50 °C.

The column was equilibrated with 0.1 M HNO_3 (3 bed volumes, 60 mL). The sample ($^{175}Yb/^{177}Lu$) was loaded onto the column in ~ 10 mL. The first elution was made using 1.5 M of HNO_3 in 200 mL followed by 30 mL of 4 M HNO_3, which removed the remaining ^{177}Lu that was retained on the column. The flow rates were evaluated at 2, 3, 4, and 5 mL/min.

3.2.3 Separation of ^{177}Lu from Yb targets. The sample preparation for the separation of the bulk amount of Yb from Lu involves dissolving a weighed amount of Yb_2O_3 (35-45 mg, 0.09 -0.1 mmole) to obtain the $Yb(NO_3)_3$. The use of Yb_2O_3 as a source of Yb is

required to accurately determine the mass of Yb, as hydrated $YbCl_3$ or NO_3^- are hygroscopic and that adds mass that would be difficult to quantify. These samples were then spiked with 500 µL of $^{175}Yb/^{177}Lu$ (~1 mCi) and ~ 9 mL of milli Q water were added to make the final volume 10 mL. The sample was loaded onto an equilibrated Ln2 column using a 20 mL syringe.

3.2.4 Separation of ^{166}Ho from Dy targets. The irradiated sample was dissolved in 5 mL of 0.05 M HNO_3 and loaded on to a column containing the Ln2 resin (11 X 200 mm). The first 100 mL fraction eluted with 0.5 M HNO_3 (fraction 1-10) contained 3.95 % of the ^{166}Dy. The next 60 mL of collected fractions (fractions 11-17) contained the remaining 94 % of the ^{166}Dy. The ^{166}Ho started to elute in fraction 21, and fractions 20-23 containing only ^{166}Ho (free of ^{166}Dy) were eluted with 30 mL of 3 M HNO_3, which contained 97 % of the total ^{166}Ho in the sample.

3.2.5 Separation of ^{161}Tb from Gd targets. The ^{161}Tb was obtained after irradiation of the enriched ^{160}Gd that has small amounts of ^{158}Gd contaminant, which undergo a neutron capture to produce ^{159}Gd. The high abundance gamma rays of ^{159}Gd (363.6 keV) and ^{161}Tb (74.6 keV) were used to track the Gd and Tb fractions, respectively. Non-radioactive Gd_2O_3 (46 mg, 0.867 of ^{nat}Gd) was dissolved in 500 µL of 3 M HNO_3 and H_2O_2 (30 %). This sample was diluted in 10 mL of Milli Q water and spiked with $^{159/161}Gd/^{161}Tb$ activity. The Ln2 column was equilibrated with 0.05 M HNO_3 and the sample was loaded. The selective elution of Gd followed by Tb was conducted by loading 0.15 M HNO_3 in 200 mL, followed by subsequent addition of 3 M HNO_3.

3.3 Results and Discussion

3.3.1 Separation of ^{177}Lu from Yb targets. The separation of the neutron irradiated enriched ^{176}Yb from the ^{177}Lu was performed to remove the bulk of the Yb target material. The separation using extraction column chromatography resulted in removing the excess Yb from the ^{177}Lu using acidic media as the mobile phase. The separation conditions to obtain a better resolution of the separating peaks such as the concentration of the mobile phase and the flow rates were evaluated and are discussed below.

The influence of eluent concentration. A successful sequential elution of Ln^{3+} on an extraction column chromatography can be obtained with optimal acid concentrations. An increase of the acid concentration results in the release of the metal ions. Although, it takes high concentrations of HNO_3 to cause the protonation of the phosphonates, the concentration used for selectively eluting the metal ions on the Ln2 resin was less than what was reported for obtaining similar outcomes (in separating ^{177}Lu from Yb targets) using the Ln resin.[20] Conversely, a dilute concentration of the acid does not have the strength to elute the Ln^{3+}, but rather increases the column elution time. The optimum acid concentration for the separation of the Yb from the Lu on the Ln2 column was 1.5 M HNO_3 and resulted in eluting the ^{175}Yb first followed by 80-85 % of ^{177}Lu , while only 15-20 % of ^{177}Lu was lost to the Yb fraction. The differences in the percent loss of ^{177}Lu were due to change in flow rates, which is discussed below.

Influence of flow rate on the separations. The flow rate was investigated to determine the optimum conditions that afforded a better separation profile. Flow rates ranging from

2-5 mL/min were evaluated while all other parameters were kept the same. There was not a discernible difference observed in the shape of the two separating peaks at the different flow rates evaluated except at 5 mL/min. As the flow rate increased, the amount of ^{177}Lu lost in the Yb fraction increased. **Table 3-2** summarizes the different flow rates that brought about an increase in the percentage loss of ^{177}Lu in the Yb fraction, which increased from 14 to 26 % with increasing flow rates from 2 to 5 mL/min.

Amount of Carrier Yb_2O_3 (mg)	Flow rate (mL/min)	Volume of fractions containing $^{175/176}$Yb (mL)	% Loss of ^{177}Lu in the Yb fraction	Volume of fractions containing only ^{177}Lu (mL)	Number of trials
45	2	120 ± 10	14	70 ± 0	2
45	3	115 ± 20	18.3 ± 4	80 ± 20	3
45	4	115 ± 10	18.5 ± 2	40 ±10	2
45	5	120	26	100	1

Table 3-2. Summary of Yb/^{177}Lu separation profile at various flow rates

As a result of the short reaction time between the extracting organophosphorous group and the lanthanides, the gap between the separating peaks becomes narrower and overlap occurs at 5 mL/min. Of the four flow rates evaluated, the majority of the ^{177}Lu was eluted in 50 mL of solvent containing a mixture of 1.5 M and 4 M HNO_3. Since the solvent flow rate was driven by a positive pressure, the bed volume of the column was slightly compressed with increasing pressure to generate a flow rate of 5 mL/min. This resulted in broadening of the Yb peak, which then overlapped with the Lu peak. A representative chromatography distribution profile of Yb/^{177}Lu using Ln2 resin at 4 mL/min is shown in **Figure 3-5.** Additional chromatography profiles of Yb/^{177}Lu at different flow rates are shown in the Appendix (**Figures A 3-2 to A 3-5**).

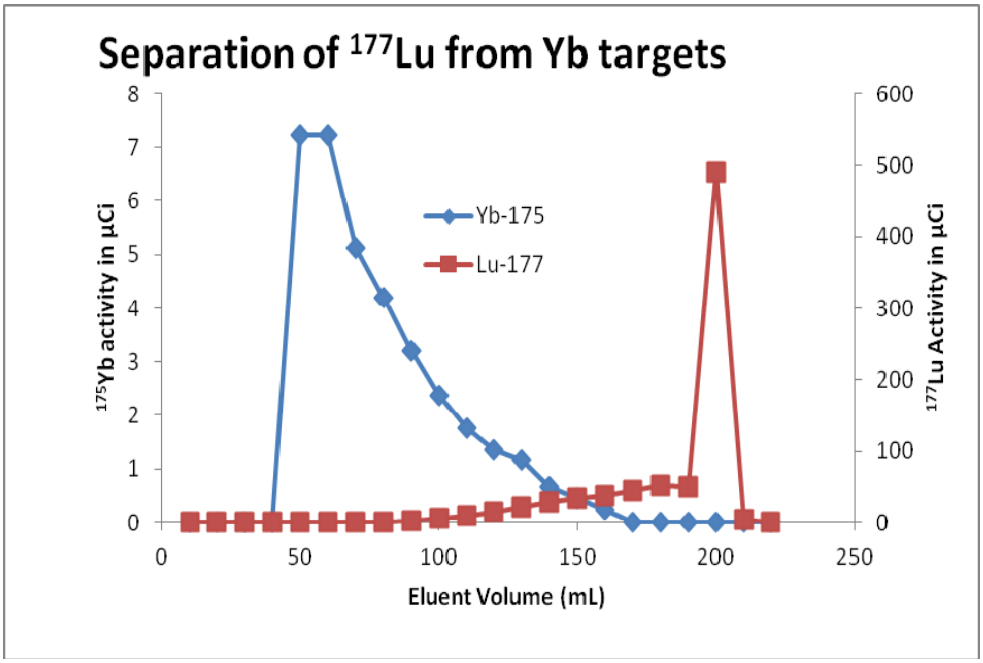

Figure 3-5. Separation of ^{177}Lu from the Yb targets.Ytterbium oxide (~ 45 mg) digested in 3M HNO_3 was spiked with ^{175}Yb/^{177}Lu and diluted to 10 mL in milli Q water. The sample was loaded onto a column pre-equilibrated with 0.5 MHNO_3 at 50 ˚C. The two radioisotopes were eluted using initially 1.5 M HNO_3 in 180 mL to elute the Yb, followed by 4M HNO_3 to elute the ^{177}Lu at a flow rate of 4 mL/min.

3.3.2 Separation of ^{166}Ho from Dy targets. The irradiated enriched Dy_2O_3 target was separated from the desired radioisotope ^{166}Ho using the Ln2 resin. The first 100 mL of the fraction eluted with 0.5 M HNO_3 (fractions 1-10, each containing 10 mL) contained 3.95 % of the ^{166}Dy. The next 60 mL collected (fractions 11-17) contained the remaining 94 % of the ^{166}Dy. The ^{166}Ho started to elute in fraction 21, and fractions 20-23 containing only ^{166}Ho (free of ^{166}Dy) were eluted with 30 mL of 3 M HNO_3, which contained 97 % of the total ^{166}Ho in the sample. The elution profile for the separation of Dy/Ho is shown in **Figure 3-6**.

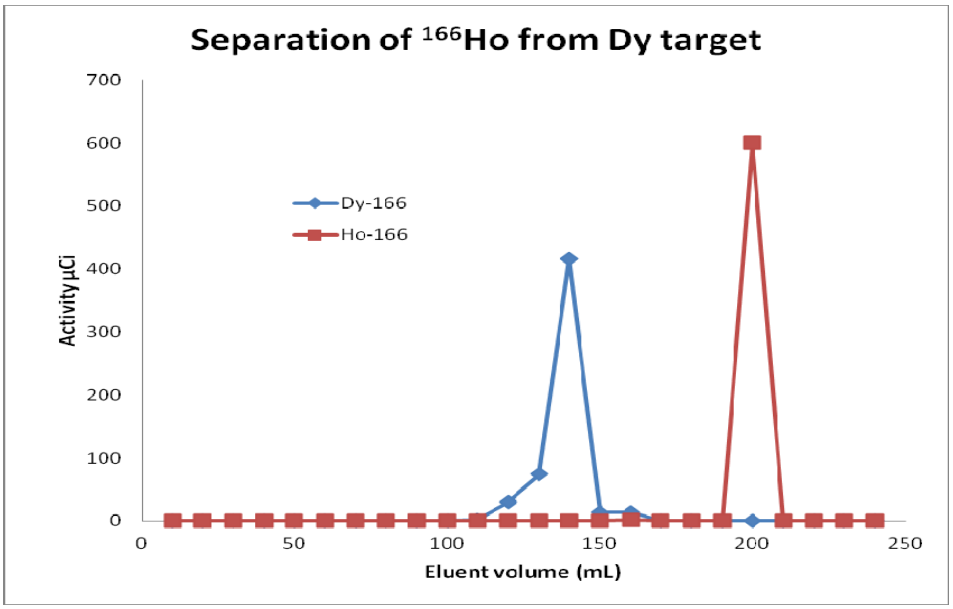

Figure 3-6. Separation of ^{166}Ho from the Dy target using the Ln2 resin. The Ln2 column was equilibrated with 0.15 M HNO_3. The Dy_2O_3 (Dy = 5 mg) sample was spiked with ^{166}Dy/^{166}Ho and diluted with milli Q water to a final volume of 10 mL. Intially 200 mL of 0.5 M HNO_3 was added at 4 mL/min to the column (temperature maintained at 50 $^{\circ}$C) followed by 50 mL of 3 M HNO_3 to elute the ^{166}Ho.

3.3.3 Separation of ^{161}Tb from Gd targets. Separation of ^{161}Tb from the Gd target was successfully performed using the Ln2 resin (**Figure 3-7**). The eluting conditions for fraction containing the ^{161}Tb target were 0.5 M HNO_3, which in comparison with mobile phases used for the separation of Yb/^{177}Lu or the Dy/^{166}Ho is a low concentration of acid. A well resolved separation of ^{161}Tb from the Gd target was obtained that is comparable to what was reported by Lehenberger and co-workers[4]. This referenced paper utilized a cation exchange Aminex resin and α-HIBA as the eluent to separate ^{161}Tb from the Dy target. Due to the slow flow rate (~0.2 mL/min), the time it took to complete the separation in the referenced paper is more than double what was found in this study (1.1 h).

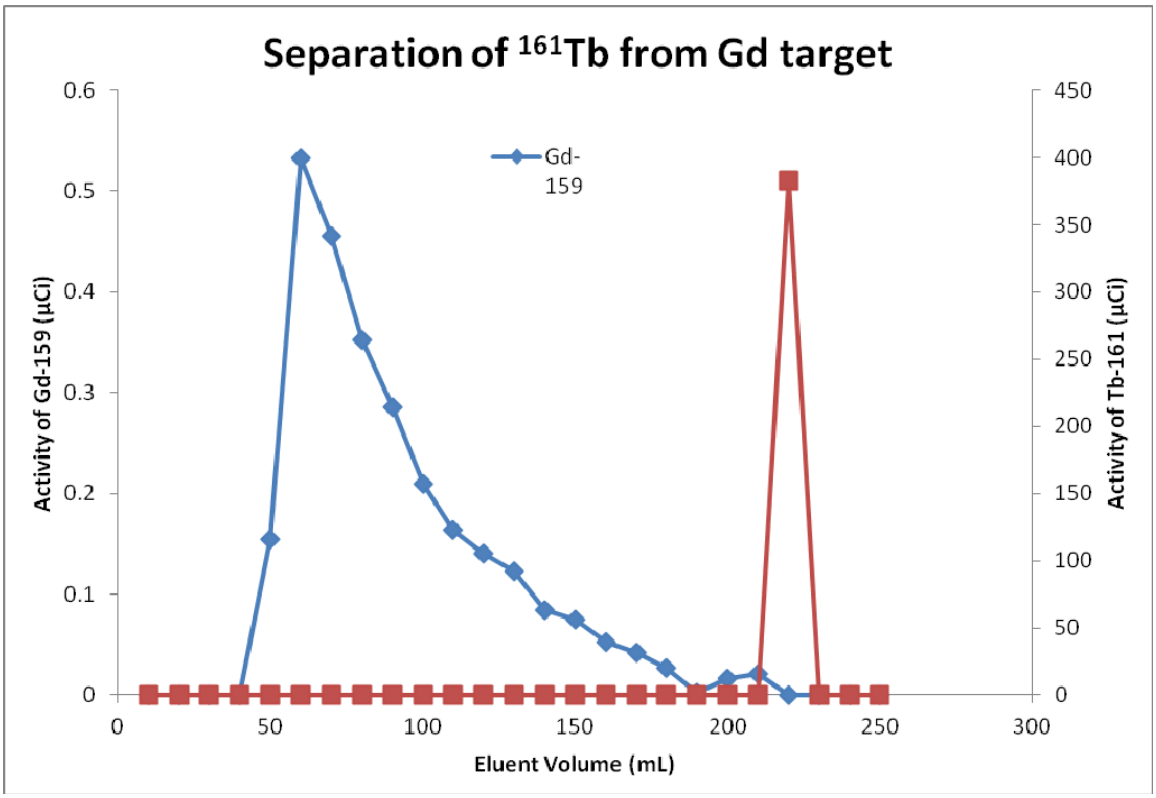

Figure 3-7. Separation of ^{161}Tb from a Gd (39.9 mg) target using the Ln2 resin. The solvent was 200 mL of 0.15 M HNO_3 followed by 30 mL of 3M HNO_3 at an elution flow rate of 4 mL/min. Under these conditions, ^{161}Tb eluted in 30 mL of the 3 M HNO_3.

3.4 Conclusion

The separation of radiolanthanides using chromatography media was evaluated. The extraction chromatography resin and cation exchange resins were investigated for separating radiolanthanides that are used for radiopharmaceutical purposes. The objective to remove the bulk of the irradiated Yb target from the ^{177}Lu product was successfully performed using the extraction chromatography media. A sequential elution of the bulk Yb and trace amounts of Lu was obtained with only 26% of the ^{177}Lu activity lost to the Yb sample. The separation performance was slightly affected by changes in flow rates.

The positive-pressure driven solvent flow exerts a high pressure resulting in resin compression. This could have an adverse effect in the resin packing since the top end of the resin is loose, and it is possible for resin movement (compression/relaxation) during the separation process.

The column performance was evaluated at different flow rates to determine a reproducible elution profile of the separating elements. Although, the exerted pressure brought about a change in the distribution profile of Yb/Lu (an increase in the loss of ^{177}Lu to the ^{175}Yb fraction with increasing flow rate), the separation of the peaks was consistent. The results obtained highlighted the resins robustness in the separation of Yb/Lu within a reasonable amount of time (1-3 h depending on the choice of flow rate). The separation times indicated here are associated with the Ln2 column. Further separation utilizing HPLC and ion-exchange column could take up to 2h. Considering the half-life of ^{177}Lu, the time it takes to process the production and separation of ^{177}Lu is quite reasonable. The separation of ^{166}Ho from the Dy targets using Ln2 column was successful in removing the Ho from the Dy fraction. The high cross-section of the enriched ^{164}Dy allows the production of the ^{166}Ho in high yields; even using a slightly smaller mass of Dy targets (12 mg) than what was used for evaluating the Yb/Lu (45 mg) separation. The separation of small mass of the enriched target from the daughter product using Ln2 chromatography is advantageous since there will be less tailing of the bulk parent nuclide. Similar encouraging results were obtained for the separation of the ^{161}Tb from the Gd target using Ln2 column.

3.5 Future Studies

The separation of radiolanthanides using extraction chromatography has shown promising results in terms of isolating the bulk amount of the enriched target isotope from the irradiated target. In order to utilize column chromatography for routine production of radiolanthanides, the conditions that affect reproducible results in the separation of radiolanthanides needs further evaluations. Due to the fines present in the Ln2 resin, the solvent flow was performed by applying positive pressure to attain the desired flow rate for good separations. During the column experiments, changes in the bed volume (expansion and contraction; the top end of the bed volume is not restricted from movement) between experiments, which was caused by the positive pressure, had adverse effects in the separation profiles of the sample. In the work of Horwitz et al. daily use of the column resulted in a 5 % shift in the cut point between the Lu and Yb fractions.[18] This change in the performance of the column could be due to the pressure exerted on the column that resulted in the change in elution profile of the sample. A column that is packed to its full capacity restricts the resin movement inside the column and the uniform distribution of pressure on the bed volume can assist in avoiding the change in elution profile of the sample. However, loading a resin having a small particle size (~ 40 μm) could cause pressure build up and is not ideal for packing a glass column with positive pressure. Therefore, solvent flow assisted with pull mechanism, instead of push, may be helpful in obtaining reproducible results.

3.6 Appendix

Enriched Yb_2O_3							
Isotope	168	170	171	172	173	174	**176**
Enrichment %	<0.05	<0.05	<0.05	<0.05	<0.05	±0.13	99.81±0.20
Enriched Dy_2O_3							
Isotope	156	158	160	161	162	163	**164**
Enrichment (%)	<0.01	<0.01	0.02±0.01	0.15±0.03	1.05±0.03	1.05±0.05	98.43±0.05
Enriched Gd_2O_3							
Isotope	152	154	155	156	157	158	**160**
Enrichment (%)	<0.01	0.01	0.18	0.36	0.25	1.00	98.2±0.1

Figure A 3-1. Analysis of the isotope distribution of enriched target compounds ^{176}Yb, ^{164}Dy, and ^{160}Gd

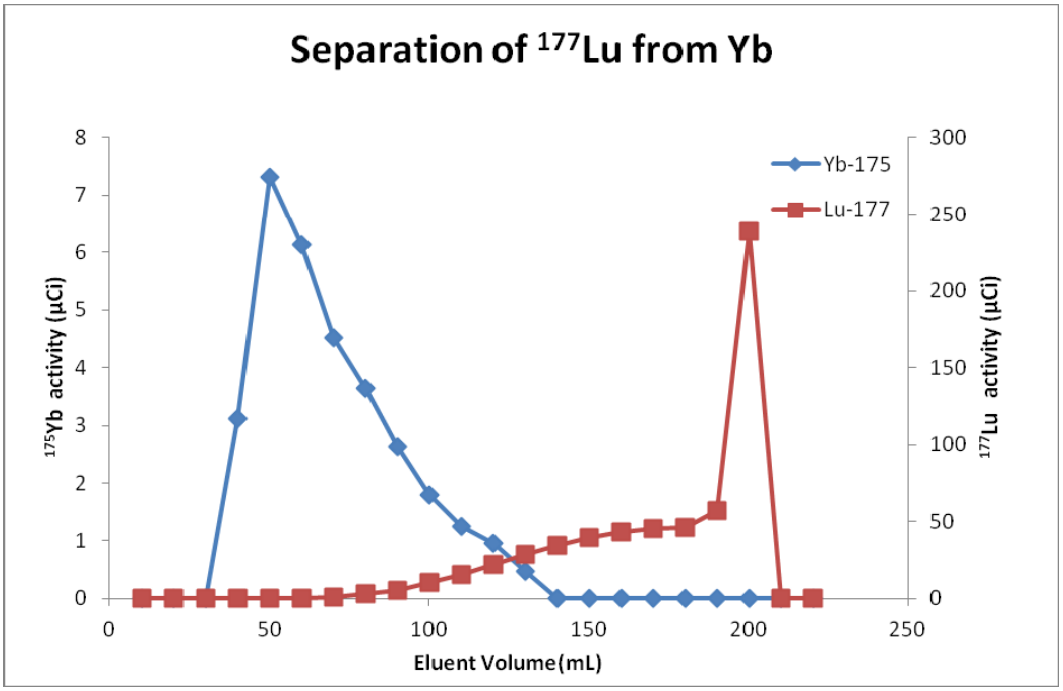

Figure A 3-2. Separation of ^{177}Lu from Yb targets that contains natural Yb (45 mg) with elution flow rate at 2 mL/min

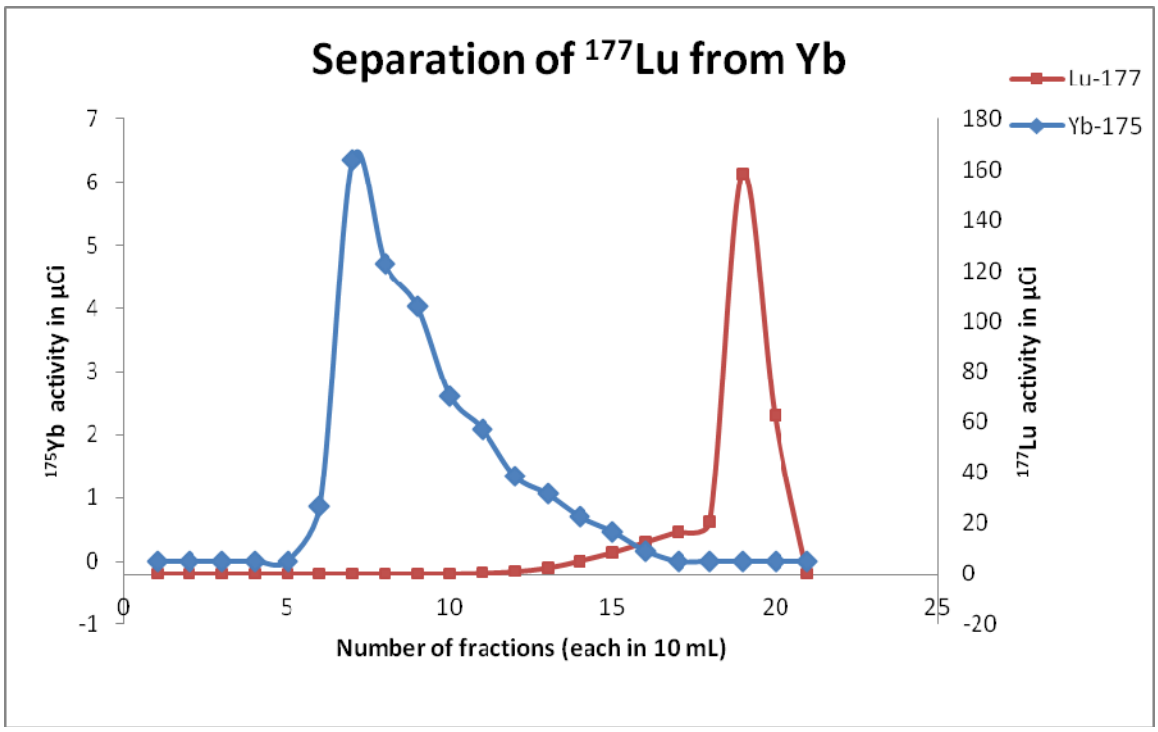

Figure A 3-3. Separation of ^{177}Lu from Yb targets that contains natural Yb (45 mg) with elution flow rate at 2.5 mL/min

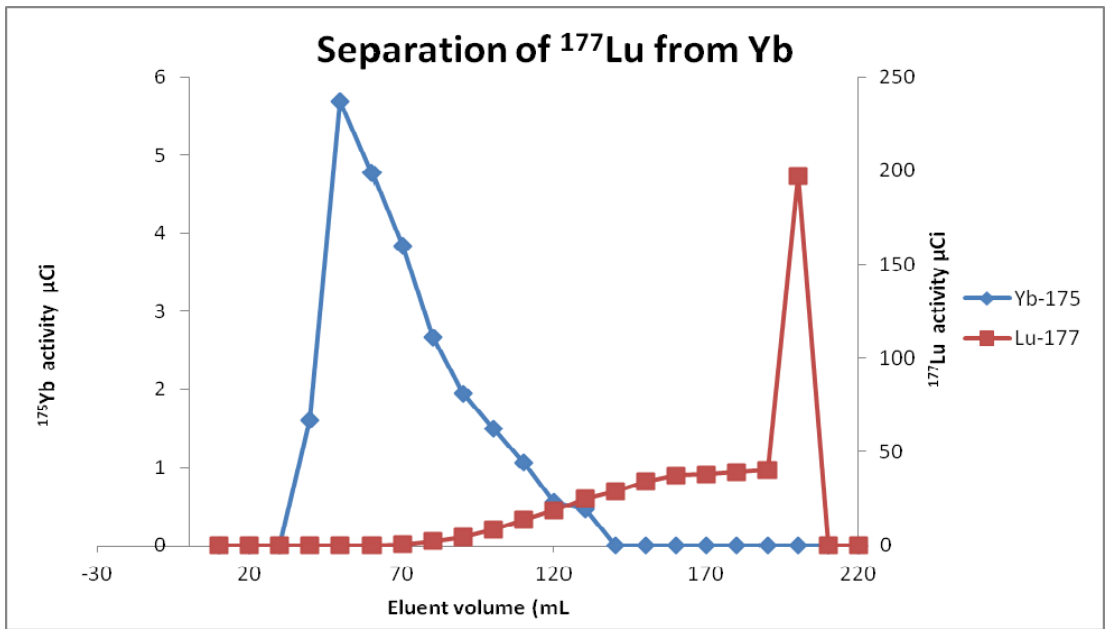

Figure A 3-4. Separation of ^{177}Lu from Yb targets that contains natural Yb (45 mg) with elution flow rate at 3 mL/min

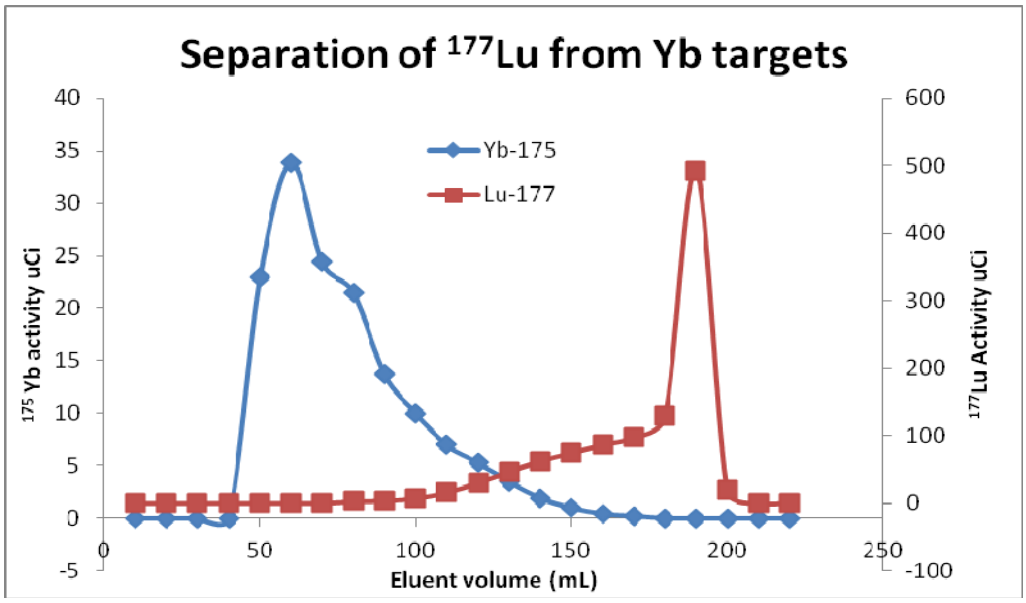

Figure A 3-5. Separation of ^{177}Lu from Yb targets that contains natural Yb (45 mg) with elution flow rate at 5 mL/min

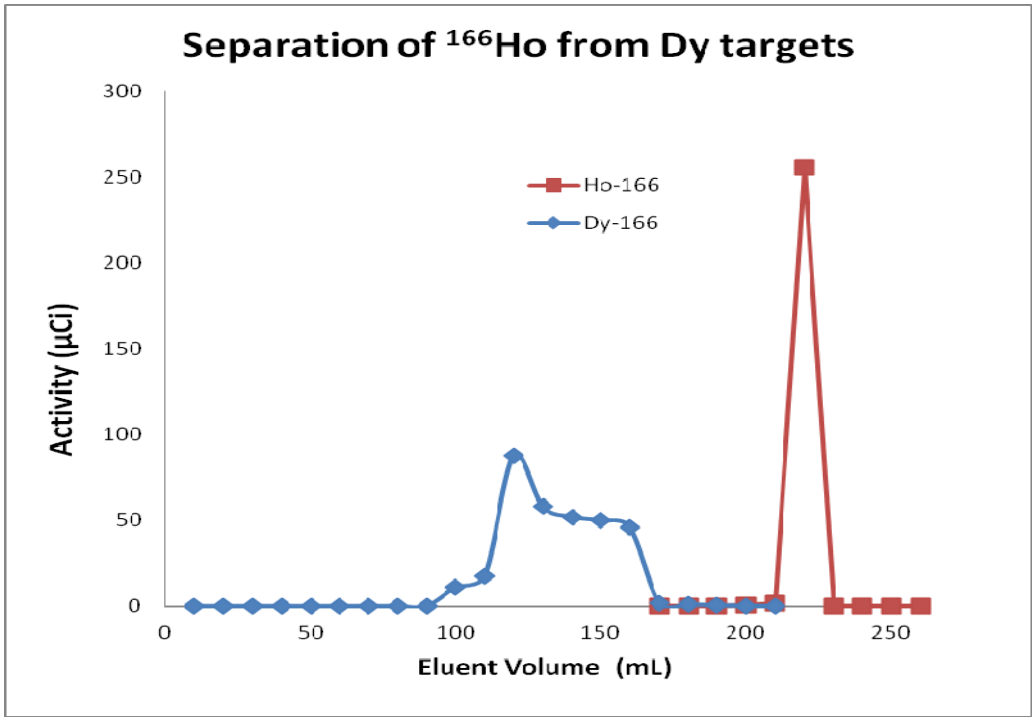

Figure A 3-6. Separation of ^{166}Ho from Dy targets that conatins cold natural Dy (12.6 mg) with elution flow rate at 4 mL/min.

Figure A 3-7. Picture of column chromatography separation using Ln2 resin as extraction media with heat exchange jacket. The flow rate of the column is controlled by adjusting flow gauge of a compressed N_2 to obtain the desired flow rate.

3.7 References

1. Pandey, U.; Mukherjee, A.; Chaudhary, P. R.; Pillai, M. R. A.; Venkatesh, M., Preparation and studies with ^{90}Y-labelled particles for use in radiation synovectomy. *Applied Radiation and Isotopes* **2001,** *55* (4), 471-475.
2. Cutler, C. S.; Smith, C. J.; Ehrhardt, G. J.; Tyler, T. T.; Jurisson, S. S.; Deutsch, E., Current and potential therapeutic uses of lanthanide radioisotopes. *Cancer Biother Radiopharm* **2000,** *15* (6), 531-45.
3. Radioisotopes and radiochemcials. http://www.murr.missouri.edu/ps_radio_isotopes.php (accessed October 1, 2012).
4. Lehenberger, S.; Barkhausen, C.; Cohrs, S.; Fischer, E.; Grünberg, J.; Hohn, A.; Köster, U.; Schibli, R.; Türler, A.; Zhernosekov, K., The low-energy β− and electron emitter 161Tb as an alternative to 177Lu for targeted radionuclide therapy. *Nuclear Medicine and Biology* **2011,** *38* (6), 917-924.
5. Smith, C. J.; Volkert Wa Fau - Hoffman, T. J.; Hoffman, T. J., Radiolabeled peptide conjugates for targeting of the bombesin receptor superfamily subtypes. (0969-8051 (Print)).
6. Lewis, M. R.; Wang, M.; Axworthy, D. B.; Theodore, L. J.; Mallet, R. W.; Fritzberg, A. R.; Welch, M. J.; Anderson, C. J., In Vivo Evaluation of Pretargeted 64Cu for Tumor Imaging and Therapy. *Journal of Nuclear Medicine* **2003,** *44* (8), 1284-1292.
7. Goodwin, D. A.; Meares, C. F.; McTigue, M.; McCall, M. J.; Chaovapong, W., Metal decomposition rates of 111In-DTPA and EDTA conjugates of monoclonal antibodies in vivo. *Nucl Med Commun* **1986,** *7* (11), 831-8.
8. Palawak, D.; Korsak, A.; Mikolajcak, R.; Janota, B.; Karczmarczyk, U.; Jakubowska, E. *Compartative Evalutaion of therapeutic radiopharmaceuticals* Radioisotope Centre POLATOM: Austria, Viena, 2007.
9. Hong, Y.-D.; Park, K. B.; Jang, B.-S.; Choi, S.-J.; Choi, S. M.; Kim, Y.-M., Holmium-166-DTPA as a liquid source for endovascular brachytherapy. *Nuclear Medicine and Biology* **2002,** *29* (8), 833-839.
10. MA, D. Radiotherapeutic potential of the ^{166}Dy/^{166}Ho delayed dose generator and of high specific activity of ^{166}Ho. University of Missouri-Columbia, Columbia, Missouri, 1996.
11. Atkins, P. W.; Shriver, D. F., *Shriver & Atkins' inorganic chemistry*. 5th ed.; Oxford University Press: Oxford, 2010; p xxiv, 824 p.
12. Huang, C.-H., *Rare earth coordination chemistry : fundamentals and applications*. John Wiley & Sons (Asia): Singapore ; Hoboken, NJ, 2010; p xxii, 575 p.
13. Nelson, F.; Murase, T.; Kraus, K. A., Ion exchange procedures : I. Cation exchange in concentration HCl and HClO4 solutions. *Journal of Chromatography A* **1964,** *13* (0), 503-535.
14. Korkisch, J.; Ahluwalia, S. S., Cation-exchange behaviour of several elements in hydrochloric acid—organic solvent media. *Talanta* **1967,** *14* (2), 155-170.

15. Stagg, W. R.; Powell, J. E., Complexes of the Trivalent Rare Earths with Isobutyrate, α-Hydroxyisobutyrate, and α,β,β'-Trihydroxyisobutyrate Ligands. *Inorganic Chemistry* **1964,** *3* (2), 242-245.
16. Sevenich, G. J.; Fritz, J. S., Addition of complexing agents in ion chromatography for separation of polyvalent metal ions. *Analytical Chemistry* **1983,** *55* (1), 12-16.
17. Chopin, G. R.; Moy, D. In *Ion-exchange studies of alpha-hydroxybutyric acid-lanthanide and actinide systems*, International atomic agency, Copenhagen, Denmark, IAA: Copenhagen, Denmark, 1960.
18. Horwitz, E. P.; McAlister, D. R.; Bond, A. H.; Barrans, R. E.; Williamson, J. M., A process for the separation of ^{177}Lu from neutron irradiated ^{176}Yb targets. *Applied Radiation and Isotopes* **2005,** *63* (1), 23-36.
19. Horwitz, E. P.; Schulz Wallace, W., Solvent Extraction in the Treatment of Acidic High-Level Liquid Waste: Where Do We Stand? In *Metal-Ion Separation and Preconcentration*, American Chemical Society: 1999; Vol. 716, pp 20-50.
20. Saed Mirzadeh, M. d., Arnold L. Beets, Furn F. Knap Jr. Method for preparing high specific activity of Lu-177. 2004.
21. Dadachova, E.; Mirzadeh, S.; Lambrecht, R. M.; Hetherington, E. L.; Knapp, F. F., Jr., Separation of carrier-free^{166}Ho from Dy_2O_3 targets by partition chromatography and electrophoresis. *Journal of Radioanalytical and Nuclear Chemistry* **1995,** *199* (2), 115-123.
22. Nayak, D.; Lahiri, S.; Ramaswami, A.; Manohar, S. B., Separation of carrier-free holmium and dysprosium produced in 70Mev $^{11}B^{5+}$ irradiated europium target by liquid–liquid extraction with HDEHP. *Ind. J. Chem* **2000,** *39A*, 1061-1065.

Chapter 4

Chemical and electrochemical reduction and separation of ^{177}Lu from ytterbium

4.1 Introduction

Separation of radiolanthanides by changing the oxidation state of one of the two neighboring elements is an alternative separation method to column chromatography. For example, the separation of a sample containing lanthanides with multiple oxidation states utilizes various methodologies to isolate the radiolanthanides of interest. This chapter discusses the separation of Yb from Lu by reducing the Yb^{3+} to Yb^{2+} using chemical and electrochemical reduction techniques.

Given the lanthanides are highly electropositive with the stable oxidation state being 3+ across the period, a reducing agent with high over potential is needed to drive the reaction to completion. The reduction of Ln^{3+} ions to a lower oxidization state can also be achieved by applying an external potential. The +2 oxidation state is only accessible for a few lanthanides (Nd, Sm, Eu, Dy, Tm, and Yb). Furthermore, the reduction potential for Sm, Eu, and Yb (Ln^{3+}/Ln^{2+}) redox couple is lower (~ 1 V) than the reduction potential for the Ln^{3+}/Ln^{0} redox coupled to generate the elemental atoms. Based on the reported standard redox potentials, a selective reduction of Ln^{3+}/Ln^{2+} for Sm, Eu, Yb is achievable without driving their oxidation state to the elemental state. This means the other lanthanides with inaccessible divalent states can be spared in the reduction process, while the neighboring elements are reduced. For example, the

reduction potential for the redox couple Yb^{3+}/Yb^{2+} is -1.05 V and that of the Yb^{3+}/Yb^{0} or Lu^{3+}/Lu^{0} is close to -2.3V, which is quiet high.[1] Therefore, the selective reduction of Yb^{3+}/Yb^{2+} can be achieved without altering the oxidation state of the Lu^{3+}. This aspect of the redox property of the lanthanides can be exploited in separation processes.

	Ln^{3+}	Ln^{2+}	Ln^{0}
Sm	[Xe] $4f^{5}$	[Xe] $4f^{6}$ **(Ln^{3+} + 1e → Ln^{2+} -1.55 V)**	[Xe] $4f^{6}$ $6s^{2}$ (Ln^{3+} + 3e → Ln^{0} -2.30 V)
Eu	[Xe] $4f^{6}$	[Xe] $4f^{7}$ **(Ln^{3+} + 1e → Ln^{2+} -0.34 V)**	[Xe] $4f^{7}$ $6s^{2}$ (Ln^{3+} + 3e → Ln^{0} -1.99 V)
Gd	[Xe] $4f^{7}$		[Xe] $4f^{7}$ $5d^{1}$ $6s^{2}$ (Ln^{3+} + 3e → Ln^{0} -2.29 V)
Tb	[Xe] $4f^{8}$		[Xe] $4f^{9}$ $6s^{2}$ (Ln^{3+} + 3e → Ln^{0} -2.30 V)
Dy	[Xe] $4f^{9}$	[Xe] $4f^{10}$ **(Ln^{3+} + 1e → Ln^{2+} -2.5V)**	[Xe] $4f^{10}$ $6s^{2}$ (Ln^{3+} + 3e → Ln^{0} -2.29 V)
Ho	[Xe] $4f^{10}$		[Xe] $4f^{11}$ $6s^{2}$ (Ln^{3+} + 3e → Ln^{0} -2.33 V)
Yb	[Xe] $4f^{13}$	[Xe] $4f^{14}$ **(Ln^{3+} + 1e → Ln^{2+} -1.05 V)**	[Xe] $4f^{14}$ $6s^{2}$ (Ln^{3+} + 3e → Ln^{0} -2.22 V)
Lu	[Xe] $4f^{14}$		[Xe] $4f^{14}$ $5d^{1}6s^{2}$ (Ln^{3+} + 3e → Ln^{0} -2.30 V)

Table 4-1. The electron configuration of the lanthanides and the common ions with the redox half reactions and the standard redox potentials in parentheses[1].

The chemical separation of the lanthanides is not without disadvantages. The chemical instability of the divalent lanthanides due to their high oxidation potential is a stumbling block in the separation process. They are considered as potent reducing agents due to their ability to reduce solvent media such as water. In this regard, the separation process of radiolanthanides is limited to anhydrous solvents under inert atmosphere. In

order to separate the two elements (Yb and Lu) by reducing the Yb^{3+} to Yb^{2+}, while the Lu remains in the 3+ oxidation, special attention is given to solvent media (the grade and quality), the counter ions present for stabilizing the Ln ions in solution, and chemical media applied to separate the radiolanthanides with two different oxidation state . The early studies conducted to separate Yb from Lu using various reducing methods are chronicled below.

In the early 1930's L.F. Yntema and R.W. Ball were able to reduce Yb^{3+} to Yb^{2+} and isolate $YbSO_4$.[2] A lanthanide chloride solution was prepared by dissolving 10 g of lanthanide oxide in $HCl_{(aq)}$, and the excess solvent removed by evaporation, while the remaining $YbCl_3$ was dissolved in H_2SO_4. In the electrolytic cell, which contained the Hg cathode and Pt anode in 0.05 N HCl (electrolyte), the sample containing $YbCl_3$ was added. A current of 0.10 A, with a current density of 0.025 A/cm^2 at the cathode, and a voltage of 110 V was applied to reduce the Yb^{3+} to Yb^{2+} and resulted in the precipitation of $YbSO_4$. Similar experiments were conducted by W. Prandt to produce Yb^{2+} based on the previous work by Yntema and Ball.[2] The electrolytic reduction was carried out in an aqueous solution of Yb/Lu sulfates using a Hg cathode and a Pt anode. The current was maintained between 0.20 and 0.40 A, the voltage drop was 110 V, and the temperature ranged from 40 to 60 ºC. The purity and percent recovery of the $YbSO_4$ was not reported.

In 1963, Asprey et al. investigated the formation of $YbSO_4$ over a Hg pool cathode.[3] An electrolytic cell was set up containing a Hg cathode and a Pt anode. During electrolysis, the anode tube was dipped into the rare earth solution. A current density between 0.02 and 0.06 A/cm^2 and a voltage between 6 and 12 V were used. The authors reported the formation of $YbSO_4$ within a few minutes and they were able to extract the

$YbSO_4$. However, due to the instability of the divalent salts, the precision of the measurements were of poor quality, but still sufficient for characterization. Separation of Eu from the lanthanides by reduction followed by column chromatography was investigated by Moskvin et al.[4] In his report a mixture of Ln^{3+} in HCl/NH_4Cl was loaded on a Jones reduction column and the subsequent elution was followed by column chromatography media containing HDEHP (fixed on teflon). This multistep separation demonstrated the reduced Eu^{2+} eluted first while the other Ln^{3+} species eluted later. The report also indicated that trace amounts of Eu^{2+} could not be separated from the mixtures of Ln^{3+} due to oxidation of Eu^{2+} to Eu^{3+} by elementary oxygen.

Although, the application to lanthanides in the referenced literature is different from what is pursued in this study, the following reports have described the successful reduction of Yb^{3+} to Yb^{2+} by electrochemical reduction, which is otherwise difficult to accomplish under ambient conditions. Rabockai reported the reversible electrochemical reduction of Yb^{3+} in aqueous solutions at various temperatures.[5] This report utilized a mercury pool and $NaClO_4$ as the working electrode and supporting electrolytes, respectively. Mercury is considered an incompatible chemical for radiopharmaceutical applications due to health concerns. Also, the aqueous supporting electrolytes have unfavorable effects on the stability of Yb^{2+} for bulk reduction and separation processes. Another reduction method reported by Nakashima et al. explored photon excitation of Yb^{3+} to reduce it to Yb^{2+}.[6] In his early publications, Nakashima indicated the irradiation of $Eu^{3+}$and Sm^{3+} ions in solutions by a laser assisted pulse excitation that resulted in the reduction of Sm^{3+} to Sm^{2+} and Eu^{3+} to Eu^{2+}. This investigation was later translated to Yb reduction chemistry and reduced Yb^{3+} to Yb^{2+} by laser irradiation. This paper indicated

an increase in concentrations of Yb^{3+} resulted in incomplete reductions. Since the separation of the reduced lanthanides was not within the scope of their investigation, no further data is available.[6]

The objective of the current study is to isolate the bulk of the irradiated enriched Yb^{3+} target from $^{177}Lu^{3+}$ in a multistep separation process. If, by some simple (one-stage) process, one could remove the Yb^{2+}, partially or entirely (chemically or by use of chromatography media), the subsequent purification process to obtain high specific activity of Lu^{3+} would be made easier. So far, encouraging results have been achieved in the separation of large amounts of Yb^{3+} target (45 mg) from ^{177}Lu using extraction column chromatography. The separation of Yb^{3+} from Lu^{3+} using chromatography column (Ln2 resin) generates a large amount of radioactive waste containing concentrated acids. Also, such a process takes hours of sample preparation and column run time that exposes workers to radiation. In order to find a more efficient separation of $^{175}Yb/^{177}Lu$, a multistep separation process that includes the reduction of Yb^{3+} to Yb^{2+} followed by a separation technique including selective precipitation of Yb^{2+}, column chromatography, or selective complexation is described. Accordingly, the work in this chapter is separated into two sections: (1) determine the best reduction method to obtain complete reduction of $Yb^{3+}$and (2) evaluate the separation techniques to isolate the divalent Yb^{2+} from Lu^{3+}.

4.2 Experimental

4.2.1 Chemicals and Reagents. Sources of reductant metals of varying mesh sizes and purity levels are listed as follows: Mg (99 %, 325 mesh, Strem Chemicals (Newburyport, MA)); Y (99.9 %, 40 mesh, 325 mesh, Sigma Aldrich (St. Louis, MO)); Zr (99.5 %, 325 mesh size, Sigma-Aldrich (St. Louis, MO)); and Al (99.5 %, 325 mesh, Alpha Aesar (Newburyport, MA)). Anhydrous $YbCl_3$ (99.9%) and $Yb(OTf)_3$ (99.9%) were acquired from Sigma-Aldrich (St. Louis, MO). Lutetium chloride was purchased from Alpha Aesar (Newburyport, MA). All solvents used for the reduction of Yb^{3+} were anhydrous (≥ 99.5 % purity) and were obtained from Sigma-Aldrich (St. Louis, MO).

4.2.2 Preparation of Yb compounds for the reduction of Yb^{3+} to Yb^{2+}. The reduction and separation experiments were conducted in a controlled atmosphere glove box operating under argon. A weighed amount of ytterbium compound ($YbCl_3$ or $Yb(OTf)_3$) was dissolved in either MeOH or EtOH. $Yb(acac)_3$ was prepared following the procedures described in the literature.[7] Briefly, $Yb(acac)_3$ was prepared by adding a mixture of 3 mmol of acetylacetone (redistilled under argon following the chemical purification procedure)[8] in 95% ethanol to a stirring solution of $YbCl_3$ (1 mmol) at 40 °C. The product was used for the reduction of Yb^{3+} without isolation.

Procedure for the chemical reduction of Yb^{3+}. The chemical reduction of Yb^{3+} in solution was performed using reductant metals. The metals and their respective standard redox potentials are listed below in **Table 4-2**.

Reductant metals	Standard redox potential (V)
$Mg \rightarrow Mg^{2+} + 2e^-$	+2.38
$Y \rightarrow Y^{3+} + 3e^-$	+2.37
$Hf \rightarrow Hf^{4+} + 4e^-$	+1.70
$Ti \rightarrow Ti^{2+} + 2e^-$	+1.63
$Al \rightarrow Al^{3+} + 3e^-$	+ 1.6
$Zr \rightarrow Zr^{4+} + 4e^-$	+1.5
$Mn \rightarrow Mn^{2+} + 2e^-$	+ 1.18

Table 4-2. The standard redox potential of metals utilized for reducing Yb^{3+} to $Yb^{2+}$is referenced.[1]

Preliminary experiments were conducted to reduce the Yb^{3+} to Yb^{2+} using glass columns filled with the metals to maximize the contact surface area and the reaction time between the metal and the Yb^{3+} sample. This setup was helpful when using large particle size metal powders that are porous for the loaded sample to elute by gravity. The other advantage of using a reduction column is that it is convenient to link the reduction column to a separation column that could be packed with a cation exchange resin or an extraction column so that the successive reduction and separation step minimizes the sample exposure to air as shown in **Figure 4-1**.

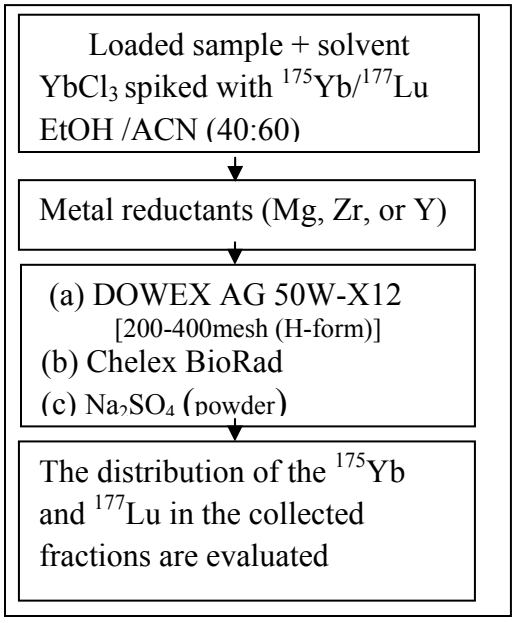

Figure 4-1. Picture of the reaction setup of reductant column connected to the separation column filled with a chromatography media. This setup uses a solvent reservoir to transfer the eluting solvent (EtOH/ACN) to the column.

To eliminate column blockage by the small particle sized metal powders, reaction mixtures that contained fine metal powders and the sample were stirred for the duration of the reaction followed by isolation of the liquid from the reaction mixtures to perform the separation process. The reductant metals were rinsed with 2 mL of the solvents that were used to dissolve the Yb salts. The sample containing Yb compounds (0.3 mmoles) was dissolved in 2 mL of MeOH or EtOH. The reaction mixture containing the reductant metal powders and the Yb salts were stirred and evaluated (by iodimetric titration; *see* below) by withdrawing the solutions from the reaction mixture with a syringe and filtering through a 0.22 μm Whatman filter disks.

4.2.3 Quantification of the reduced Yb^{2+}. The iodimetric titration method was used to determine the amount of Yb^{3+} reduced by the metal reductants. A known amount of the Yb^{2+} Cl_2 or $Yb^{2+}(OTf)_2$ (green colored samples) was isolated from the redox reaction mixture and titrated with a fresh solution made of iodine dissolved in a solvent mixture of EtOH and ACN (35:65 v/v). In the iodimetric titration of Yb^{2+}, the solution containing the Yb^{2+} was stirred with a known volume of I_2 that was added to the mixture that changed the green colored solution to colorless; the excess I_2 was titrated with a standardized solution of sodium thiosulfate. The number of moles of Yb^{2+} was determined by subtracting the moles of thiosulfate used to complete the titration from the moles of I_2 added to the mixture (**Equations 4-1 & 4-2** show the chemical reaction between Yb^{2+} and I_2). The efficiency of the reductant metal was determined by taking the moles of Yb^{2+} divided by the total moles of Yb^{3+}used for the reaction and multiplied by 100 to establish the percent yield.

$$2Yb^{2+} + I_2 \rightarrow 2Yb^{3+} + 2I^- \qquad \text{Equation 4-1}$$

$$I_{2\ excess} + 2S_2O_3^{2-} \rightarrow 2I^- + S_2O_6^{2-} \qquad \text{Equation 4-2}$$

4.2.4 Electrochemical Reduction. The electrochemical data were obtained with a Bio-analytical Systems Inc. (BAS) CV-50 instrument. The non-aqueous electrolytes (tetraethylammonium chloride, tetrabutyl ammonium perchlorate electrochemical analysis, > 99 % from Sigma Aldrich, St Louis], and tetrabutylammonium tetrafluoroborate (ACS grade 98% from Sigma Aldrich)) were dissolved in anhydrous ethanol/acetonitrile solutions to make 1 mM concentrations. A non-aqueous 0.1 M Ag/AgCl reference electrode was prepared following a referenced procedure [9]). The working electrodes evaluated were glassy carbon, carbon paste, and titanium wires (99.9% metal basis; 0.127 mm, from Alpha Aesar). The carbon paste working electrode was prepared by following a literature method using glassy carbon powder and mineral oil.[10] The counter electrode was a platinum wire (Bioanalytical Systems). The cyclic voltammetry experiments were evaluated at scan rates of 50 mV/sec and 100 mV /sec. The applied potential operating window for the CV experiments was 100 mV to -2000 mV.

For the bulk electrolytic reduction of Yb^{3+}, H-cell electrochemical glassware was used and the cathodic and anodic compartments were filled with tetraethylammonium chloride (electrolytes) in anhydrous EtOH/ACN mixtures, while $YbCl_3$, $Yb(OTf)_3$, or $Yb(acac)_3$ were added to the cathodic cells. For the bulk electrolysis the glassy carbon paste and a platinum rod were used in the cathodic and anodic compartments, respectively. The reaction vessel was purged with argon gas prior to use and continuously purged during the course of electrolysis.

4.2.5 Separation of Yb^{2+} from Lu^{3+} by selective precipitation. Ytterbium chloride (0.38 mmole) was dissolved in 2 mL of MeOH/ACN that also contained radioactive $^{175}Yb/^{177}Lu$. This sample was then added to Mg or Y (100 mg) metal reductants and the reaction mixture was stirred for 30 min. The solution was isolated from the mixture and added to tetramethylammonium sulfate (1.1 mmole) that was dissolved in 1 mL of MeOH. An instant precipitation following the addition was observed. The reaction vessels were centrifuged and the supernatant and pellet fractions were separately counted to determine the distribution profile of ^{175}Yb and ^{177}Lu in each of the fractions.

4.2.6 Separation of Yb^{2+} from Lu^{3+} using chromatography media. Labset glassware kits from Chemglass with screw cap ends were assembled for the reduction and separation experiments (**Figure 4-1**). A constant flow of solvent (EtOH/ACN mix), purged under N_2, was passed through the joined glass columns. The first column was filled with the reductant metals (Mg, Zr, or Y) and the second was filled with the separating reagents (DOWEX AG 50W x 8, Chelex-100 resin, or Na_2SO_4). A sample containing $YbCl_3$ was spiked with $^{175}Yb/^{177}Lu$ and loaded onto the column using a syringe and allowed to react with the reductant metal, and then eluted onto the separation column by gravity solvent flow.

4.2.7 Separation of Yb^{2+} from Lu^{3+} by complex formation. Ytterbium chloride (0.38 mmole) was dissolved in 2 mL MeOH/ACN mixture and spiked with $^{175}Yb/^{177}Lu$ (50 μL, 622 μCi). The sample was added to a reductant metal (Mg, 100 mg). After the reaction was stirred for 30 min, the solution was isolated, filtered through a Whatman filter disk, and 500 μL of the Yb/Lu reaction mixture was added to 0.2, 0.3, 0.5, or 0.8 M HDEHP in 500 μL. At high concentrations of HDEHP (0.5 and 0.8M), multiple layers of solution

formed. The samples were centrifuged to separate the layers and an aliquot from each layer was evaluated for $^{175}Yb/^{177}Lu$ by spotting on C-18 reversed phase TLC plates to evaluate the Yb^{2+} vs Yb^{3+} HDEHP speciation. The developing solution for theTLC plates was 20/80 acetone/hexane. The TLC plates were analyzed using an AR-2000 Bioscan. The Yb/Lu sample that forms a complex with HDEHP moved toward the solvent front on the C-18 reversed phase TLC plates, whereas the Yb/Lu that did not form a complex with HDEHP remains at the origin.

4.3 Results and Discussions

The multistep separation process involving chemical or electrochemical reduction of the Yb^{2+} followed by separation from the Lu^{3+} was evaluated. The first step was to determine the effectiveness of the method of reduction (Yb^{3+} to Yb^{2+}) that leads to the complete reduction of Yb^{3+}, whereas the second step explored separating the two species, Yb^{2+} and Lu^{3+} that differed in their oxidation states.

4.3.1 Electrolytic reduction of Yb^3 to Yb^{2+}. In order to achieve complete reduction of Yb^{3+} to Yb^{2+} a set of experiments was performed by applying a potential to the Yb^{3+} compound. The different redox inert metals that were used as electrodes did not show evidence of reducing the Yb^{3+} under various sets of conditions, namely prolonged time of current flow, solvent mixtures, and potential. By using the glassy carbon electrode, a reversible Yb^{3+} -Yb^{2+} Cl_x couple (E°= -0.8 V) was observed by the cyclic voltammetry (**Figure 4-2**). In addition, $Yb(acac)_3$ resulted in a similar reversible scan with the reduction potential close to -1.6 V. The higher potential recorded for complexed Yb^{3+} compounds indicate that the coordinating ligands are acting as electron donors, resulting

in an increase in potential for the reduction to occur. This result indicates that alternative methods that could assist in the dissolution of Yb salts in organic solvents by forming complexes with ligands is not ideal due to the higher potentials required to reduce Yb^{3+}. A study reported by Dennis et al. showed the changes in the Ce^{3+}/Ce^{4+} redox couple can be produced by changing the chelating ligand.[11] Based on this report, the electron withdrawing effect of the ligand donor atoms contributed to slightly higher reduction potentials required to reduce the lanthanides ions. The electron density effect is pronounced in lanthanide ions because the f-orbitals are inaccessible to the binding electrons from the ligand orbitals.

Previous studies involving electrolytic reduction of Sm^{3+} and Yb^{3+} compounds.

A successful reversible electrolytic reduction of Yb $(OTf)_3$ has been reported by Parrish et al. with redox potentials varying between the $Yb(OTf)_2$ and YbI_2 compounds[12] . This report suggested that the supporting electrolytes in acetonitrile (*T*-Bu_4NX; X = Cl^-, I^-, and Br^-) undergo ligand exchange with the triflate and the halide forms of ytterbium. The experimental redox potential for $Yb(OTf)_3$ in the presence of a tetraalkyl ammonium iodide and bromide electrolytes was -1.2 and -1.7 V, respectively.

An attempt to perform bulk electrolysis on Yb^{3+} using carbon paste as the cathode did not exhibit reduction. The solvent mixture used (MeOH/ACN) to dissolve the Yb^{3+} and the electrolyte was not compatible with the carbon paste. The carbon paste, tantalum, and titanium metal working electrodes did not show even psuedo-reversible cyclic voltammetric scans. A flat scan swipe that went through a highly negative potential without indication of any sort of peak suggested the reduction of the Yb^{3+} ion did not occur. This was true for $YbCl_3$ and $Yb(OTf)_3$ compounds. Voltammetric scans similar to

the one shown on **Figure 4-3** were observed and show the ineffectiveness of the working electrodes discussed.

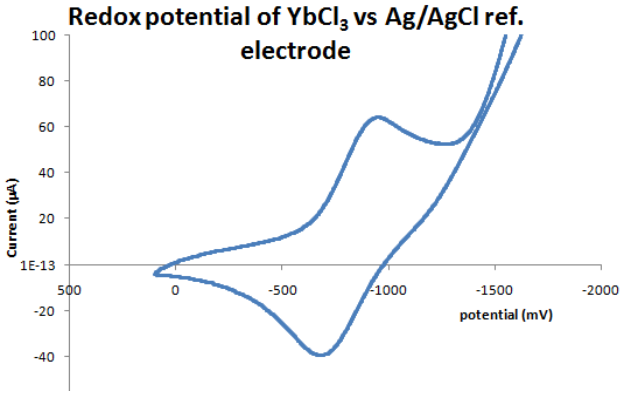

Figure 4-2. Cyclic voltammetry of $YbCl_3$ in TEACl as the supporting electrolyte and MeOH/ACN as the solvent using glassy carbon as the working electrode.

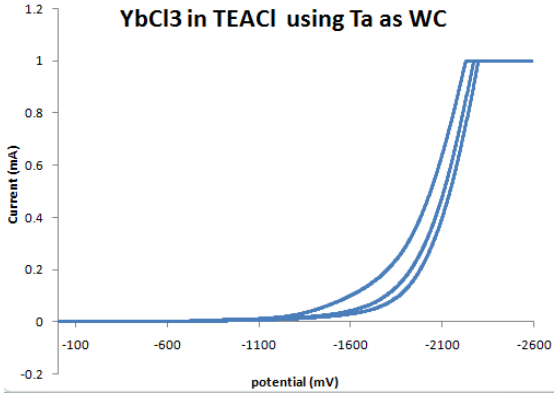

Figure 4-3. Cyclic voltammetry of $YbCl_3$ in TEACl using Ta as a working electrode. Similar scans were observed for Ti metal wire as working electrode with the $Yb(OTf)_3$ analyte.

The calculated redox potential of $Yb(OTf)_3$ vs Ag/AgCl reference electrode in EtOH/ACN solvents is -0.715 V. The total potential required for the complete reduction of Yb^{3+} was close to -1.0 V. A bulk electrolysis was conducted using glassy carbon paste as the working electrode with a potential of -2.5 V, well above the experimentally determined value. The result from the bulk electrolysis experiment, showed no indication

of reduced Yb^{2+} in the solution. After a prolonged experiment of applying potential to the Yb^{3+} compound, gradual accumulation of insoluble particulates covered the electrode surface. This could be due either to the electrode incompatibility with the solvent mixture (EtOH/ACN) or from the electrolytes decomposition at higher voltage. There was not a discernible current flow or observable color change from using the glassy carbon paste as the working electrode.

4.3.2 Chemical Reduction of Yb^{3+} to Yb^{2+}. The efficiency in reducing the Yb^{3+} to Yb^{2+} was related to the strength of the standard reduction potential of the metals used as reductants. Higher mesh number or lower particle size was effective in reducing Yb^{3+} due to the high surface area. The reduction of Yb^{3+} with high yield was investigated to determine the optimum conditions. Among the variables evaluated to accomplish the objectives, a series of changes in the reagents used ($YbCl_3$, $Yb(OTf)_3$, and $Yb(acac)_3$), metal reductants, temperature, and solvent mixtures were investigated and found to have exhibited pronounced effect in the amount of Yb^{3+} reduced. The reason for evaluating only these listed ytterbium compounds were because of the limitation in the practical work up to prepare the Yb targets. In order to maintain the Yb^{2+} stable in solution, the starting Yb compound has to be anhydrous. Of the three forms of the Yb compounds evaluated, the $Yb(OTf)_3$ could easily be dehydrated and reduced to its +2 oxidation state.[13]

The amount of Yb^{3+} reduced by the reductant metal was directly related to the standard redox potential of the metals used. Although all of the evaluated reductant metals have a redox potential well above the potentials needed to reduce Yb^{2+}, the solvent system utilized for the reduction might weaken their potency as a reductant.

Magnesium and yttrium metals afforded reduction of Yb^{3+} to Yb^{2+} with the highest yields. A vigorous reaction was often observed when using these two metals resulting in an instant color change to bright green, which is indicative of reduction of Yb^{3+}. While the other metals (Zr, Hf, Ti, and Al) have sufficient potential to reduce Yb^{3+}, the yield from the reduction process was small to nothing. A slight faint green color was observed on the surface of the metal but the amount of Yb^{2+} formed was not enough to quantify. **Table 4-2** below lists the percentage yields obtained by using metals for the reduction of Yb^{3+}.

	Solvent mixtures	% Yield of Yb^{2+}						
		Mg	Y	Mn	Zr	Hf	Ti	Al
$YbCl_3$	EtOH/ACN (35:65)	72.0 ± 5	90.0 ±7	20±2.5	0	0	0	0
	MeOH/ACN (35:65)	60.0 ± 2	87±1.3	0	0	0	0	0
$Yb(OTf)_3$	EtOH/ACN (35:65)	10.0 ± 1.8	0	0	0	0	0	0
	MeOH/ACN (35:65)	0	0	0	0	0	0	0

Table 4-2. The result from the reduction of Yb^{3+} using reductant metals in different solvent conditions. The amount of Yb^{2+} obtained after the reduction was determined by iodometric titration. In some of the evaluated reductant metals there was no observable color change in the reaction mixtures.

4.3.3 Counter ion or complexing ligand effect(s) on the reducing metals. The counter ions or complexing ligands of Yb^{3+} have an effect on the redox potential of Yb due to their interaction with the Yb^{3+} ion by either donating or withdrawing electron density.[14] For this reason, the redox potential required to reduce Yb^{3+} varies depending on the form of Yb^{3+} ($YbCl_3$, $Yb(Otf)_3$, or $Yb(acac)_3$) used for the reduction process. Ytterbium nitrate is an alternative source used for the target irradiation for production of ^{177}Lu. However,

these studies did not include the NO_3^- due to its redox susceptibility in the presence of reductants and formation of NO_x species.[15]

In general, from the set of Yb^{3+} starting materials used for the reduction process, $YbCl_x$ $(MeCN)_yCl^-$ and $Yb(MeCN)^{3+}$ $(OTf)_3$ demonstrated reduction by using metal reductants. However, of the two forms of Yb^{3+} compounds, the triflate takes a longer time for the reduction to occur (2 h). This was evident after using Mg or Y as the reductant metals.

4.3.4 Solvent effect. Since the reduced Yb^{2+} is easily oxidized back to Yb^{3+} in the presence of water or oxygen, the solvents used to dissolve the Yb^{3+} salts must be anhydrous and oxygen free. The ytterbium salts that were utilized for this study were soluble in methanol and ethanol, and partially soluble in isopropyl alcohol. Pure alcohol solvents were superior in dissolving the Yb salts, but the strong reaction on adding the metal reductants that evolved heat and gas followed by a sudden disappearance of the green color suggested Yb^{2+} was oxidized to Yb^{3+} by undergoing the following chemical reactions.

$$Mg_{(s)} + 2ROH \xrightarrow{\Delta} Mg(OR)_2 + 2H^+ \quad R= -CH_2CH_3 \text{ or } -CH_3$$

$$H^+ + 2e^- \rightarrow H_{2\,(g)}$$

Magnesium is capable of forming alkoxide species as the above equation indicates.[16-18] Also, the formation of the Mg-alkoxide species proceeds at elevated temperatures. This reaction produces H^+ that can undergo a one electron reduction to form H_2 gas (H_2 gas bubbles were observed during the reaction). Magnesium metal and

Yb^{2+} are potent in reducing H^+ to H_2, since Yb^{2+} ion was in the liquid phase, it is safe to assume Yb^{2+} reduced H^+, resulting in oxidation back to Yb^{3+}.

In order to circumvent the aggressive reaction of the metals in the presence of Yb^{3+} compounds that leads to the oxidation of Yb^{2+} to Yb^{3+}, various modifications were made to control the random temperature changes. By cooling the reaction mixtures using external cooling mantles (also dry-ice incubation), heat and bubble occurrences (that were evident in reactions conducted in room temperatures) were eliminated. However, an attempt to keep the reaction mixture at < -10 °C resulted in the amount of Yb^{2+} formed reduced to 38% ±0.02. Other approaches used to ease the rapid temperature increase included the use of solvent mixtures such as alcohols, acetonitrile, and tetrahydrofuran to accommodate the solubility issues of Yb^{3+} salts and conduct the reaction under cooler temperatures. **Table 4-3** lists the solvent mixtures examined to obtain the highest yield of reduced Yb^{2+}. There were a few solvent mixtures (e.g., MeOH/cyclohexane) that were either incompatible or did not keep the Yb^{3+} salt in solution. While THF and 1,4-dioxane are regarded as complexing solvents that should stabilize divalent lanthanides,[14] the Yb^{3+} compounds constantly crashed out of solution in these solvents and required alcohol mixtures to keep the Yb^{3+} salt in solution. The EtOH/ACN mixtures were the ones that gave the highest yield of Yb^{2+}, (72 % and 90% using Mg and Y metals, respectively).

The advantage in using solvent mixtures is that in the presence of a proton acceptor solvent (nitrogen of the ACN) the proton of the alcohol will tend to form hydrogen bonds with the nitrile groups of ACN.[19] As a result, the oxidized metal (e.g., Mg^{2+}) will be stabilized by forming an alkoxy bond. Also, formation of a hydrogen bond

with the nitriles will lessen the chance of the dissociated protons being reduced to H_2 gas by Yb^{2+}, which is an unfavorable outcome that leads to oxidation of Yb^{2+} to Yb^{3+}.

Solvent system	Percent Yield of Yb^{2+}	δ	observation
MeOH	32.0	± 4.0	
EtOH	36.3	±2.0	
THF			Not soluble
10% MeOH/THF			
40% MeOH/THF	61.37	±2.0	
10% MeOH/ACN			murky solution
35 % MeOH/ACN	40.33	±3.0	
40% MeOH/ACN	32.33	±4.0	
50% MeOH/ACN	27.67	±2.0	
25 % MeOH/EtOAc	23.36	±2.0	
40% MeOH/dioxane	0		
10% EtOH/THF	0		
40% EtOH/THF	0		
10% EtOH/ACN	0		Not soluble
25% EtOH/ACN	39.00	±4.0	
35% EtOH/ACN	72.00	±5.0	
40% EtOH/ACN	68.33	±3.0	
40% EtOH/ACN ascorbic added	0		Murky solution
50% EtOH/ACN	56.00	±5.0	
28% EtOH/dioxane	0		
40% EtOH/dioxane	0		
40% MeOH/Cylohexane			not compatible with alcohol
40% MeOH/hexane			
40% MeOH/toluene			

Table 4-3 Reduction of $YbCl_3$ using Mg as the reductant metal. *Iodometric titration* methodology was applied to determine the amount of Yb^{2+} in solution. (δ = standard deviation with n = 3)

4.3.5 1,4-Dioxane and THF as complexing solvents. The effects of complexing solvents such as 1,4-dioxane and THF on the Yb^{2+} was prominent in stabilizing the reduced Yb^{2+}. In the early publications by Clifford et al. there was a suggestion that complexing

reagents such as THF stabilized the rather short-lived Sm^{2+} or Yb^{2+} compounds [14, 20]. When using THF as a solvent mixture to stabilize the Yb^{2+} ion, however, insoluble particulates formed on the surface of the reductant metal. This observation suggested the presence of THF could have facilitated Yb^{2+} precipitation. Similar observations were reported by Collin et al. in an attempt to reduce Sm^{3+} to Sm^{2+} and indicated occasional precipitation occurred on the surface of the reductant metal when they used THF as the solvent.[21]

4.3.6 Separation of ^{177}Lu from Yb. The reaction mixture containing Yb^{3+} compounds were spiked with ^{175}Yb/^{177}Lu and the separation of the Yb from Lu was evaluated counting the samples using HPGe and analyzing the emitted energies spectrum. The separation was classified into three parts: column separation, solid phase extraction, and liquid-liquid extraction using complexing reagents. After allowing the Yb^{3+} compounds to react with metal reductants, the second step was to (1) pass the reaction mixture through a column containing an ion exchange resin, (2) extract a complexed Yb^{2+} from the Lu^{3+} reaction with the reductant metals, and (3) extract the reduced Yb^{2+} as a solid.

(1) The column separation was conducted using Chelex and DOWEX resins (according to the manufacturer's specifications, the resins are compatible with the solvent system used in this experiment (i.e., alcohol/ACN mixtures)). The reason for using cation exchange resins was to separate the Yb^{2+} from the Lu^{3+} (the expected order of elution profile would be Yb^{2+} first followed by $^{177}Lu^{3+}$). The Chelex resin is selective for divalent metal ions due to the binding affinity of the metals to the carboxylic acid groups of the resin at a specific pH. The difficulty encountered in using resins as the chromatography media was that they are designed to perform well in wet media (i.e., in the presence of

water). This could possibly be the reason why the separation of the reduced Yb^{2+} from ^{177}Lu using chromatography media did not perform well since the Yb^{2+} is easily oxidized in the presence of water. An attempt to dry the resins (Chelex or DOWEX 50W X 4) caused column channeling during column equilibration, which made the subsequent separation trials unsuccessful. Both Chelex and DOWEX chromatography resin that are capable of binding lanthanides with high affinity[22-24] managed to only retain 40 % of the Yb/Lu, whilst the remaining activity (60% of the Yb/Lu with an equivalent ratio as the loaded sample) passed through column.

4.3.7 Separation of Yb/Lu by complexation. Solvent extraction using phosphonates have been reported for removing rare-earth metals from reaction mixtures.[25-26] Di-2-ethylhexylphosporic acid (HDEHP) is used to extract lanthanides in non-polar organic phases. In the case of La HDEHP complexation, the Ln^{3+} bonds the HDEHP with the HDEHP forming hydrogen bonds with the adjacent phosphates (**Figure 4-4)**. The differences in the oxidation number between Yb^{2+} and Lu^{3+} could potentially result in forming HDEHP complexes that differs by the number of coordinating HDEHP (Yb^{2+} and Lu^{3+}). The alkylated branched chains of HDEHP with six carbon atoms per chain are more lipophilic and have a stronger affinity for hydrocarbons. One approach investigated was to add HDEHP to the reaction mixtures containing the reduced Yb^{2+} /Lu^{3+} and isolate Yb^{2+} from the Yb^{3+}complex using reversed phase C-18 plates. Complexed Ln^{3+} moves with the solvent front with mixtures of organic solvents (hexane/acetone) as a mobile phase and since there was only one observed peak by TLC, the Yb^{2+} may have been oxidized in the presence of the phosphonate groups. The chemical equation below indicates the dissociation of H^+ from the Ln-ligand reactions.

$$Ln^{3+} + 3(HDEHP)_2 = Ln(HDEHP)_3 + 3H^+$$

The dissociating hydrogen ions from the phosphonate groups of the HDEHP could potentially oxidize the Yb^{2+}, resulting in the formation of the trivalent Yb^{3+} HDEHP complex.

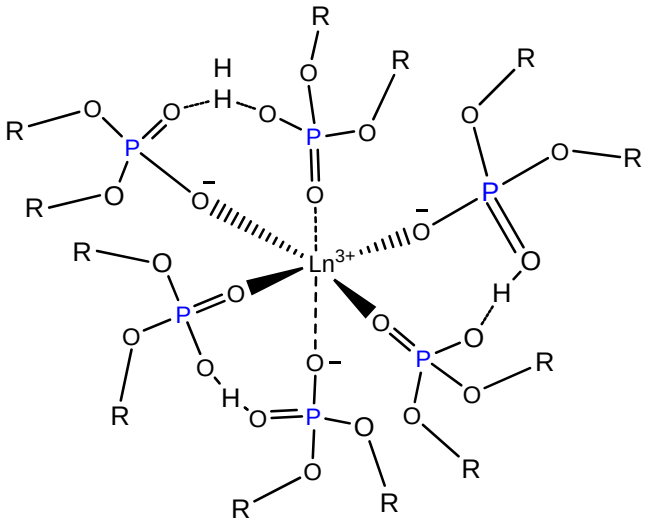

Figure 4-4. Structure of Ln^{3+}(HDEHP)3 complexes.[25] (R= hexyl)

4.3.8 Separation by solid extraction. The studies reported by Bilewicz et al. and Chakravarty et al. discuss the efficiency of a multistep separation of the ^{177}Lu from irradiated Yb^{3+} samples by reduction and solid state extraction. [27,28] The separation step that follows the reduction step takes advantage of the selective precipitation of Yb^{2+}as the insoluble $YbSO_4$. Although, each report used a different reduction method (Bilewicz used sodium amalgam (Na/Hg) and Chakravarty used electrolysis with mercury as a cathode to reduce the Yb^{3+} to Yb^{2+}), both studies reported successful separation of the Yb from the ^{177}Lu owing to the insoluble $YbSO_4$ or low level deposition of ^{177}Lu in the Hg phase (Bilewicz reported 73 % total recovery of ^{177}Lu, while Chakaravarty reported the

extraction of ^{177}Lu was ~99 % yield). Therefore, an attempt was made to capture the $YbSO_4$ in the solid state. A diagram of the reduction of Yb^{3+} and separation of Yb^{2+} from Yb^{3+} process is shown below in **Figure 4-5**.

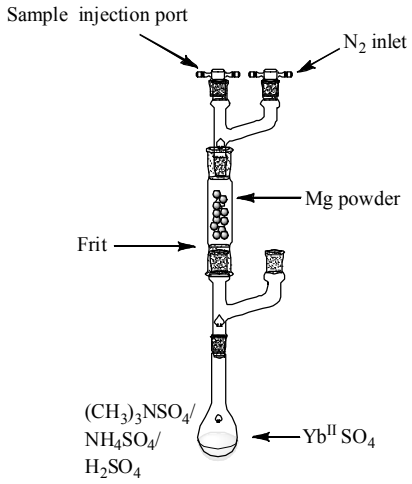

Figure 4-5. Separation of Yb^{2+} from Lu by reduction using reductant metals (e.g., Mg) and precipitation of the divalent Yb with sulfates.

The precipitation of Yb^{2+} in the presence of sulfates that are soluble in the solvent mixtures (40/60: EtOH/ACN) conditioned to keep the Yb^{3+} salts in solution and yield the maximum reduction of Yb^{3+} was investigated. The tetraalkylammonium sulfates (TMAS) and sulfonates were the primary reagents chosen for the Yb^{2+} precipitation process. The selective precipitation of Yb by the sulfates did not yield the desired outcome as both Yb^{3+} and Lu^{3+} precipitated out of solution. This suggests that in order to selectively remove Yb^{2+} as $YbSO_4$, the solvent has to be aqueous.

4.4 Conclusion

Electrochemistry. The reduction of Yb^{3+} to Yb^{2+} by applying a potential to the sample has been evaluated. The electrodes chosen to perform the reduction of the Yb^{3+} were either incompatible with the solvents (strong organic solvents) or decomposed electrolytes at higher potentials or passivation of the surface of the electrode was observed. The electrolyte decomposition significantly hindered the bulk electrolysis. The cyclic voltammetry experiment to reduce Yb^{3+} to Yb^{2+} resulted in reversible scans for the $YbCl_3$ using glassy carbon electrodes to enhance the surface area. The bulk electrolysis using carbon paste electrodes, however, encountered electrode surface erosion due to the interaction between the solvent (ACN) and the carbon paste.

Chemical reduction of Yb^{3+} to Yb^{2+}. Based on what has been evaluated thus far, the chemical reduction of Yb^{3+} to Yb^{2+} is ideal in terms of its chemical safety and its performance in reducing the bulk of the Yb sample. Although, the amount of Yb used in the experiments is slightly higher (100 mg) than what is regularly used in similar referenced literatures (~ 50 mg), the chemical yields obtained from this reduction system are encouraging. The separation of Yb^{2+} from the Lu^{3+} by selective precipitation has been reported by Bilewicz.[27] Following this report, the current study attempted to isolate the reduced Yb^{2+} by precipitation but was unsuccessful in selective precipitation of Yb^{2+}. The solubility of divalent $YbSO_4$ in aqueous solvent is less than trivalent $Yb_2(SO_4)_3$, however, since the study utilized organic solvents, the precipitation using sulfates was not selective for Yb^{2+}. The precipitation of the sample by tetraalkyl sulfates resulted in precipitation of $Yb^{2+/3+}$ and the Lu^{3+}, which is an undesired outcome as the objective of the separation process was to isolate the Yb^{2+} in solid state for debulking purposes and the Lu^{3+} in the

liquid phase. Due to the high water content of the chromatography media, the reduced Yb^{2+} compounds were instantly oxidized on contact with the cation exchange resins. Conversely, anhydrous ammonium sulfate powders that were loaded on a column in the hope of forming the $YbSO_4$ resulted in elution of both Yb and Lu without retention on the column.

The multistep separation of the Lu^{3+} from the Yb^{3+} targets offers convenience in handling and processing radiolanthanides by minimizing the processing time and avoids generating high volumes of unwanted, radioactive wastes as is the case with column chromatography. Also, the solvents utilized for the reductions can easily be removed from the sample due to their low boiling points. It has been shown from this experiment that Yb^{3+} can be readily reduced with the reductant metal Mg and Y.

4.5 Future Studies

The multistep separation of ^{177}Lu from the Yb^{3+} that involves reduction of the Yb^{3+} has been explored. The separation of the divalent Yb from the Lu^{3+} required attention since the Yb^{2+} redox unstable, hence the chemical utilized for the separation has to be non-aqueous and handled under inert atmosphere. Although, the current separation by complexation did not yield the desired outcome, it is the conceivable option to perform the separation of Yb form Lu by picking ligands that are redox active. There were various attempts made to stabilize the reduced Yb^{2+} during the separation process. But it was difficult to fulfill the objectives due to Ln ions are attracted to oxy-ions that can easily oxidize the Yb^{2+}. Therefore, it is rather beneficial to pick a ligand that undergoes redox and forms a stable complex thereby changing its chemical structure as a

result of its complexation with Yb^{2+}. This approach is more advantageous since the Lu^{3+} does not participate in the redox reaction and can be isolated in the solvent of choice (even in aqueous media), because guarding the Yb^{2+} from oxidation is no longer needed.

The types of ligands that undergo one electron reduction and form stable complexes with carbonyl functional groups have been well explored in the organic chemistry in which divalent metal ions participate in the reactions as catalysts.[29] A review article that covered the catalytic reduction of highly conjugated ketones elaborated on the various methods utilized to obtain a pinacole-coupled product. **Figure 4-6** shows a general reaction that represents one electron reduction of ketones by catalytic Ln^{2+} ion to result in lanthanide pinacolates.

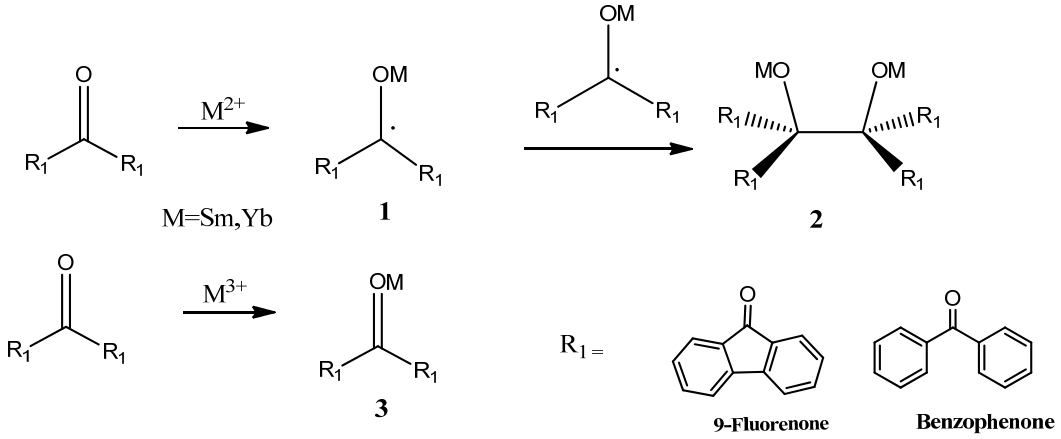

Figure 4-6. Basic mechanism of pinacol coupling reactions

The focus on this reaction scheme is the intermediate metal pinacolates, and depending on the steric effect from the conjugated ligand, the yield in forming a stable pinacolate compound can increase. The yield from the one electron reduction of the fluorenone and benozophenone results in a ketyl intermediate. The product from the pinacol coupling reaction (2) could only be formed in the presence of metals at lower

oxidation states acting in a single electron transfer. A trivalent lanthanide may form product (3) but will not be part of the product (2) since each of the coupling adduct comes in with a ketyl radical as indicated in the intermediate (1). A number of reports used either Sm or Yb metals as the catalytic reductants and while most of them chose the metal as the source of the reductant species, there are a few reports that explored the options of using divalent Sm or Yb to reduce the carbonyl oxygen.[30] By applying the pinacole coupling reaction to the separation of Yb/Lu, the arduous work to protect the oxidation of Yb^{2+}can be avoided.

4.6 References

1. Atkins, P. W.; Shriver, D. F., *Shriver & Atkins' inorganic chemistry*. 5th ed.; Oxford University Press: Oxford, 2010; p xxiv, 824 p.
2. Ball, R. W.; Yntema, L. F., The separation of ytterbium by electrolytic reduction. Observation on the rare earths XXXVI. *Journal of the American Chemical Society* **1930,** *52* (11), 4264-4268.
3. Asprey, L. B.; Ellinger, F. H.; Staritzky, E. Rare Earth Research II: Proceedings of the Third Conference on Rare Earth Research, Vores, K., Ed. 1964; pp 11-24.
4. Peppard, D. F., Liquid-Liquid Extraction of Metal Ions. In *Advances in Inorganic Chemistry*, Emeléus, H. J.; Sharpe, A. G., Eds. Academic Press: 1966; Vol. Volume 9, pp 1-80.
5. Rabockai, T., Electrochemical reduction of ytterbium in perchloric media. *Journal of Electroanalytical Chemistry and Interfacial Electrochemistry* **1977,** *76* (1), 83-89.
6. Nakashima, N.; Yamanaka, K.-i.; Yatsuhashi, T., Reduction of Yb(III) to Yb(II) by Two-Color Two-Photon Excitation. *The Journal of Physical Chemistry* **2013,** *117* (35), 8352.
7. Xijuan, Y.; Rronghu, W.; Huiyu, S.; Qingde, S., Study on dihydrated praseodymium acetylacetonate by photoacoustic spectra with broad wavelength range. *Journmal of Rare Earths* **2003,** *21* (2), 135.
8. Armarego, W. L. F.; Chai, C. L. L., *Purification of Laboratory Chemicals* 6ed.; Elsevier, 2009.
9. Gores, H. J.; Barthel, J., Non-aqueous electrolyte solutions. *Naturwissenschaften* **1983,** *70* (10), 495-503.
10. Švancara, I.; Vytřas, K.; Kalcher, K.; Walcarius, A.; Wang, J., Carbon Paste Electrodes in Facts, Numbers, and Notes: A Review on the Occasion of the 50-Years Jubilee of Carbon Paste in Electrochemistry and Electroanalysis. *Electroanalysis* **2009,** *21* (1), 7-28.
11. Wester, D. W.; Palenik, G. J.; Palenik, R. C., Electrochemical studies of cerium chelate complexes. *Inorganic Chemistry* **1985,** *24* (25), 4435-4437.
12. Parrish, J. D.; Little, R. D., Electrochemical generation of low-valent lanthanides. *Tetrahedron Letters* **2001,** *42* (44), 7767-7770.
13. Huang, C.-H., *Rare earth coordination chemistry : fundamentals and applications*. John Wiley & Sons (Asia): Singapore ; Hoboken, NJ, 2010; p xxii, 575 p.
14. Shabangi, M.; Sealy, J. M.; Fuchs, J. R.; Flowers Ii, R. A., The effect of cosolvent on the reducing power of SmI_2 in tetrahydrofuran. *Tetrahedron Lett.* **1998,** *39* (25), 4429-4432.
15. Erkfeldt, S.; Palmqvist, A.; Petersson, M., Influence of the reducing agent for lean NOx reduction over Cu-ZSM-5. *Appl. Catal., B* **2011,** *102* (Copyright (C) 2012 American Chemical Society (ACS). All Rights Reserved.), 547-554.
16. Eva H. Morkved, H. O., and Helge Kjosen, Prepration of octa(alkoxy) Azaphthalocyanines. *Acta Chemica Scandinavica* **1999,** *53*, 1117-1121.

17. Yamaguchi, O.; Kawabe, K.; Shimizu, K., Formation of MgGeO3 from the hydrate prepared by hydrolysis of magnesium and germanium oxides. *Journal of the Chemical Society, Dalton Transactions* **1983,** (9), 2139-2141.
18. Lin, J. M.; Li, H. H.; Zhou, A. M., Synthesis of Benzyl/Allyl Alkyl Ethers from Corresponding Magnesium Alkoxides. *Tetrahedron Letters* **1996,** *37* (29), 5159-5160.
19. Kondo, Y., The Finkelstein Reaction in Acetonitrile–Alcohol Mixtures. An Approach to an Anion Solvation by Means of a Multi-step Solvation Model *Bulletin of the Chemical Society of Japan* **1975**.
20. Imamoto, T.; Ono, M., The Reaction of Samarium(III) Iodide with Samarium Metal in Tetrahydrofuran, A New Method for the Preparation of Samarium(II) Iodide. *Chemistry Letters* **1987,** *16* (3), 501-502.
21. Collin, J.; Giuseppone, N.; Machrouhi, F.; Namy, J.-L.; Nief, F., New synthesis and reactions of [Sm(OTf)2(DME)2], a salt-free samarium(II) triflate. *Tetrahedron Letters* **1999,** *40* (16), 3161-3164.
22. Hashimoto, K.; Matsuoka, H.; Uchida, S., Production of no-carrier-added ^{176}Yb(n, gama)^{177}Yb beta decay ^{177}Lu process. *Journal of Radioanalytical and Nuclear Chemistry* **2003,** *255* (3), 575-579.
23. Knight, C. H.; Cassidy, R. M.; Elchuk, S.; Elliot, N. L.; Green, L. W.; Recoskie, B. M., Dynamic ion exchange chromatography for the determination of number of fissions in uranium dioxide fuels. *Analytical Chemistry* **1986,** *58* (6), 1181-1186.
24. Cassidy, R. M.; Miller, F. C.; Knight, C. H.; Roddick, J. C.; Sullivan, R. W., Evaluation of dynamic ion exchanger for the isolation of metal ions for characterization by mass and .alpha.-spectrometry. *Analytical Chemistry* **1986,** *58* (7), 1389-1394.
25. Marie, C.; Hiscox, B.; Nash, K. L., Characterization of HDEHP-lanthanide complexes formed in a non-polar organic phase using 31P NMR and ESI-MS. *Dalton Transactions* **2012,** *41* (3), 1054-1064.
26. El-Reefy, S. A.; Awwad, N. S.; Aly, H. F., Liquid–Liquid Extraction of Uranium from Phosphoric Acid by HDEHP–CYANEX-921 Mixture. *Journal of Chemical Technology & Biotechnology* **1997,** *69* (2), 271-275.
27. Bilewicz, A.; Żuchowska, K.; Bartoś, B., Separation of Yb as $YbSO_4$ from the ^{176}Yb target for production of ^{177}Lu via the Yb(n, γ)^{177}Yb$\rightarrow$^{177}Lu process. *Journal of Radioanalytical and Nuclear Chemistry* **2009,** *280* (1), 167-169.
28. Chakravarty, R.; Das, T.; Dash, A.; Venkatesh, M., An electro-amalgamation approach to isolate no-carrier-added ^{177}Lu from neutron irradiated Yb for biomedical applications. *Nuclear Medicine and Biology* **2010,** *37* (7), 811-820.
29. Hou, Z.; Fujita, A.; Zhang, Y.; Miyano, T.; Yamazaki, H.; Wakatsuki, Y., One-Electron Reduction of Aromatic Ketones by Low-Valent Lanthanides. Isolation, Structural Characterization, and Reactivity of Lanthanide Ketyl Complexes. *Journal of the American Chemical Society* **1998,** *120* (4), 754-766.
30. Hou, Z.; Wakatsuki, Y., Reactions of Ketones with Low-Valent Lanthanides: Isolation and Reactivity of Lanthanide Ketyl and Ketone Dianion Complexes. *Organometallics* **1999,** *2*.

VITA

Nebiat Sisay was born in August 22, 1981, in Addis Ababa, Ethiopia. He graduated from Southern University at New Orleans with a Bachelors of Science with honors in Chemistry (2008). He participated in two summer (2006 and 2007) undergraduate internship programs at the University of Missouri-Columbia under Dr. Silvia S. Jurisson before he joined Dr. Jurisson's research group for his graduate studies. He received his Ph.D. in Chemistry with a specialization in radiopharmaceutical chemistry from the University of Missouri-Columbia (2014). He is planning to complete a postdoctoral appointment where he will continue research in the area of radiochemistry.